



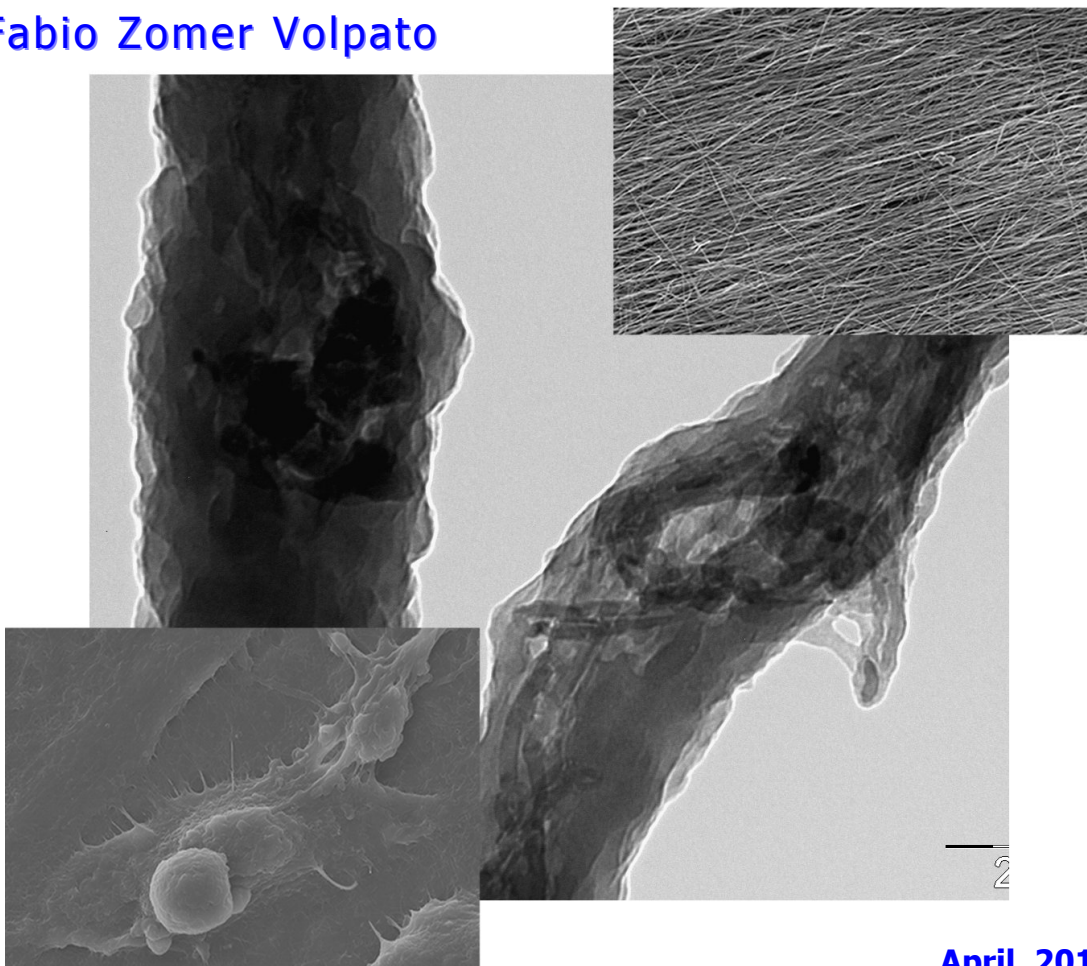
UNIVERSITY  
OF TRENTO - Italy

Department of Materials Engineering  
and Industrial Technologies

Doctoral School in Materials Engineering – XXII cycle

## Composites for Biomedical Applications

Fabio Zomer Volpato



April 2010





UNIVERSITY  
OF TRENTO - Italy

Department of Materials Engineering  
and Industrial Technologies

Doctoral School in Materials Engineering – XXII cycle

---

---

# **Composites for Biomedical Applications**

**Fabio Zomer Volpato**

Advisor:

Prof. Claudio Migliaresi

**April 2010**



# Contents

<b>1</b>	<b>INTRODUCTION AND OBJECTIVES</b>	<b>15</b>
1.1	Introduction . . . . .	15
1.2	Objectives . . . . .	17
1.2.1	Specific Objectives . . . . .	17
<b>2</b>	<b>STATE OF THE ART</b>	<b>19</b>
2.1	Tissue Engineering . . . . .	19
2.2	Scaffolds in Tissue Engineering . . . . .	21
2.3	Polymers in Tissue Engineering . . . . .	21
2.3.1	Natural polymers . . . . .	22
2.3.2	Synthetic polymers . . . . .	23
2.4	Composites in Tissue Engineering . . . . .	23
2.5	Surface Features . . . . .	24
2.5.1	Micro patterning . . . . .	25
2.5.2	Nano patterning . . . . .	25
2.6	Carbon Nanotubes . . . . .	26
2.6.1	Single-walled carbon nanotubes . . . . .	27
2.6.2	Multi-walled carbon nanotubes . . . . .	28
2.6.3	Production technique . . . . .	29
2.6.3.1	Chemical Vapor Deposition (CVD) . . . . .	29
2.6.3.2	Arc-Discharge . . . . .	30
2.6.3.3	Laser ablation . . . . .	30

2.6.4	Properties . . . . .	30
2.6.4.1	Mechanical properties . . . . .	30
2.6.4.2	Electrical properties . . . . .	31
2.6.4.3	Optical properties . . . . .	31
2.6.5	Carbon nanotubes in tissue engineering . . . . .	32
2.6.5.1	Carbon nanotubes biocompatibility . . . . .	33
2.7	Electrospinning Technique . . . . .	34
2.7.1	Electrospinning theory . . . . .	37
2.7.1.1	Droplet generation . . . . .	37
2.7.1.2	Taylor's cone formation . . . . .	38
2.7.1.3	Launching of the jet . . . . .	38
2.7.1.4	Elongation of straight segment . . . . .	39
2.7.1.5	Whipping instability region . . . . .	40
2.7.1.6	Solidification into nanofiber . . . . .	41
2.7.2	Main parameters that influence fiber morphology . . . . .	41
2.7.2.1	Electrical field . . . . .	41
2.7.2.2	Polymer concentration . . . . .	42
2.7.2.3	Flow rate . . . . .	42
2.7.2.4	Working distance . . . . .	42
2.7.3	Electrospinning for biomedical applications . . . . .	43
<b>3</b>	<b>MATERIALS AND METHODS</b>	<b>45</b>
3.1	Polyamide 6 - PA6 . . . . .	45
3.2	Functionalized Multi-Walled Carbon Nanotubes . . . . .	46
3.3	Fabrication Technique . . . . .	46
3.4	Characterization Methods . . . . .	49
3.4.1	Carbon nanotubes analyses . . . . .	49
3.4.1.1	Transmission electron microscopy - TEM . . . . .	49
3.4.1.2	X-Ray photoelectron spectroscopy - XPS . . . . .	49
3.4.2	Nanofiber morphology . . . . .	50
3.4.2.1	Scanning electron microscopy - SEM . . . . .	50

<i>CONTENTS</i>	3
3.4.2.2 Transmission electron microscopy - TEM	50
3.4.2.3 Atomic force microscopy - AFM . . . . .	51
3.4.3 Thermal analysis . . . . .	51
3.4.3.1 Differential scanning calorimetry - DSC	51
3.4.4 Mechanical analysis . . . . .	52
3.4.4.1 Tensile analysis . . . . .	52
3.5 Biological Evaluation . . . . .	52
3.5.1 Protein adsorption analyses . . . . .	53
3.5.1.1 Protein adsorption . . . . .	53
3.5.1.2 Electrophoresis . . . . .	54
3.5.2 Cell seeding and culture . . . . .	54
3.5.3 Cell proliferation . . . . .	55
3.5.4 Cell viability . . . . .	56
3.5.5 Cell morphology . . . . .	57
3.6 Statistical Analysis . . . . .	57
<b>4 RESULTS AND DISCUSSION</b>	<b>59</b>
4.1 Carbon Nanotubes Analysis . . . . .	59
4.2 Nanofiber Production and Morphology . . . . .	61
4.3 Thermal Analysis . . . . .	66
4.4 Mechanical Analysis . . . . .	71
4.5 Biological Analysis . . . . .	74
4.5.1 Protein analyses . . . . .	74
4.5.2 Proliferation analysis . . . . .	77
4.5.3 Cell viability . . . . .	80
4.5.4 Cell morphology . . . . .	86
<b>5 CONCLUSIONS</b>	<b>95</b>
<b>6 FUTURE INVESTIGATIONS</b>	<b>99</b>
<b>7 ACKNOWLEDGEMENTS</b>	<b>101</b>

4

*CONTENTS*

**Bibliography**

**103**

# List of Figures

2.1	Tissue Engineering approach representation. ( <a href="http://biomed.brown.edu">http://biomed.brown.edu</a> ). . . . .	20
2.2	Molecular structures of a single-walled carbon nanotube (SWCNT) and of a multi-walled carbon nanotube (MWCNT). ( <a href="http://www-ibmc.u-strasbg.fr/">http://www-ibmc.u-strasbg.fr/</a> ). . . . .	27
2.3	TEM image of a single-walled carbon nanotube. ( <a href="http://www.electroiq.com">http://www.electroiq.com</a> ). . . . .	28
2.4	TEM image of a multi-walled carbon nanotube. ( <a href="http://endomoribu.shinshu-u.ac.jp/">http://endomoribu.shinshu-u.ac.jp/</a> ). . . . .	29
2.5	Electrospinning diagram drawn by Cooley in 1902, where A is a solution of polymer (e.g., collodion or cellulose nitrate in ether or acetone) delivered into the high-voltage direct current (DC) electric field via tube B to form electrospun nanofibers collected on a drum F. [1] . . . . .	35
2.6	Number of article publications in the past years relevant to electrospinning. [2] . . . . .	36
2.7	Most common electrospinning apparatus. [3] . . . . .	37
2.8	a) Optical image of the Taylor's cone and tapering linear segment of a jet emanating from a microfabricated silicon tip. (b) Diagram of different geometries of Taylor's cone obtained in practice. [4] . . . . .	39

2.9	Trajectories of the jet in the whipping instability region during the electrospinning of PCL in 15 wt% acetone solution (applied voltage is 5 kV and gap distance is 14 cm). [5] . . . . .	40
3.1	Hydrolytic degradation of amide groups in the polyamide backbone. . . . .	46
3.2	TEM micrography of the supplied MWCNTs. Source: Cheap Tubes. . . . .	47
3.3	Electrospinning safety box, S1 shows the static system and S2 the dynamic system. . . . .	49
3.4	Apparatus control box. . . . .	50
4.1	TEM image of the supplied multi-walled carbon nanotubes. 60	
4.2	XPS survey spectra of the supplied MWCNTs. . . . .	60
4.3	C1s fitting of XPS survey spectra. . . . .	61
4.4	O1s fitting of XPS survey spectra. . . . .	61
4.5	The influence of applied voltage on the fiber alignment of PA6, when the target tangential speed is 3.33 m/s. (A) 20 kV, (B) 15 kV and (C) 5 kV. . . . .	62
4.6	Random PA6 (A) and aligned PA6 (B) produced networks. 63	
4.7	Random PA6/CNT (A) and aligned PA6/CNT (B) produced networks. . . . .	63
4.8	Histogram representing the random and aligned PA6 fiber diameter distribution. . . . .	64
4.9	Histogram representing the random and aligned PA6/CNT fiber diameter distribution. . . . .	65
4.10	Transmission electron micrography of PA6/CNT electrospun fiber. . . . .	65

4.11 AFM images depicting the surface topography of the (A) PA6 and (B) PA6/CNT fibers. . . . .	66
4.12 Fiber profile acquired from the AFM images, (A) PA6 and (B) PA6/CNT. . . . .	66
4.13 Partial thermogram depicting the water adsorption region.	68
4.14 First scan partial thermogram depicting the melting region.	69
4.15 Partial thermogram depicting the crystallization region. .	70
4.16 Second scan partial thermogram depicting the melting region. . . . .	71
4.17 PE/MWCNT NHSK structure produced by solution crystallization of PE on MWCNTs at 103 °C in p-xylene for 30 min. (a) SEM image of MWCNTs decorated by disc-shaped PE single crystals. (b) TEM image of the PE/MWCNT NHSK structure. (c) Schematic representation of the PE/CNT NHSK structure. PE forms lamellar single crystals on CNT surface with polymer chains parallel to the CNT axis. [6] . . . . .	72
4.18 Typical stress-strain curves of orthogonal and parallel regarding the spinning direction. . . . .	73
4.19 Protein adsorption after treatment with 0.1% SDS, where (Std.) HImark Standard, (1) TCP control, (2) Random PA6, (3) Aligned PA6, (4) Random PA6/CNT and (5) Aligned PA6/CNT. Imperial <sup>TM</sup> stain. . . . .	75
4.20 Protein adsorption after treatment with 0.1% SDS, where (Std.) HImark Standard, (1) TCP control, (2) MG63 medium and (3) inactive FBS. ProteoSilver <sup>TM</sup> stain. . .	75
4.21 Binding strength analysis of (Std.) HImark Standard, (1) TCP control, (2) Random PA6, (3) Aligned PA6, (4) Aligned PA6/CNT and (5) Random PA6/CNT. . . . .	76

4.22	Alamar Blue proliferation assay of the tested networks cultured with MG63 cell line. * $p < 0.0001$ and ** $p < 0.5$ . . .	78
4.23	Alamar Blue proliferation assay of the tested networks cultured with MRC5 cell line. * $p < 0.0001$ and ** $p < 0.5$ . . .	79
4.24	Fibroblasts surrounded by (collagen fibrils) a scaffold. . .	80
4.25	Cell viability analysis of MG63 cell culture on different surfaces for 3 days. (A) Random PA6, (B) Aligned PA6, (C) Random PA6/CNT and (D) Aligned PA6/CNT networks. . .	81
4.26	Cell viability analysis of MG63 cell culture on different surfaces for 7 days. (A) Random PA6, (B) Aligned PA6, (C) Random PA6/CNT and (D) Aligned PA6/CNT networks. . .	82
4.27	Cell viability analysis of MG63 cell culture on different surfaces for 14 days. (A) Random PA6, (B) Aligned PA6, (C) Random PA6/CNT and (D) Aligned PA6/CNT networks. . . . .	83
4.28	Cell viability analysis of MRC5 cell culture on different surfaces for 3 days. (A) Random PA6, (B) Aligned PA6, (C) Random PA6/CNT and (D) Aligned PA6/CNT networks. . . . .	84
4.29	Cell viability analysis of MRC5 cell culture on different surfaces for 7 days. (A) Random PA6, (B) Aligned PA6, (C) Random PA6/CNT and (D) Aligned PA6/CNT networks. . . . .	85
4.30	Cell viability analysis of MRC5 cell culture on different surfaces for 14 days. (A) Random PA6, (B) Aligned PA6, (C) Random PA6/CNT and (D) Aligned PA6/CNT networks. . . . .	86
4.31	SEM images of MG63 cell culture on different surfaces for 3 days. (A) Random PA6, (B) Aligned PA6, (C) Random PA6/CNT and (D) Aligned PA6/CNT networks. . . . .	87

4.32	SEM images of MG63 cell culture on different surfaces for 7 days. (A) Random PA6, (B) Aligned PA6, (C) Random PA6/CNT and (D) Aligned PA6/CNT networks. . . . .	88
4.33	SEM images of MG63 cell culture on different surfaces for 14 days. (A) Random PA6, (B) Aligned PA6, (C) Random PA6/CNT and (D) Aligned PA6/CNT networks. . . . .	89
4.34	SEM images of MRC5 cell culture on different surfaces for 3 days. (A) Random PA6, (B) Aligned PA6, (C) Random PA6/CNT and (D) Aligned PA6/CNT networks. . . . .	90
4.35	SEM images of MRC5 cell culture on different surfaces for 7 days. (A) Random PA6, (B) Aligned PA6, (C) Random PA6/CNT and (D) Aligned PA6/CNT network. . . . .	91
4.36	SEM images of MRC5 cell culture on different surfaces for 14 days. (A) Random PA6, (B) Aligned PA6, (C) Random PA6/CNT and (D) Aligned PA6/CNT networks. . . . .	92
4.37	Micrography depicting the upper cell layer alignment after 14 days of culture with MG63. Aligned (A) PA6 and (B) PA6/CNT network. . . . .	93
4.38	High magnification SEM micrography depicting the cellular ingrowth on the scaffolds surface after 14 days of culture with MG63. Aligned (A) PA6 and (B) PA6/CNT network. . . . .	93
4.39	High magnification SEM micrography illustrating the cellular ingrowth on the scaffolds surface after 14 days of culture with MRC5. (A) Aligned PA6 and (B) Random PA6/CNT network. . . . .	94
4.40	High magnification SEM micrography depicting the cellular penetration in the outer nanofibers of the aligned PA6/CNT at 3 days of culture with MRC5. . . . .	94



# List of Tables

3.1	Manufactures datasheet for the functionalized 30-50nm MWCNTs. . . . .	47
3.2	Electrospinning parameters used in the project. . . . .	48
4.1	Quantitative analysis of the C1s and O1s peaks. . . . .	61
4.2	Most adapted parameters applied for the networks production. . . . .	62
4.3	Thermal analysis results representing the pure PA6 and composite system. . . . .	67
4.4	Crystallinity percentage of the networks after 1st and 2nd scan. . . . .	68
4.5	Mechanical properties of PA6 and PA6/CNT. . . . .	73



# Nomenclature

AFM Atomic force microscopy

AM Alveolar macrophage

CLM Conocal laser microscopy

CNT Carbon nanotube

DSC Differential scanning calorimetry

FBS Fetal bovine serum

FDA Fluorescein diacetate

HFIP Hexafluoro-iso-propanol

MG63 Human osteogenic sarcoma

MRC5 Embryonic human lung

MWCNT Multi-walled carbon nanotube

NHSK Nanohybrid shish-kebab structure

PA6 Polyamide 6

PBS Phosphata buffered saline

PI Propidium iodide

PMMA Polymethyl methacrylate

RPM Revolutions per minute

SDS Sodium dodecyl sulfate

SEM Scanning electron microscopy

SWCNT Single-walled carbon nanotube

TCP Tissue culture plate

TEM Transmission electron microscopy

XPS X-Ray photoelectron spectroscopy

# Chapter 1

## INTRODUCTION AND OBJECTIVES

### 1.1 Introduction

Important work in terms of healing and reconstruction of human tissue has become a reality due to extensive research and development in the medical and engineering fields [7, 8]. Injury, disease, congenital malformation and the world's life expectancy growth enlarged the demand for replacement of human tissue and organs. Currently, there are a variety of materials and processes to regenerate and replace (with adequate fidelity) human tissue. Bone, cartilage, skin, cardiovascular prosthesis, and partial organ tissue regeneration and reconstruction are now possible and have shown promise for a large portion of individuals that have special needs because of tissue loss or organ failure [9, 10, 11, 12, 13, 14].

Tissue engineering is broad field, which applies a number of fabrication techniques to produce scaffolds to implantation. Among the techniques used for fabricating scaffold materials, electrospinning has emerged as a promising technique. During electrospinning an external electrical field is applied to a polymer melt or solution, generating elec-

trostatic forces that induce the formation of nanometric fibers. The technique has been constantly improved since its first presentation in 1902 by J. F. Cooley and W. J. Morton [4, 1, 15], particularly in the biomedical field, where it has been used for research in drug delivery, tissue scaffolding and wound care systems [16, 17, 18].

Electrospinning has been applied to process a wide range of materials due to its adaptation potential. Polymers, ceramics and composites have been produced using electrospinning for biomedical applications [19, 20, 21, 22, 23]. In particular, the technique has been used to combine the properties of two or more materials to reach the desired scaffold. In biomedical applications, composites of a polymeric matrix and ceramic fillers have been mainly used for drug delivery systems and for improving the mechanical properties of medical devices.

Ceramic fillers such as silica, alumina, calcium phosphates and carbon nanotubes have shown to significantly improve the mechanical behavior of the composite systems [24, 25, 26, 27, 28, 29]. Among the ceramic fillers widely applied in the biomedical field, special attention has been dedicated to carbon nanotubes in the past decade. Carbon nanotubes rank among the highest-modulus and strongest fibers known [30, 31] and are therefore expected to be excellent reinforcing fillers in polymeric composites. Furthermore, their structure allows several types of surface functionalities, which can be designed for optimal matrix compatibility.

In this work, carbon nanotubes were used as fillers in a polymeric matrix of polyamide 6. A slowly resorbable polymer was used to avoid the carbon nanotubes release, since their biocompatibility is still under investigation with controversial results [32, 33, 34]. The purpose of this research was to produce a system with tunable morphological and mechanical properties, easy of production and that could guide the biological response. This thesis presents the production and physical and biological characterization of random and aligned PA6 and PA6/MWCNT networks

for biomedical applications.

## 1.2 Objectives

The aim of this work is to develop and characterize a novel nano- and micro-structured composite system made of biocompatible polymeric matrix with aligned domains of carbon nanotubes for biomedical applications.

### 1.2.1 Specific Objectives

- Develop a novel composite system with tuneable morphology and mechanical properties.
- Align carbon nanotubes along with the polymeric matrix.
- Analyze the physical modifications on the polymeric matrix when CNTs are added.
- Investigate the variation of protein adsorption caused by the CNTs addition.
- Evaluate the biological response, in terms of proliferation, viability and morphology, when CNTs are added to the system.



# Chapter 2

## STATE OF THE ART

### 2.1 Tissue Engineering

Several authors have defined tissue engineering differently in the past years [8, 35]. However, the most used definition in the scientific world was given by Langer et al., which defined Tissue Engineering as “an interdisciplinary field that applies the principles of engineering and life sciences toward the development of biological substitutes that restore, maintain, or improve tissue function” [8]. In figure 2.1 the typical approach used in tissue engineering is presented.

Injury, disease, and congenital malformation have always been part of the human experience. As the world population life expectancy increases, the demand for replacement of human tissue and organs increases. Important developments in the multidisciplinary field of tissue engineering have permitted a novel set of tissue replacement parts and implementation strategies [36, 37, 38]. Advances in biomaterials, stem cells, growth and differentiation factors, and biomimetic environments have created unique opportunities to fabricate tissues in the laboratory from the combination of scaffolds (artificial extracellular matrices), cells, and biologically active molecules.

Among the major challenges now facing tissue engineering is the need for more complex functionality, as well as both functional and biomechanical stability in tissues destined for transplantation. The structure and properties of the artificial scaffolds are critical to guarantee normal cell behaviour and performance of the cultivated tissue.

Scientists have developed numerous tissue replacement materials in the past decades. Diverse tissues have been reproduced in laboratory [16, 39, 40, 41]. Biodegradable and biostable polymers [42, 43], either natural or synthetic, ceramic materials [44, 9], either natural or synthetic, and composites [45, 46, 47] have been processed into scaffolds for tissue engineering.

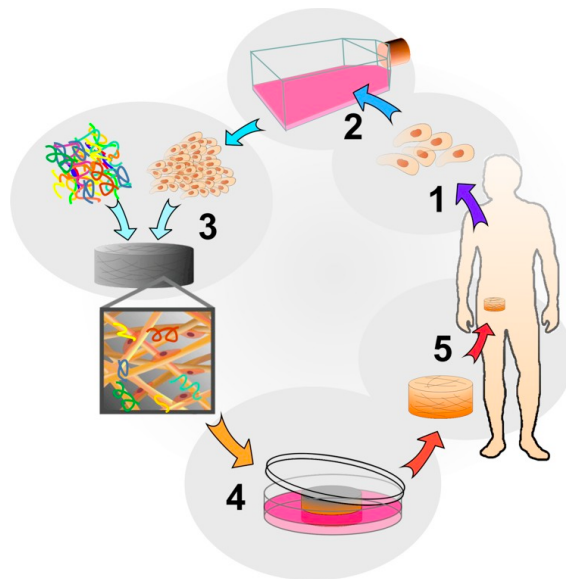


Figure 2.1: Tissue Engineering approach representation. (<http://biomed.brown.edu>).

## 2.2 Scaffolds in Tissue Engineering

Tissue engineering aims to produce three-dimensional (3D) scaffolds that can mimic the biologic and mechanical function of natural extracellular matrix (ECM). Scaffolds provide a 3D substrate for cells to form new tissues with appropriate structure and function. Furthermore, scaffolds can allow the delivery of cells and appropriate bioactive factors (such as cell adhesion peptides and growth factors) to specific locations in the body with high efficiency [48]. Scaffolds are also supposed to provide mechanical support against in vivo forces to maintain the predefined 3D structure during tissue development.

To support the replacement of normal tissue without inflammation, the implanted material should be biodegradable and bioresorbable. Incompatible materials are destined for inflammatory or foreign-body response that eventually leads to rejection and/or necrosis [49, 50]. Degradation products, if produced, should be removed from the body via metabolic pathways at an adequate rate that keeps the concentration of these degradation products in the tissues at a tolerable level [51]. The scaffold should also provide an environment in which appropriate regulation of cell behavior (adhesion, proliferation, migration, and differentiation) can occur so that functional tissue can form.

## 2.3 Polymers in Tissue Engineering

Polymer is a high molar mass molecule, which is composed by number of repeating units called monomers. They are a large class of natural and synthetic materials with a wide variety of properties. Polymers occur in nature and can be found in living species, such as proteins, collagen, and DNA. Synthetic polymers consist of a large group of materials that have become of common use in our life.

Tissue engineering applies the knowledge in polymers technology (production and properties) to develop new biomaterials where ideal properties and functional customization such as injectability, synthetic manufacture, biocompatibility, nano-scale fibers, low concentration, resorption rates can be engineered. To achieve the goal of tissue reconstruction, scaffolds must meet some specific requirements. High porosity and adequate pore size are required to facilitate cell migration and diffusion throughout the whole structure of both cells and nutrients. Biodegradability is often an essential factor. Tissue engineering scaffolds should preferably be absorbed by the surrounding tissues. The rate at which degradation occurs has to coincide as much as possible with the rate of tissue formation.

### 2.3.1 Natural polymers

Natural polymers can be classified as proteins (silk, collagen, gelatin, fibrinogen, elastin, keratin, actin and myosin), polysaccharides (cellulose, amylose, dextran, chitin and glycosaminoglycans) or polynucleotides (DNA, RNA) [52]. The macromolecular similarities of natural polymers with natural tissues generally increase biocompatibility and reduce immunologic responses. This further leads to the avoidance of issues related to toxicity and stimulation of a chronic inflammatory reaction, as well as lack of recognition by cells, which are frequently provoked by many synthetic polymers.

Natural polymers are known to degrade by the effect of naturally occurring enzymes and the possibility to control the degradation rate by chemical cross-linking or other chemical modifications. In comparison to synthetic polymers, this class is frequently known have inadequate mechanical properties for load-bearing applications [52]. Their complex structure difficult the identification of the most suitable manufacturing techniques (compression molding, extrusion) to process them [53]. In addition, the properties of natural polymers are not predictable neither

reproducible.

Scaffolds from natural polymers have been intensively studied in the past years. Collagen [39, 54], gelatin [55, 56] and silk fibroin [57, 42] are some of the polymers studied for tissue engineering applications.

### 2.3.2 Synthetic polymers

Synthetic polymers are chemically synthesized polymers and represent the largest group of materials applied in tissue engineering. The predictable and reproducible mechanical and physical properties such as tensile strength, elastic modulus and degradation rate [58] are some of the factors that led to the increase number of applications in tissue engineering. Nevertheless, this class of polymers has a higher risk of toxicity, immunologic response and infection than natural polymers due to their more complex structures and process techniques.

Some synthetic polymers are hydrolytically unstable and degrade in the body while others may remain essentially unchanged for the lifetime of the patient. Biodegradable polymers have been applied in tissue engineering to repair nerves, skin, vascular system and bone. Typical biodegradable polymers used for biomedical purposes are hydrophobic polyester, such as polyglycolide (PGA) [55, 43], and polylactide (PLA) [59, 60], polyurethanes (PUs) [61, 62] and polyamides (PAs) [63, 64].

## 2.4 Composites in Tissue Engineering

Composite materials can be defined as a material composed of two or more chemically and physically distinct phases (metallic, ceramic or polymeric), which are separated by an interface. This class of materials has been applied for many years in structural engineered parts due to its excellent mechanical properties [65, 66]. Composites are usually classified based on its matrix (metals, ceramics or polymers) or reinforcement (particulates, short or continuous fibers, nanofillers) components [65].

Taking advantage of this well known technology, researchers have been applying composite materials in tissue engineering to enhance mechanical properties and cell function, and deliver special molecules [67, 28, 68].

Composites as well as any implanted material applied in tissue engineering must exhibit specific mechanical properties related to the tissue that will be repaired or replaced. Furthermore, the materials must retain their properties when implanted in vivo so that they can provide the necessary support for cell attachment and proliferation.

In tissue engineering, biocompatible polymers have been mostly applied as matrix for composite materials along with ceramic fillers [69, 70, 71]. Generally, polymers are known to be flexible and exhibit a lack of mechanical strength and stiffness, however they are simple to mold and can easily form complex structures. While ceramics are stiff and brittle. Composites aim to combine the properties of both materials to enhance tissue reconstruction.

## 2.5 Surface Features

One of the most important ambitions of the biomedical field is to understand how individual cells communicate and interact between themselves and the physical and chemical environment in which they reside. Recently, there have been improvements and developments of new technologies that have allowed scientists to observe and manipulate the environment around cells at the micron and nanoscale, which permits investigation of how the surrounding environment impacts cellular functions. In the microenvironment, cells are able to interact at the micro to the nano scale (e.g. cells can range from 10 to 100 microns in diameter, while proteins are down to the nanometer size).

Advances in fabrication processes at the micro- and nano-metric levels in the last decade have allowed bioengineers to produce novel patterned biomaterials, which are able to guide cell functions and organization.

Since the morphology of a tissue plays an important role on the remodeling process, novel engineered devices/scaffolds target to mimic the natural tissues to enhance biocompatibility and reduce unexpected immunological responses. It has been reported that the topographic patterning can be used to control cell functions such as proliferation, organization, migration and differentiation [36, 72, 73, 74].

### 2.5.1 Micro patterning

Microscale topographic features have been shown to regulate many aspects of cell functions.

Huang *et al.* [72] demonstrated that while myoblasts tend to differentiate and orient randomly when cultured in vitro, when cultured on patterned membranes with 10 micron wide grooves spaced 10 microns apart they differentiate into organized, parallel myotubes with decreased proliferation and increased myotube length compared to the myoblasts on unpatterned surfaces.

Nanofibers are nano/submicrometric fibers composed of natural and/or synthetic polymers that can be patterned into various orientations and shapes to influence cell and tissue behavior. Oriented nanofibers influence cells similarly to matrix micropatterning or micro topographical patterning. Patel *et al.* [74] reported that aligned electrospun fibers significantly induced neurite outgrowth and enhanced skin cell migration during wound healing compared to randomly oriented nanofibers.

### 2.5.2 Nano patterning

Several authors have published in vitro and in vivo experiments showing that nanostructured materials, which mimic the nanometer topography of the native tissues, improve biocompatible responses, and result in better tissue integration in medical implants [75, 76, 77]. Nevertheless, there is still lacks on the comprehension of how cells sense these features.

Dalby *et al.* [76] showed that endothelial cells develop a distinct and

arcuate morphology when cultured on poly(4-bromostyrene) with islands of 13 nm high. They also demonstrated that cells respond better to 13 nm islands than 35 or 95 nm.

Popat et al. [77] demonstrated that marrow stromal cells showed higher adhesion, proliferation, ALP activity and bone matrix deposition when cultured on nano tubular titania in comparison with a flat titania surface.

## 2.6 Carbon Nanotubes

Carbon nanotubes (CNTs) are an example of a carbon-based nanomaterial, which since its discovered by Sumio Iijima in 1991 [78], have emerged as one of the most intensively investigated nanomaterial. The physicochemical properties that are highly desirable for the use in the commercial, environmental, and medical sectors are the reasons why CNTs have been intensively investigated. Essentially, there are two forms of CNTs: single-walled (SWCNT) and multi-walled (MWCNT). The molecular structure of single-wall and multi-wall carbon nanotubes can be visualized as a rolled-up graphene sheets, as present in figure 2.2. The CNTs structure is based on the orientation of the tube axis with respect to the hexagonal lattice and can be completely specified by its chiral vector  $\vec{C}_h$ , which is denoted by the chiral indices (n, m), as presented in equation 2.1.

$$\vec{C}_h = n\vec{a}_1 + m\vec{a}_2 \quad (2.1)$$

where, integers (n, m) are the number of steps along the zig-zag carbon bonds of the hexagonal lattice, with  $\vec{a}_1$  and  $\vec{a}_2$  the unit vectors.

The bonding in carbon nanotubes is essentially  $sp^2$ , similar to the bonding in graphite. The outstanding mechanical, electrical, thermal and chemical properties of CNTs have been related to its molecular structure since the curvature of CNT induces a quantum confinement and a  $\sigma - \pi$

rehybridization [79, 80].

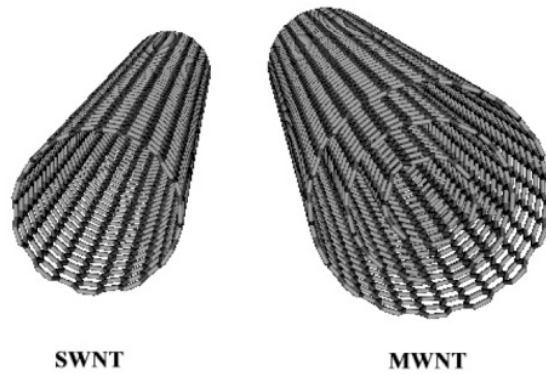


Figure 2.2: Molecular structures of a single-walled carbon nanotube (SWCNT) and of a multi-walled carbon nanotube (MWCNT). (<http://www-ibmc.u-strasbg.fr/>).

### 2.6.1 Single-walled carbon nanotubes

Single-walled carbon nanotubes (SWCNTs) consist of a single rolled-up graphene sheet with diameters ranging from 0.4 to 3 nm, while their length can vary according to the synthesis process (up to 300  $\mu\text{m}$ ). SWCNTs may be either metallic or semiconducting, depending on their chiral vector [81, 82, 83]. A TEM image of a SWCNT is presented in figure 2.3.

SWCNT exhibit excellent electric properties that are not shared by the MWCNT, which candidate them for miniaturizing electronics beyond the micro electromechanical scale currently used in electronics. Tissue engineering also employ the particular properties of SWCNTs in pharmacological drug delivery, optical labeling, contrast agents, among others. Nevertheless, a negative affect of SWCNTs is the impossibility to be efficiently functionalized. The functionalization process breaks down the

C=C double bond, which introduce discontinuities in the structure of the tube, therefore modifying its intrinsic properties.

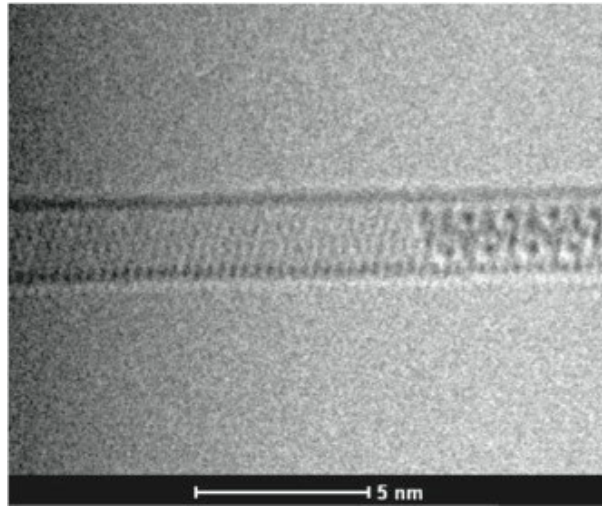


Figure 2.3: TEM image of a single-walled carbon nanotube. (<http://www.electroiq.com>).

### 2.6.2 Multi-walled carbon nanotubes

Multi-walled nanotubes (MWCNTs) consist of multiple rolled up graphene sheets (concentric tubes) distanced by 0.34 nm. The diameter of a MWCNT can vary according to the fabrication parameters, reaching up to 200 nm. MWCNTs exhibit excellent mechanical properties and is the most utilized for composite applications due to the loading transfer capability. A TEM micrography of a multi-walled carbon nanotube can be observed in figure 2.4.

A particular kind of multi walled nanotube is the double-walled carbon nanotube (DWCNT), which presents similar morphology and properties to SWCNT but can be effectively functionalized with other chemicals in order to add new properties, once the functionalization occurs in the

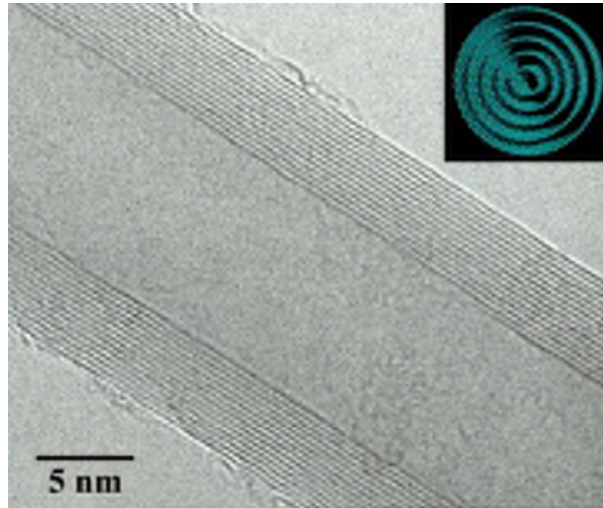


Figure 2.4: TEM image of a multi-walled carbon nanotube. (<http://endomoribu.shinshu-u.ac.jp/>).

outer tube, maintaining the inner tube intact.

### 2.6.3 Production technique

Carbon nanotubes can be produced by different kinds of techniques. The most applied and established synthesis methods are Chemical vapor deposition, arc-discharge and laser ablation. A brief description of these techniques is given below.

#### 2.6.3.1 Chemical Vapor Deposition (CVD)

The CVD process involves the decomposition of hydrocarbons (methane, acetylene, ethylene, etc.) on catalyst particles (e.g. Co, Ni, Fe), which are deposited on the substrate [80]. Usually, the hydrocarbons are decomposed in a tube reactor at temperatures ranging from 550 to 750 °C. The synthesis of CNTs is often plasma enhanced (PECVD). Depending on the growth conditions (catalyst material, gas, temperature, flow-rate, and synthesis time), MWCNTs range from 10-400 nm in diameter and

0.1-50  $\mu\text{m}$  in length [80].

### 2.6.3.2 Arc-Discharge

This process apply a direct current (DC) in two carbon electrodes which generate an arc. The electrodes are kept under an inert gas atmosphere (Ar, He), which increases the speed of carbon deposition. The arc-discharge method produces high-quality SWCNTs and MWCNTs. Nevertheless, the presence of a catalyst is necessary to grow SWCNTs. A subsequent separation of CNTs from the substrate and metal particles is necessary and causes impurities in the final product. The major contaminants are amorphous carbon, fullerenes, catalysts and graphite particles. The CNTs produced by arc-discharge are highly crystalline.

### 2.6.3.3 Laser ablation

The laser ablation method, a pulsed or continuous laser is applied to vaporize a target consisting of a mixture of graphite and metal catalysts (e.g. Co, Ni). The system is kept in inert atmosphere, usually helium or argon gas. The laser-produced MWCNTs are relatively short (300 nm) with the inner diameter in the range of 1.5-3.5 nm, where the SWCNTs have length from 5-20  $\mu\text{m}$ , and diameter between 1-0.4 nm [80].

## 2.6.4 Properties

### 2.6.4.1 Mechanical properties

The extraordinary mechanical properties of carbon nanotubes arise from  $\sigma$  bonds between the carbon atoms. Experimental measurements together with theoretical calculations show that nanotubes exhibit the highest Young's modulus (elastic modulus E) and tensile strength among known materials. Krishnan *et al.* [30] reported the experimental value of the elastic modulus of single-walled CNTs that can arrive up to 2.4

TPa. Yu *et al.* [31] published an study where they applied an AFM to measure the ultimate strength of MWCNTs, which ranged from 20 to 63 GPa. These values surpasses any well-known materials for their high tensile strength, such as steel and synthetic fibers.

The exceptional mechanical properties of CNTs increased the interest for the application of nanotubes where high tensile strength, extraordinary flexibility and lightweight materials are requested, such as tissue engineering.

#### 2.6.4.2 Electrical properties

The nanometer dimensions of the carbon nanotubes together with the unique electronic structure of a graphene sheet make the electronic properties of these structures highly unusual. The electric properties of carbon nanotubes have being on of the most studied properties of the CNTs due to the possible applications on the electronic industry. CNTs present a high symmetry and extremely small size, which allow outstanding quantum effects and electronic, magnetic, and lattice properties. Studies have confirmed several important electronic properties of the nanotubes such as the quantum wire effect of SWCNT, SWCNT bundle, and MWCNT as well as the metallic and semi-conducting characteristics of a SWCNT [84, 82, 85].

#### 2.6.4.3 Optical properties

Defect-free nanotubes, especially SWCNTs, offer direct band gap and well-defined band and sub-band structure, which is ideal for optical and optoelectronic applications. Literature works refer specifically to the absorption, photoluminescence and Raman spectroscopy when the optical properties of CNTs are discussed, especially because these properties allow quick and reliable characterization of the nanotube quality in terms of non-tubular carbon content, structure (chirality) of the produced nan-

otubes, and structural defects.

The optical spectra have been established for individual SWCNTs and ropes using resonant Raman, fluorescence [86], and ultraviolet to the near infrared (UV-VIS-NIR) spectroscopies [87]. In addition, electrically induced optical emission [88] and photoconductivity [89] have been studied for individual SWCNTs.

### 2.6.5 Carbon nanotubes in tissue engineering

Carbon nanotubes has emerged as a promising nanomaterial, which has great potential for multiple uses in tissue engineering. The rise in interest for CNTs stems from their unique structure that can be tailored to closely mimic the nano-scale of native biological structures (i.e. collagen), while also displaying interesting electrical and mechanical properties besides the fact of their low density. Recently, several studies have been published on the application of CNTs in the biomedical field, with numerous authors having applied CNTs in neuronal regeneration [90, 91, 92] and cartilage tissue engineering [93]. However, bone tissue regeneration has shown to be the most interesting field for the application of this class of nanomaterial [94, 95, 96, 97].

Special attention has been given to understand the interactions between CNTs and cells [90, 98, 99, 100, 101, 102]. Zanello *et al.* [101] examined the proliferation and function of osteoblast cells seeded onto five differently functionalized carbon nanotubes. This work demonstrated that bone cells prefer electrically neutral CNTs, which sustained osteoblast growth and bone-forming functions. Webster *et al.* [38] investigated the adhesion properties of osteoblasts, fibroblasts, neurons, and astrocytes on polycarbonate urethane/carbon nanofiber/nanotube composites. The experiments revealed that cell functions of the neural and osteoblast cells increased, while glial scar tissue formation (astrocytes) and fibrous tissue encapsulation (fibroblast) decreased.

Carbon nanotubes have also been previously used to enhance the

electrical conductivity and mechanical properties of polymeric matrixes in order to provide controlled electrical stimulation to cells and increase the mechanical support for tissues. Supronowicz *et al.* [68] demonstrated that when osteoblasts were cultured under an alternating current on a CNT-doped poly lactic acid there was an enhancement on the proliferation by 46%, and an increase in calcium deposition by 307%. Schmidt *et al.* [41] reported a significant increase in neurite outgrowth and spreading of P12 cell line when cultured in a oxidized polypyrrole substrate under electrical stimulation if compared to the substrate without stimulation. Furthermore, carbon nanotube-reinforced chitosan matrix has been studied and reported by Wang *et al.* [103], which reported that the addition of 0.8 wt% of CNTs into the chitosan matrix improved the mechanical behaviour of the composites by 93% and 99% for the elastic modulus and tensile strength, respectively. In addition, Ruan *et al.* [70] showed an enhancement of 140% on ductility and 25% on tensile strength of composites based on 1 wt% of carbon nanotube-reinforced ultrahigh molecular weight polyethylene.

#### 2.6.5.1 Carbon nanotubes biocompatibility

The main topic of this research is the use of carbon nanotubes in a polymeric matrix, which is known to be resorbable in a period of time, for biomedical application. Thus, the research would not be complete without review the CNTs toxicity. Historically, the first toxicity evaluations of CNT were carried out in 2004 by Lam *et al.* [104] and Warheit *et al.* [32], in which they demonstrated the pulmonary toxicological effect of single-wall carbon nanotubes in mices. Since these works, there has been an increase in interest of carbon nanostructures in the biomedical field, and as a result, a number of studies and publications have been dedicated to this topic. However, amid the large resource of publications on this topic results are still controversial [104, 32, 33, 105, 106, 107, 108]. Jia *et al.* [105] showed that when SWCNTs and MWCNTs were incu-

bated with alveolar macrophages (AM), significant increase ( $\sim 35\%$ ) in cytotoxicity was observed after 6 h of exposure. They also presented the dose dependency of CNTs, where SWCNTs appear to significantly impair phagocytosis of AM at low doses ( $0.38 \text{ mg/cm}^2$ ). On the contrary, when MWCNTs were used at high dosage ( $3 \text{ mg/cm}^2$ ) necrosis and degeneration was observed. Manna *et al.* [107] studied SWCNT in contact with human keratinocyte cells, and observed an increase in oxidative stress and the inhibition of cell proliferation of the keratinocytes when in contact with nanotubes. However, Cherukuri *et al.* [33] studied the detection of SWCNTs when uptaken by macrophage cells and observed that the cells can actively ingest significant quantities of nanotubes ( $3.8 \text{ }\mu\text{g/ml}$ ) without showing toxic effects. Leeuw *et al.* [106] studied *Drosophila* larvae when fed with food containing  $\sim 10$  ppm of disaggregated SWCNTs and found no short-term toxicity or impaired growth or viability of the *Drosophila* larvae.

Recently, Ren *et al.* [34] addressed in a review that CNTs might not be as toxic as previous published. They raised the fact that no uniform criterion for these analyses is found in the literature (e.g. amount of impurities, tested cell line, different culture medium and nutrients, different ratio between medium and nanotubes) and this might contribute to some of the controversial results.

However, from the detailed analyses of the literature, we observed that the cytotoxicity of carbon nanotubes is mostly related to the CNTs high concentration and amount of impurities. Nevertheless, several authors are still studying the interaction between CNT and the biological environmental.

## 2.7 Electrospinning Technique

The electrospinning technique was first reported and patented by J. F. Cooley in 1902, where he presented a method to produce yarns through

the application of a high voltage power. The US patent (#692631) was entitled “Apparatus for electrically dispersing fibres” [1]. Cooley acknowledged the principles that form fibers instead droplets such as fluid viscosity, volatility of the solvent and the balance between electrical field and surface tension of the solution. In his first scheme of the electrospinning apparatus, shown in figure 2.5, he presented the deposition of a viscous polymer solution on a positively charged electrode (brass sphere) placed close to an electrode of opposite charge to obtain the electrospun fibers. The theory was described as the result of “electrical disruption of the fluid.”

Further contribution were made by G. I. Taylor in the 1960s to the fundamental understanding of the behavior of droplets under an electrical field [15]. Taylor mathematically modeled the shape of the cone formed by the solution droplet, which has become known as Taylor cone.

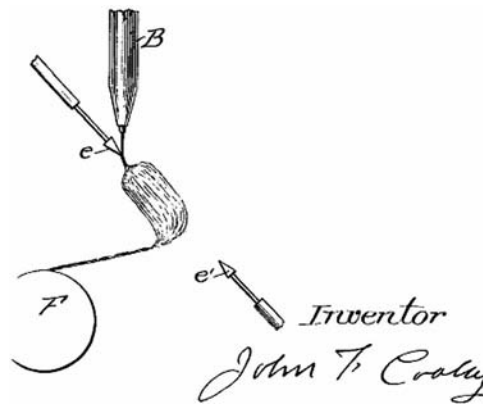


Figure 2.5: Electrospinning diagram drawn by Cooley in 1902, where A is a solution of polymer (e.g., collodion or cellulose nitrate in ether or acetone) delivered into the high-voltage direct current (DC) electric field via tube B to form electrospun nanofibers collected on a drum F. [1]

Doshi and Reneker re-discovered the electrospinning as a potential source of nano-structured materials in 1995, which during studies of elec-

trospinning it was observed that fibers could be easily formed with diameters on the nanometer scale [109]. Huang observed that between 1995 and 2000 fewer than 10 journal papers on the electrospinning topic were published annually; however since the 2000's this number has been exponentially growing to reach over 800 papers published in 2007 (figure 2.6), which reflects the growing in interest in the technique [110]. Since 1995 there have been further theoretical developments of the driving mechanisms of the process. Work on the shape of the Taylor cone, the ejection of a fluid jet [111] and the description of the bending (whipping) instability behavior [112] have been carried out. Further studies on the geometry of the applied electric field in order to control the nonlinear whipping instability have been attempted [113, 112, 114].

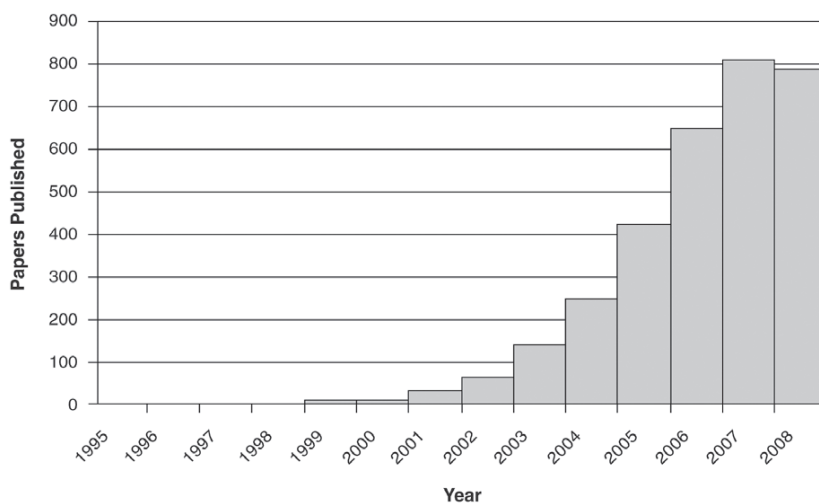


Figure 2.6: Number of article publications in the past years relevant to electrospinning. [2]

Currently, the electrospinning apparatus has not change significantly from the firsts schemes, as can be seen in figure 2.7. In laboratories equipments most of the basic hardware components remain the same. However, the greatest improvement is related to the availability of more

stable power supply and continuous pumps to regulate the delivery of polymer solution to the charged electrodes that allows better nanofiber quality. Nowadays, electrospinning is considered the most cheap and simple technique to produce structured polymer fibers with diameters in the range from few micrometers down to the nanometer size, which are of substantial interest for various kinds of applications.

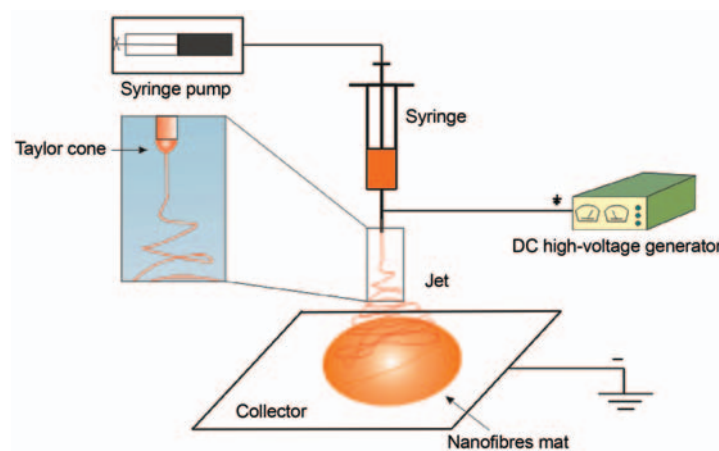


Figure 2.7: Most common electrospinning apparatus. [3]

## 2.7.1 Electrospinning theory

### 2.7.1.1 Droplet generation

In the electrospinning process the charging of a polymer solution droplet is the initial step. Usually, a polymer solution is pumped at a low flow rate into a capillary tip. In the absence of an applied electric field, the surface tension of the liquid, and the gravitational force, are the only two forces acting on the meniscus of the droplet. Due to the electric field, charge separation will take place in a droplet that is electrically conductive. Where the capillary is positively charged, for instance, the positively charged species migrate to the surface of the droplet and

the negatively charged species accumulate in its interior until the electric field within the liquid droplet is zero. Charge separation will generate a force that is countered by the surface tension within the droplet [2, 3]. The velocity at which these ionic species move through the liquid is determined by the magnitude of the electric field and the ionic mobility of the species.

### 2.7.1.2 Taylor's cone formation

The deformation of relatively small charged droplets under an electric field, from a sphere to an ellipsoid, has been studied for years (Macky 1931). The effect diminishes as  $r$  increases, because the electric field just outside the droplet varies inversely with  $r^2$  [15]. For droplets of water, such deformation has been observed at fields exceeding 5000V/cm. The elongated droplet assumes a cone-like shape and a narrow jet of liquid is ejected from the capillary [15], as seen in figure 2.8. The Taylor's cone is formed at the critical voltage,  $V_C$ , applied to a droplet at the end of a capillary of length  $h$  and radius  $R$  [15] as presented in equation 2.2.

$$V_C^2 = (2 \cdot L/h)^2 \cdot (\ln(2 \cdot h/R) - 1.5) \cdot (0.117 \cdot \pi \cdot R \cdot T) \quad (2.2)$$

Observing the process in a range of different liquids, Taylor determined the equilibrium between surface tension and electrostatic forces to be achieved when the half angle of the cone was 49.38°. This value can, however, be different for different polymer solutions and melts.

### 2.7.1.3 Launching of the jet

The coulombic repulsion present in the droplet are usually not sufficient to launch the polymer jet due to the abundant entanglement of polymer chains in concentrated solution. Nevertheless, the surface area has to be increased to accommodate the charge accumulation on the jet surface, and this occurs through the formation of fibers. A slim fibril

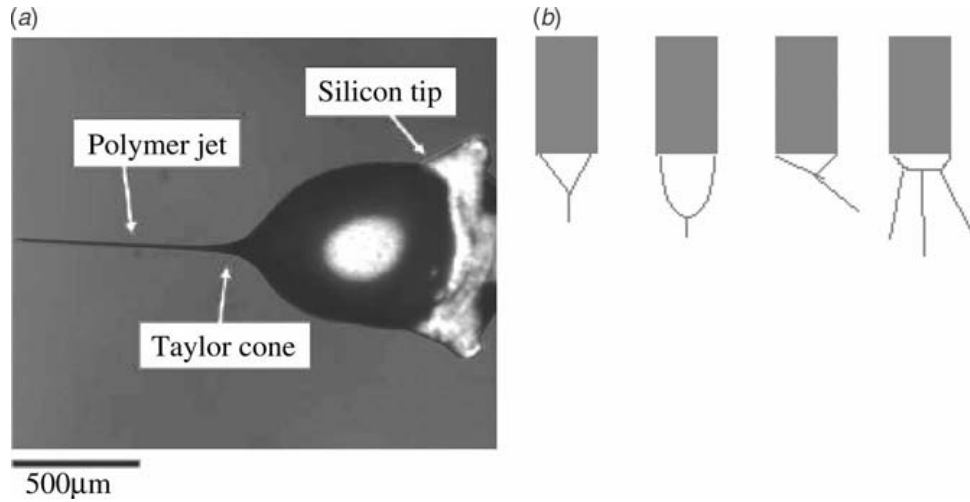


Figure 2.8: a) Optical image of the Taylor's cone and tapering linear segment of a jet emanating from a microfabricated silicon tip. (b) Diagram of different geometries of Taylor's cone obtained in practice. [4]

emanates from the cone to create additional surface area needed to accommodate surface charges, and it initially travels directly towards the grounded collector.

#### 2.7.1.4 Elongation of straight segment

The jet initiation occurs almost immediately after the applied voltage exceeds the critical voltage to the polymer solution. The coulombic repulsion of surface charges on the jet has an axial component that elongates the jet in its passage towards the collector [4]. Studies revealed that the velocity of the jet as well as the variance in jet velocity increase with distance from the Taylor's cone [115]. As a result, the jet diameter decreases rapidly due to both extension and evaporation of the solvent. The initially straight jet reduces in diameter as it accelerates towards the collector, and the tapering is pronounced in the region below the Taylor's cone.

### 2.7.1.5 Whipping instability region

The originally straight jet segment regularly becomes unstable and displays bending, undulating movements during its passage towards the collector. The type of instability obtained is dependent on the electric field, with stronger fields favouring whipping instability.

High-speed imaging studies concluded that the jet undergoes into a series of loops of increasing diameter, spiralling down towards the collector [116]. The unstable cone-shaped jet is created by the rapid symmetric movement of a single jet, as presented in figure 2.9.

Reneker's images of larger loops closer to the collector show higher order bending instability where the jet being looped forms right- and left-handed coils [116]. Both the rate of increase in surface area during whipping instability and the solvent evaporation rate are high in this regime, further reducing the jet diameter.

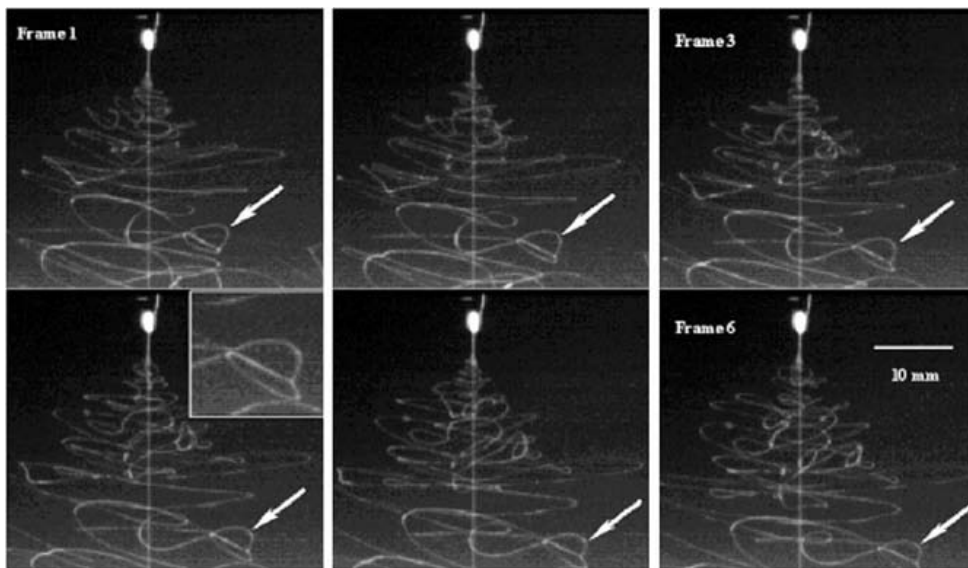


Figure 2.9: Trajectories of the jet in the whipping instability region during the electrospinning of PCL in 15 wt% acetone solution (applied voltage is 5 kV and gap distance is 14 cm). [5]

### 2.7.1.6 Solidification into nanofiber

The duration available to the jet undergo whipping instability is also governed by the rate of evaporation of the solvent. With a solvent of high vapor pressure, the elongational viscosity of the jet may reach levels too high to achieve any further deformation quite early in the whipping instability stage, yielding thick nanofibers. Solvent volatility is therefore a key consideration in controlling fiber diameter. With appropriate selection of solvents and process parameters, extremely fine nanofibers can be electrospun [117].

The nanofibers obtained under the best electrospinning conditions are generally of circular cross-section, continuous, and bead free. However, the literature on electrospinning reports other geometries of nanofibers [118, 5, 119].

## 2.7.2 Main parameters that influence fiber morphology

### 2.7.2.1 Electrical field

In electrospinning the liquid jet travels across the gap distance from the highly charged tip to the grounded collector plate. The presence of a surface charge is responsible for the acceleration of the initial jet towards the grounded collector. Logically, the charge density will be particularly sensitive to the solvent used. Either nanofiber diameters will suffer changes with the solvent composition.

The density of surface charges is affected by the applied voltage. Therefore, the fiber stages presented previously are affected. Instability and stretching of the jet increases with the applied voltage, consequently, the fiber diameter is reduced. The importance of the electrical field in determining nanofiber morphology has been extensively reported [120, 110, 121].

### 2.7.2.2 Polymer concentration

The concentration of polymer in solution often determines if it will electrospin and generally has a dominant effect on the fiber diameter as well as fiber morphology. The concentration governs the adequate chain entanglement, which control the fiber uniformity and morphology. Higher concentrations generally yield nanofibers of larger average diameter but the quantitative relationship between the solution concentration and fiber diameter appears to be variable [4, 2, 122].

Viscosity is usually identified as the dominant variable that determines fiber diameter [123]. The minimum viscosity needed varies with the molecular weight of the polymer as well as the nature of the solvent used. Nevertheless, solution viscosity is primarily adjusted by changing polymer concentration, varying the solvent composition at a constant concentration of polymer can also be used for the purpose.

### 2.7.2.3 Flow rate

The rate at which the polymer solution is pumped into the tip can be defined flow rate. Preferably, the feed rate must match the rate of removal of solution from the tip to produce continuous nanofibers of uniform diameter.

At lower feed rates electrospinning may only be intermittent with the Taylor's cone being unstable, but at higher feed rates larger fiber diameters and beads often result. Increasing the feed rate under conditions where the applied potential is not a limiting factor results in a higher average fiber diameter [124]. The importance of the flow rate in determining nanofiber morphology has been extensively reported [54, 125].

### 2.7.2.4 Working distance

The working distance is distance between the tip of the needle and the target and it is directly correlated to the whipping instability and solidification stages. The most affected are the whipping instability stage

where the fibers have their most elongation, and the solidification stage where the solvent evaporates along the instability stage and the fiber is able to stretch and solidify. When the working distance is reduced the whipping and solidification stages are shortened, which affect the space that fibers have to elongate and dry. Mainly, the result are thicker and “wet” fibers. On the other hand, when the distance is excessive mainly broken fibers are produced as result of the fast evaporation of the solvent and the harder fibers at the whipping stage.

### 2.7.3 Electrospinning for biomedical applications

The application of electrospun fibers for biomedical applications has raised particular interest in the past few years. Fiber dimension, tailorable surface chemistry, high porosity and large surface area are some of the properties that made electrospinning appealing for scaffolds for tissue engineering [120, 126, 127, 121], diagnosis [128, 129], artificial blood vessels [16, 130] and controlled drug delivery [21, 55, 38, 131]. Among the biomedical research fields there have being a specific attention on two particular areas, which are focused on nanofiber-based three-dimensional scaffolds for tissue engineering and the design of nanofiber devices for drug delivery.

Human cells can attach and organize well around fibers with diameters smaller than those of the cells [132], especially because most of the human tissues and organs are organized in nanofibrous forms or structures. A great amount of research has been dedicated to the production of electrospun tissue scaffolds. In this regard, nanoscale electrospun scaffolds can provide an optimal template for cells to seed, migrate, and grow. Electrospinning appears as a technique that allows the production of reproducible and biocompatible three-dimensional scaffolds for cell ingrowth. Furthermore, a successful regeneration of biological tissues and organs calls for the development of structures that are beneficial for cell deposition and cell proliferation. However, electrospinning typi-

cally is used to produce thin two-dimensional (2D) layers. While three-dimensional (3D) nanofibrous scaffolds have been fabricated by layering these 2D networks [133].

Delivery of drug/pharmaceuticals to patients has always been an important concern in medicine. Particular attention has been given to new technologies in order to better control the drugs release profile, absorbance, distribution as well as the patient convenience and compliance. Electrospinning has been introduced as a significant technique that can produce polymer nanofibers to drug delivery purposes. The principle is based on the increase of the dissolution rate of a particular drug by the increase of the carrier surface area. In fact, several authors have been studying the delivery kinetics of pharmaceuticals when entrapped in electrospun nanofibers [134, 135].

# Chapter 3

## MATERIALS AND METHODS

### 3.1 Polyamide 6 - PA6

Polyamide 6, also called Nylon 6 or  $\epsilon$ -caprolactam, is a semi-crystalline thermoplastic polymer widely used for many applications, such as clothing, the automobile industry and recently in the biomedical field. It is known to exhibit good mechanical and insulating properties, as well as biocompatibility [136, 12]. The polyamide mechanical properties are controlled by its semi-crystalline structure, where the amorphous regions contribute to the elasticity while the crystalline regions contribute to its strength and rigidity. The regularity and symmetry of its backbone make the polyamide a highly crystalline polymer, which makes it suitable for fiber production. However, the amount of crystallinity depends on the synthesis details as well as on the kind of polyamide. The crystalline regions present two distinct forms: the monoclinic alpha phase, which is thermodynamically more stable, and the pseudo-hexagonal gamma phase [137].

Polyamides are hygroscopic and susceptible to hydrolysis as shown in figure 3.1. The water molecule attacks the amorphous regions of the polymer and reduces its molecular weight. The consequence of this event

is the reduction of the mechanical properties. An advantage of highly crystalline polymers is that they are less susceptible to hydrolytic degradation.

In the biomedical field, polyamide has shown to possess good biocompatibility with various human cells and tissues [138, 63, 64]. Specifically, the strong hydrogen bonds between the amide groups allow scientists to explore the chemical interaction with other structures [139].

The polyamide 6 used in this work was supplied by Aquafill, Italy.

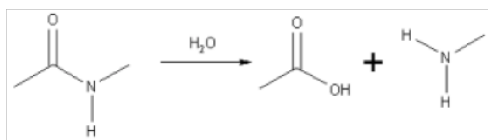


Figure 3.1: Hydrolytic degradation of amide groups in the polyamide backbone.

## 3.2 Functionalized Multi-Walled Carbon Nanotubes

The functionalized multi-walled carbon nanotubes used in this work was supplied by Cheap Tubes, USA. The TEM micrograph and its datasheet for MWCNT is presented in figure 3.2 and table 3.1. The selection of functionalized MWCNTs is related to the mechanical properties of load transfer [140, 141] and the possibility of chemical interaction with the polymeric matrix [139].

## 3.3 Fabrication Technique

Electrospinning has been well documented for the wide range of structures it can produce by adjusting specific parameters such as type of

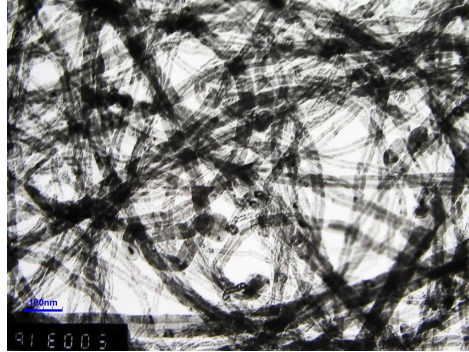


Figure 3.2: TEM micrograph of the supplied MWCNTs. Source: Cheap Tubes.

30-50nm MWCNTs Datasheet	
Outer Diameter	30-50 nm
-COOH Content	0.73 wt%
Length	10-20 $\mu\text{m}$
Purity	> 95 wt%
Ash	< 1.5 wt%

Table 3.1: Manufactures datasheet for the functionalized 30-50nm MWCNTs.

collector, applied voltage, flux rate, distance from the target, polymer concentration and solution conductivity [142, 143, 17, 18]. Recognizing this, preliminary studies were conducted to determine the optimum test parameters to achieve the project objectives. The polymer concentrations were defined through adaptation from previous literature publications [4, 110, 2]. The solutions were tested at determined target distance and electrical field to evaluate the fiber quality of each set of parameters, while the type of collector and flux rate were fixed. The parameters used are presented in table 3.2. Hexafluoro-iso-propanol was used as solvent for the experiments, specifically due to its low boiling point (58.2 °C) and strong affinity with polyamide.

The electrospinning apparatus used for this project was designed in-

	Random PA6	Aligned PA6	Random PA6/CNT	Aligned PA6/CNT
Polymer Concentration (%)	15	15	8	8
CNT Concentration (%)	–	–	0.2	0.2
Electrical Field (kV/cm)	0.3 - 0.8	0.3 - 0.8	0.3 - 0.8	0.3 - 0.8
Voltage (kV)	4.5 - 20	4.5 - 20	4.5 - 20	4.5 - 20
Working Distance (cm)	15 - 25	15 - 25	15 - 25	15 - 25
Flux Rate (mL/h)	0.3	0.3	0.3	0.3
Tangential Speed at the Surface (m/s)	–	5.83	–	5.83

Table 3.2: Electrospinning parameters used in the project.

house and consists of a polymethylmetacrilate (PMMA) box that has two systems, as shown in figure 3.3, two high voltage DC generator (ES30, GAMMA High Voltage Instruments), which generates high voltage from 0 to 30 kV and two syringe pumps (MA 1 70-2208, Harvard Apparatus). The control panel is presented in figure 3.4.

The first system (S1) is used to electrospin in a fixed target and in a vertical direction (downwards). The second, and most utilized, system (S2) is horizontal electrospinning. In this system it is possible to consider the co-electrospinning, in which two solutions are spun in contemporaneous. The target is the mandrill that is connected to a brushless motor and to a grounded electrode. The motor can spin the mandrill to velocities up to 3500 rpm and by modifying the mandrill diameter it is possible to alter the tangential speed at the surface. A system of solution, capillary metal needle, capillary tube, and syringe is used to flow the material inside the electrical field.

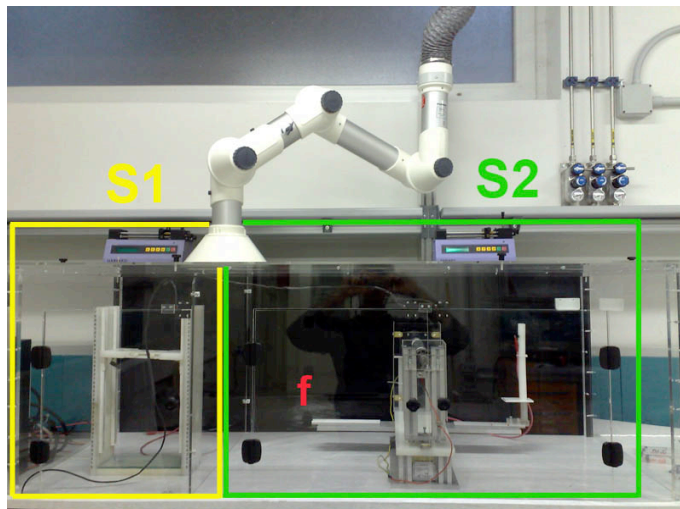


Figure 3.3: Electrospinning safety box, S1 shows the static system and S2 the dynamic system.

## 3.4 Characterization Methods

### 3.4.1 Carbon nanotubes analyses

#### 3.4.1.1 Transmission electron microscopy - TEM

Transmission electron microscopy (CM12, Philips) was employed to evaluate the quality of the supplied carbon nanotubes. MWCNTs were suspended in HFIP and subsequently deposited into a TEM grid.

#### 3.4.1.2 X-Ray photoelectron spectroscopy - XPS

The quantitative analysis of the supplier declared functionalization amount was carried out with XPS. The XPS measurements were carried out using an ESCA200 instrument (Scienta-Gammatdata ESCA 200 Uppsala, Sweden). Wide scans were acquired in the BE energy range 1200 – 0 eV using a 500 eV pass energy while high resolution core line spectra were performed setting the analyzer pass energy at 150 eV and the energy step



Figure 3.4: Apparatus control box.

at 0.05 eV. As the samples are conductive, they did not require charge compensation which led to an energy resolution of 0.3 eV.

## 3.4.2 Nanofiber morphology

### 3.4.2.1 Scanning electron microscopy - SEM

The fiber network morphologies were observed using SEM (Supra 40, Zeiss) in terms of fiber quality and presence of defects. The samples were gold sputtered before observation. The diameter distribution of the fibers was determined by the measurement of 30 individual nanofibers from the SEM images using image analysis software (Image J, National Institutes of Health/USA). Measurements were random performed on fibers in five different regions of the micrograph.

### 3.4.2.2 Transmission electron microscopy - TEM

Transmission electron microscopy was employed to evaluate the distribution of carbon nanotubes within the thinnest fibers. TEM grids were used as collector during electrospinning as a preparation method for the

observation.

### 3.4.2.3 Atomic force microscopy - AFM

Nanofiber topography was evaluated by AFM (NT-MDT Solver, Zelenograd) analysis in semi contact mode with tips of 40 nm curvature radius at 150 kHz resonant frequency. The fiber profile was extracted from the AFM images.

### 3.4.3 Thermal analysis

#### 3.4.3.1 Differential scanning calorimetry - DSC

Differential Scanning Calorimetry (DSC) was employed in order to detect the influence of the filler and process on the melting and crystallization behaviour of the resulting material and to detect the presence of residual solvent. The tests were carried out on PA6 and PA6/CNT reinforced composites by using a differential scanning calorimeter (Mettler DSC30, Mettler Toledo, USA). Measurements were performed under nitrogen flow of 100 ml/min. Two consecutive heating curves were performed: first the samples were heated at a rate of 5 °C/min from 0 °C to 300 °C and then cooled till 20 °C at 5 °C/min, the second heating curve followed the same parameters as the previous. The melting enthalpy ( $\Delta H_m$ ) was determined from the corresponding peak areas in the heating and cooling thermograms. The crystallinity content ( $X_c$ ) was calculated by the application of equation 3.1.

$$X_c = \frac{\Delta H}{(\Delta H_0) \cdot wP} \quad (3.1)$$

where  $\Delta H$  is the apparent enthalpy of fusion per gram of material,  $\Delta H_0$  is the latent heat of fusion of 100% crystalline polymer, taken as

190 J/g [144, 145], and  $wP$  is the weight fraction of polymer in the composites.

### 3.4.4 Mechanical analysis

The methods available to measure the mechanical properties of electrospun nets derive from the techniques applied for films and textile materials. Nowadays, it is still not available a standard that regulates the procedures to carry out these measurements. Therefore, some caution in interpreting the data is warranted. Several parameters can influence the mechanical properties such as homogeneity and polydispersity of the fibers, type of solvent, presence of imperfections or defects [146, 3]. Thus, it is difficult to compare different studies and/or materials, and a correct experimental procedure should be described.

#### 3.4.4.1 Tensile analysis

Tensile analyses were carried out for PA6 and PA6/CNT composite networks. Tests were conducted in a universal testing machine (4502, Instron) with 10 mm/min cross-head speed rate and 25 mm gauge length. The networks were cut into rectangular sheets of 5 x 35mm. The analysis of the tensile behavior was performed in two main directions according to the spinning direction, 0° and 90°. Tensile stress of each sample was calculated on the nominal cross-section area which neglects the presence of voids. Five samples of each network at both angles were submitted to the test.

## 3.5 Biological Evaluation

In this work, two cell lines were cultured on the scaffolds in order to evaluate how the produced networks would behave when in contact with different tissues. Hard (human osteoblasts-like) and soft (human fibroblasts-like) tissue models were considered to be a important evalu-

ation of the tested materials. Osteoblasts are responsible for bone formation, more specifically for the mineralization of the osteoid matrix. In essence, osteoblasts are sophisticated fibroblasts that express all genes that fibroblasts express with the addition of the genes for bone sialoprotein and osteocalcin[147]. Fibroblasts are responsible to maintain the structural integrity of connective tissues by continuously secreting precursors of the extracellular matrix. Fibroblasts secrete the precursors of all the components of the extracellular matrix, primarily the ground substance and a variety of fibres. The composition of the extracellular matrix determines the physical properties of connective tissues.

### 3.5.1 Protein adsorption analyses

#### 3.5.1.1 Protein adsorption

The samples were incubated for 30 min with 500 $\mu$ L culture medium at 37 °C. The incubation period, volume, and sample dimension (10 mm of diameter) were selected to match the cell seeding conditions. The TCP well surface was used as control for all analyses. After incubation, the medium was removed and the samples were gently washed with deionized water, placed into clean TCP well and subjected to the proper protein desorption procedure. Two procedures were used to analyse the protein adsorption, the qualitative total desorption and the protein binding strength. For a qualitative measure of protein desorption, the samples and control were submitted to a 1 hour incubation in 0.1% of SDS at 37 °C. While for the binding strength study, the materials were subjected to protein elution according to an experimental protocol based on the sequential washing of the sample surfaces by media with different chemical strength. The specimens were washed three times with water followed by sequentially wash steps with isopropanol/water solutions at increasing concentrations (10, 30, 50, and 70% v/ v), and then a final wash with 0.1% SDS [11, 57]. At each step, 500  $\mu$ L of eluting medium were added

to the materials for 20 min at room temperature while the SDS wash lasted for 1 hour at 37 °C under static conditions.

### 3.5.1.2 Electrophoresis

One-dimensional (1D) electrophoresis was performed to characterize the protein desorption from the networks and controls. The desorbed proteins were freeze-dried and resuspended in sample buffer (NuPAGE<sup>TM</sup> LDS Sample Buffer, Invitrogen, Italy). Six microliters of each resuspended sample were then loaded on a sodium dodecyl sulfate polyacrylamide electrophoresis gel (NuPage<sup>TM</sup> Novex 3–8% (Tris-acetate), Invitrogen, Italy). The selected gel is suitable for the detection of high-molecular weight (40–500 kDa) proteins. Each gel was loaded with two molecular weight protein standards (HiMark<sup>TM</sup> and SeeBlu<sup>TM</sup> Plus2, Invitrogen, Italy), fresh culture medium (1:20 in sample buffer) and inactive fetal bovine serum (1:40 in sample buffer) as control lanes. The gels were run in an XCell SureLock<sup>TM</sup> Midi-Cell (Invitrogen, Italy) at 150 V constant voltage. After electrophoresis, the gels were stained following the manufacturer's protocol using a silver-based stain (ProteoSilver<sup>TM</sup>, Sigma-Aldrich, Germany) or a comassie-blue based stain (Imperial<sup>TM</sup>, Pierce, USA) and further digitalized with an imaging system (GEL LOGIC 200, Kodak, USA).

### 3.5.2 Cell seeding and culture

Human osteoblasts-like cell line MG63 (Human osteogenic sarcoma) and human fibroblasts-like cell line MRC5 (Embryonic human lung) were cultured on random and aligned electrospun nets. Cell lines were supplied by Istituto Zooprofilattico Sperimentale della Lombardia e dell' Emilia Romagna (Brescia, Italy). Prior to cell seeding, samples were cut into 10 mm diameter circles and sterilized in ethanol 70% overnight at 4 °C.

Samples were rinsed 3 times with sterilized PBS and allowed to dry under the hood. Samples were pre incubated in 0.5 ml of medium for 30 minutes at 37 °C and 5%  $CO_2$  before cell seeding to allow protein adsorption.

The MG63 and MRC5 medium were prepared from RPMI 1640 medium (ECB9006L, Euroclone, Italy) supplemented with 10% inactive fetal bovine serum, 1% glutamax, 1% non essential amino acids, 1% antibiotic and 1% sodium pyruvate. Phenol red free medium was used in order to avoid interference with the proliferation assay as recommended from the supplier.

Cells were seeded onto 4 identical samples for each analysis at a concentration of  $8.9 \cdot 10^3 \text{ cells/cm}^2$  and  $3.2 \cdot 10^4 \text{ cells/cm}^2$  for MG63 and MRC5, respectively. The seeding concentration was defined considering the kinetics of proliferation of each cell line. Fresh culture medium was replaced every 2 days. Culture times were 3, 7 and 14 days. The morphology of the adhered cells was observed using SEM for each culture time. Cell viability was evaluated by confocal microscopy, while proliferation was assessed by alamar blue analysis.

### 3.5.3 Cell proliferation

Proliferation evaluation was performed using the Alamar Blue assay (DAL1025, Invitrogen, Italy). The analysis is based on the reduction capability of living cells to determine in a quantitative manner the cellular viability/proliferation. Living cells are able to reduce the molecule resazurin, the active agent of Alamar Blue assay, into resorufin, a bright red compound with a high fluorescence yield. The reagent is non toxic and is able to cross the cell membrane. Alamar Blue reagent was diluted in culture medium in a concentration of 1:10. Samples were incubated for 4 hours in 500  $\mu\text{L}$  of Alamar Blue dilution and 100  $\mu\text{L}$  of the reactant was successively transferred to a 96 well plate to further measurement at a spectrophotometer (Multiskan EX, Thermo Labsystems). Absorbance

was measured in two different wavelengths, 570 nm and 620 nm, which corresponds to the absorbance of resorufin and the background, respectively.

The acquired absorbance was treated to have the reduction percentage of resazurin by the living cells. Equation 3.2 was used to calculate a correction factor in order to eliminate the effect of the oxidation of alamar blue solution and the reduction percentage was calculated by the application of equation 3.3.

$$Ro = \frac{AO_{570nm}}{AO_{620nm}} \quad (3.2)$$

$$AR_{570nm} = A_{570nm} - (A_{620nm} \cdot Ro) \cdot 100 \quad (3.3)$$

where, Ro is the correction factor;  $AO_{570nm}$  the absorbance of oxidized form at 570 nm;  $AO_{620nm}$  the absorbance of oxidized form at 620 nm;  $AR_{570nm}$  the percentage of reduced resazurin into resorufin;  $A_{570nm}$  the measured absorbance at 570 nm and  $A_{620nm}$  the measured absorbance at 620 nm.

### 3.5.4 Cell viability

Evaluation of cell viability on the seeded scaffolds was performed by confocal laser microscopy (CLM) (Nikon Eclipse, Nikon, Japan) after staining with fluorescein diacetate-propidium iodide (FDA-PI) (F1303, Molecular Probes Inc., USA). FDA stains viable cells green, while PI stains necrotic and secondary apoptotic cells red. The assay was performed according to previously published methods [148]. Briefly, before observation the samples were rinsed in distilled PBS and further incubated with an FDA/PBS (2  $\mu$ L/998  $\mu$ L) solution for 15 min at 37 °C. To eliminate the excess dye, samples were rinsed 3 times in PBS and further incubated with a PI/PBS (20  $\mu$ L/980  $\mu$ L) solution for 2 min at room temperature.

### 3.5.5 Cell morphology

The networks for SEM observation were fixed and dehydrated after defined culture periods as follows: the samples were soaked in Glutaraldehyde 25% in Cacodylic buffer 0.1M for 30 minutes at 4 °C, then rinsed in Cacodylic buffer 0.1M for 3 times. Dehydration was conducted as follows: samples were soaked for 10 minutes in ethanol solutions of concentration 30%, 50%, 70%, 90% and 20 minutes in 100%, then allowed to dry under the hood. The samples were gold sputtered before observation.

## 3.6 Statistical Analysis

All values are expressed as mean  $\pm$  standard deviation. Statistical analyses were performed with Kaleidagraph software applying the t-student variable.



# Chapter 4

## RESULTS AND DISCUSSION

### 4.1 Carbon Nanotubes Analysis

Carboxyl functionalized MWCNT were used in this research. The morphology and functionalization were controlled as preliminary studies.

The morphology was accessed by TEM analysis and the result is present in figure 4.1. It was observed that there is a large diameter dispersion as well as the presence of defects on the nanotubes walls. The defects are probably the consequence of the functionalization process.

In order to evaluate the functionalization claimed from the supplier, an XPS analysis was carried out. The XPS survey spectra of the nanotubes is presented in figure 4.2. The carbon presence is evidenced at 284 eV while the oxygen appears at 530 eV. The carbon and oxygen peak areas have been fitted in order to evaluate the presence of the specific bonds. The carbon and oxygen fitting are presented in figures 4.3 and 4.4, respectively. The quantitative analysis done by the fitting of the peaks is presented in table 4.1. The analysis has shown that the atomic abundance of oxygen is approximately 6.54%, from which 3.53% refers to hydroxyl groups, 2.19% represent the carboxyl groups and 0.81% of water.

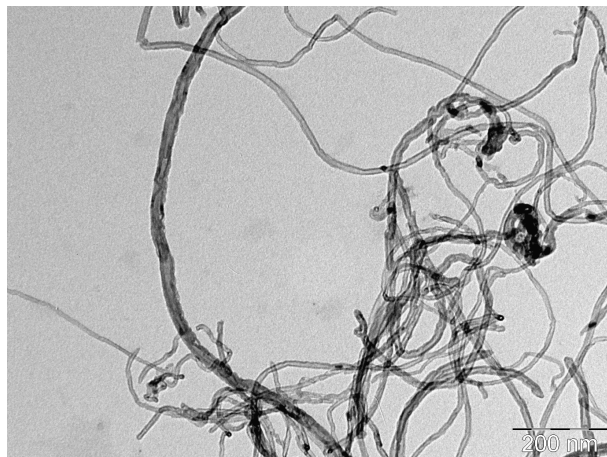


Figure 4.1: TEM image of the supplied multi-walled carbon nanotubes.

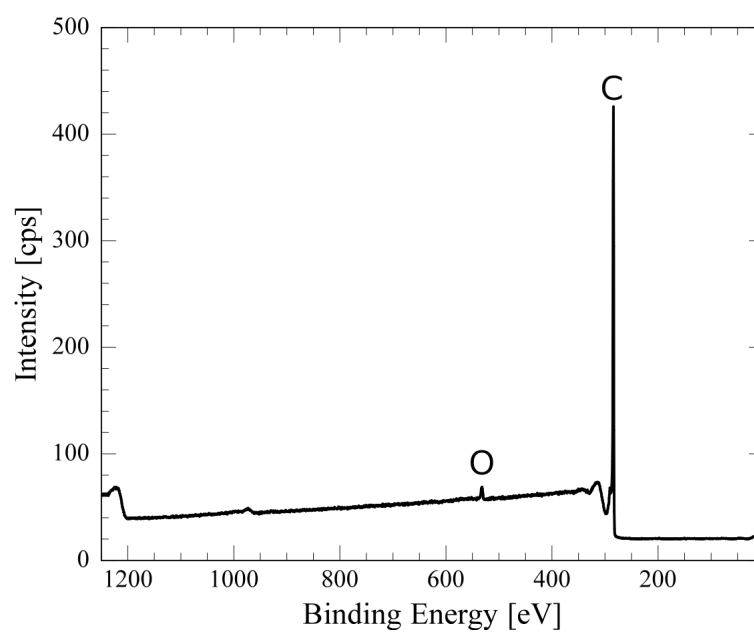


Figure 4.2: XPS survey spectra of the supplied MWCNTs.

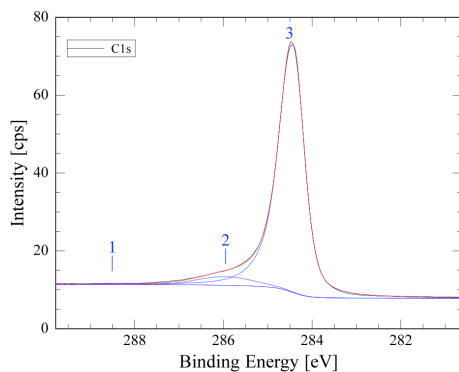


Figure 4.3: C1s fitting of XPS survey spectra.

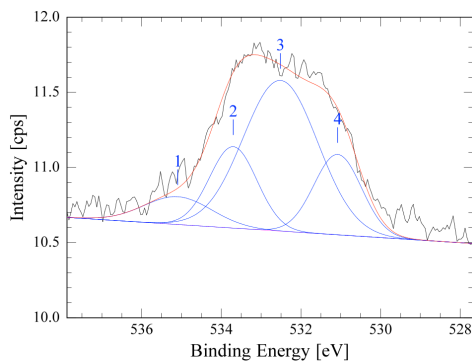


Figure 4.4: O1s fitting of XPS survey spectra.

	Area	BE (eV)	Height	Fwhm	at%	Atom
C1s001	6.66	288.50	0.21	1.50	0.56	-(C=O)-OH
C1s002	70.67	285.95	2.21	1.50	5.98	-C-OH
C1s003	1099.15	284.42	63.55	0.56	92.96	C-C
O1s001	7.87	535.09	0.185	2.00	8.18	H <sub>2</sub> O
O1s002	16.16	533.70	0.542	1.40	16.78	-(C=O)-O*H
O1s003	46.98	532.51	1.00	2.20	48.80	C-O*-H
O1s004	15.95	531.08	0.53	1.40	16.56	-(C=O*)-OH

Table 4.1: Quantitative analysis of the C1s and O1s peaks.

## 4.2 Nanofiber Production and Morphology

Since the aim of this study was to investigate the potential of polymer/CNT composites as a biomaterial candidate, a series of tests were performed to determine the effect of several parameters on the fiber quality and morphology, as presented in table 3.2. The parameters choice impacts the operating conditions significantly. A clear overview is presented in figure 4.5 where the influence of applied voltage on fiber alignment of PA6 is demonstrated. It can be observed that as the applied voltage increases the alignment of the fibers significantly decreases. This is a

consequence of the increased speed of the ejected polymer which is higher than the collector capability of organizing them. Following the series of tests previously described, the most adapted parameters are presented in table 4.2, while SEM images the best produced networks are presented in figures 4.6 and 4.7.

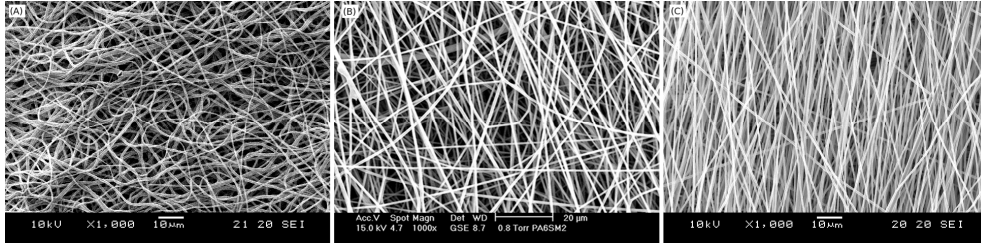


Figure 4.5: The influence of applied voltage on the fiber alignment of PA6, when the target tangential speed is 3.33 m/s. (A) 20 kV, (B) 15 kV and (C) 5 kV.

	Random PA6	Aligned PA6	Random PA6/CNT	Aligned PA6/CNT
Polymer Concentration (%)	15	15	8	8
CNT Concentration (%)	–	–	0.2	0.2
Electrical Field (kV/cm)	0.32	0.32	0.4	0.4
Voltage (kV)	8	8	10	10
Working Distance (cm)	25	25	25	25
Flux Rate (mL/h)	0.3	0.3	0.3	0.3
Tangential Speed at the Surface (m/s)	–	5.83	–	5.83

Table 4.2: Most adapted parameters applied for the networks production.

To better distinguish the size and distribution of fibers produced by electrospinning, histograms were prepared for the experimental groups and are presented in figures 4.8 and 4.9. The results of the PA6 and PA6/CNT based networks show a uni-modal distribution of fiber size for the aligned networks, while the random networks showed a broader

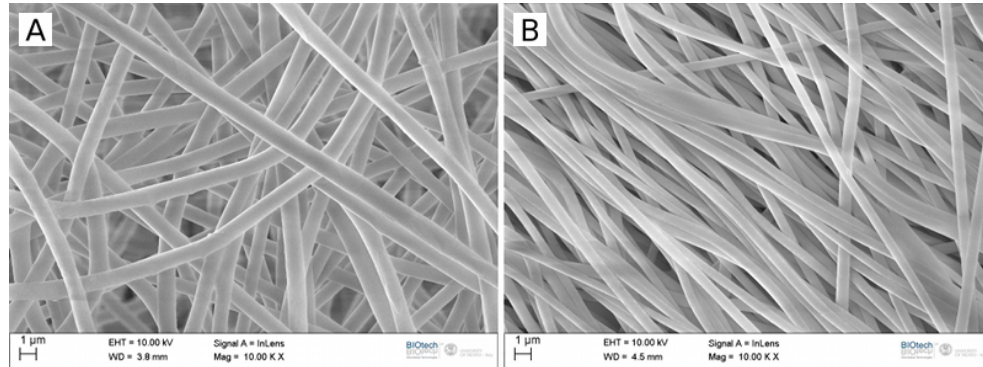


Figure 4.6: Random PA6 (A) and aligned PA6 (B) produced networks.

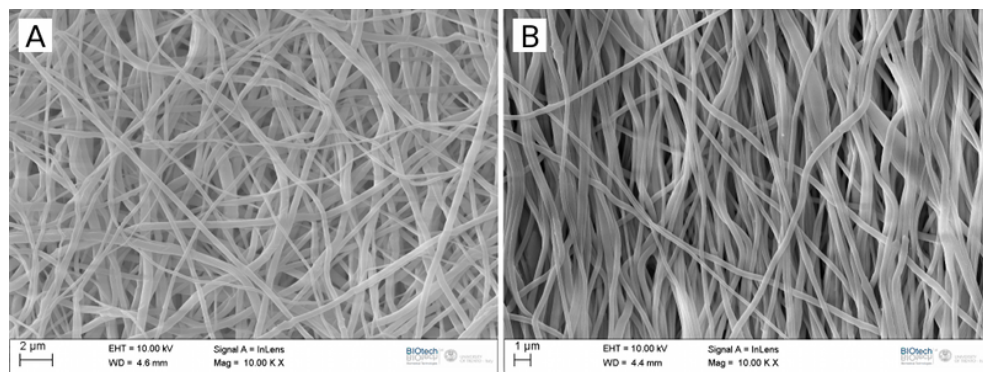


Figure 4.7: Random PA6/CNT (A) and aligned PA6/CNT (B) produced networks.

fiber distribution. Furthermore, the aligned networks present lower fiber diameters in comparison to the random ones. Presumably, these are the effects of the collector configuration, which is a mandrel at high speed. The high speed of the collector induces the stabilization of the whipping zone, converging to a uni-modal fiber distribution and increases the fiber stretching, which reduces the fiber diameter of the aligned networks.

Additional information that can be extracted from the histograms is the clear reduction of the fiber diameter of the composite networks. There are two explanations for this behavior. As discussed in section 2.7.2,

two of the main parameters that influence fiber morphology are polymer concentration and solution conductivity. As presented in table 4.2, the composite networks have been produced with a lower polymer concentration in order to balance the increase on electrical conductivity. The addition of carbon nanotubes has increased the electrical conductivity of the solution, which regulates the velocity in which the jet is formed and ejected. Moreover, the combination of lower polymer concentration and higher conductivity led to the significant decrease of the fiber diameter. Lastly, it should be distinguished that the higher conductivity presented by the composite solution has a negative effect on the fiber alignment as seen in figures 4.6 and 4.7.

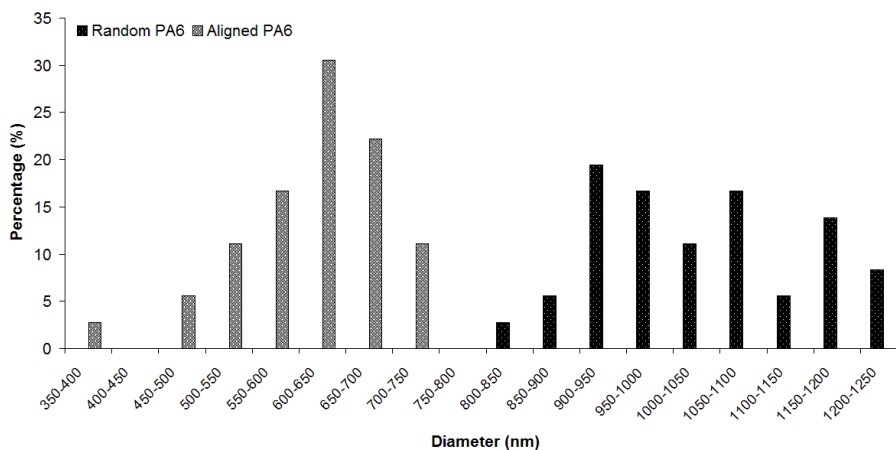


Figure 4.8: Histogram representing the random and aligned PA6 fiber diameter distribution.

As presented in previous studies [149, 150, 19], carbon nanotubes are able to align within the nanofiber axis due to the converging nanoscale jet that constrains and reduces the number of available orientations in the flow field [4]. To confirm this phenomena, the orientation of the CNTs within the polymer fibers was investigated using TEM with results presented in figure 4.10. The TEM analysis clearly indicates a near-perfect orientation of the CNTs within the axial direction of the polymer fibers.

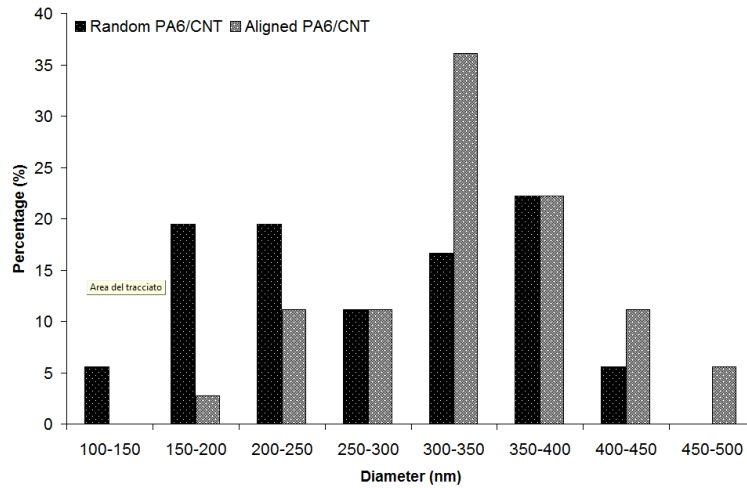


Figure 4.9: Histogram representing the random and aligned PA6/CNT fiber diameter distribution.

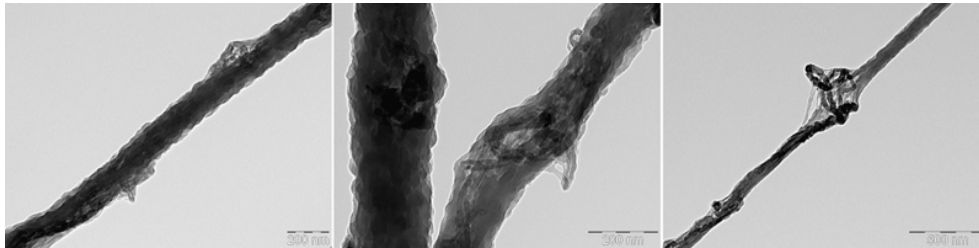


Figure 4.10: Transmission electron micrography of PA6/CNT electro-spun fiber.

In addition to the alignment of nanotubes within the polymer fibers, it was also possible to verify the presence of roughness and defects at the fiber surface most probably caused by fiber stretching. The presence of surface roughness and defects provides evidence for the presence of the nanofillers beneath the surface and residual aggregates within solution.

To further ascertain the surface topography obtained by TEM, an AFM analysis was performed at the nanofiber's surface with the results are presented in figure 4.11. From the AFM analysis, the presence of surface roughness on the composite in comparison to the control nanofibers

is confirmed. The profile of the fibers was acquired from the AFM images and is presented in figure 4.12. We chose to present the profile instead of the value of surface roughness because we believe the value would not be statistically significant. The difficult to perform the analysis led to the acquisition of one image per type of material.

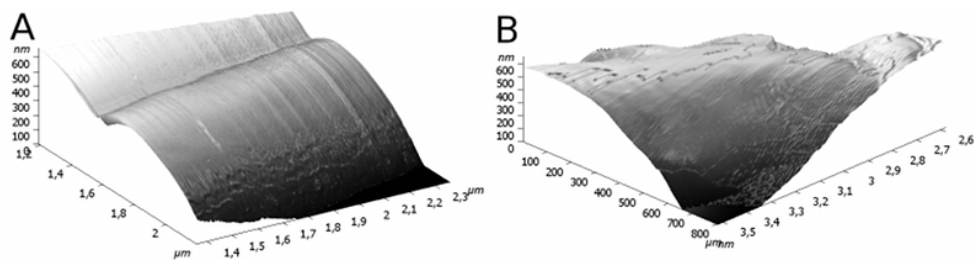


Figure 4.11: AFM images depicting the surface topography of the (A) PA6 and (B) PA6/CNT fibers.

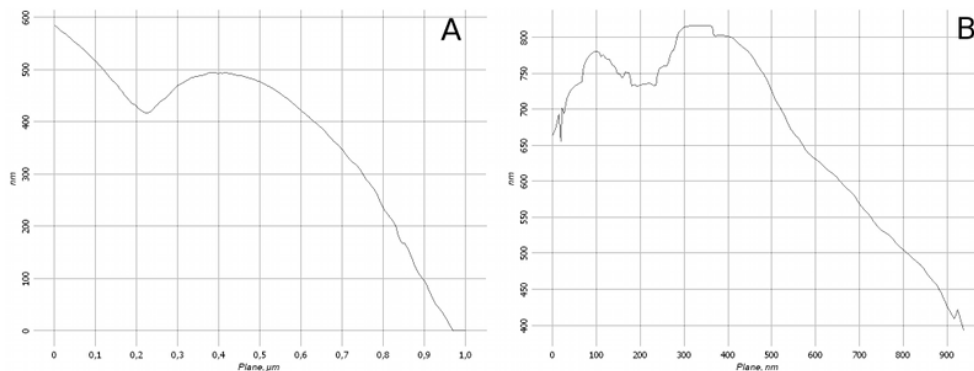


Figure 4.12: Fiber profile acquired from the AFM images, (A) PA6 and (B) PA6/CNT.

### 4.3 Thermal Analysis

Differential scanning calorimetry was employed in order to evaluate the influence of the CNT filler and the process on the melting and crystal-

lization behavior. The partial thermograms representing the glass transition temperature, 1st scan melting, recrystallization and 2nd scan melting are presented in figures 4.13, 4.14, 4.15 and 4.16, respectively. The evaluation results and crystallinity analysis are summarized in tables 4.3 and 4.4, respectively.

	Random PA6	Aligned PA6	Random PA6/CNT	Aligned PA6/CNT
Heating (1st Scan) water absorption				
Onset Temperature (°C)	57.83	63.18	36.21	36.66
Endset Temperature (°C)	105.24	101.19	97.19	106.17
Integral (mJ)	-464.12	-633.20	-565.52	-515.12
Normalized Integral (J/g)	-29.01	-38.14	-32.88	-30.85
Heating (1st Scan)				
Onset Temperature (°C)	216.48	216.45	207.87	210.63
Endset Temperature (°C)	228.95	229.45	230.21	231.39
Integral (mJ)	-913.41	-1048.43	-1009.29	-1154.45
Normalized Integral (J/g)	-57.09	-63.16	-58.68	-69.13
Cooling				
Onset Temperature (°C)	195.82	194.86	200.56	206.34
Endset Temperature (°C)	182.35	177.83	179.94	184.39
Integral (mJ)	1077.60	1064.20	931.80	1047.77
Normalized Integral (J/g)	67.35	64.11	54.17	62.74
Heating (2nd Scan)				
Onset Temperature (°C)	204.88	204.09	202.88	206.31
Endset Temperature (°C)	226.54	226.78	225.27	227.81
Integral (mJ)	-1245.84	-1208.15	-1060.48	-1224.29
Normalized Integral (J/g)	-77.87	-72.78	-61.66	-73.31

Table 4.3: Thermal analysis results representing the pure PA6 and composite system.

The thermograms showed in the first scan the presence of an endothermic peak relative to the water absorption, as shown in figure 4.13. It is well known that polyamide absorb moisture due to their amine groups,

which interact with the water molecules [151, 152]. We assume that these peaks are related to water and not residual solvent because of the high enthalpy measured. Nevertheless, we do not exclude the presence of a slight amount of HFIP. The shifting of the water desorption peaks to lower temperatures is related to the heating rate used (5 °C/min) and the high surface area of the samples. No significant difference in water content can be observed between the produced materials, what means that the presence of nanotubes do not affect the water absorption of the samples.

	Crystallinity (%)	
	1st Scan	2nd Scan
Random PA6	30.1	41.0
Aligned PA6	33.2	38.3
Random PA6/CNT	31.7	33.3
Aligned PA6/CNT	37.3	39.6

Table 4.4: Crystallinity percentage of the networks after 1st and 2nd scan.

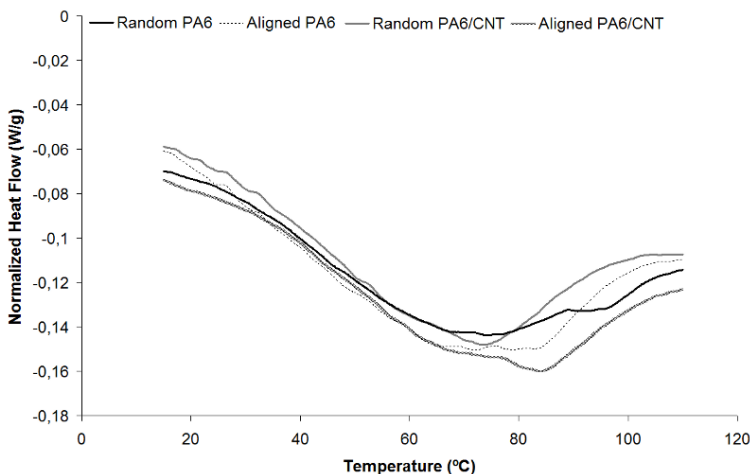


Figure 4.13: Partial thermogram depicting the water adsorption region.

The crystalline behavior of the materials are influenced either by the

process and the CNTs presence as showed in the thermograms. The influence of the electrospinning process can be observed in the first heating scan (figure 4.14) where the crystallinity is higher in the aligned networks. This phenomenon occurs because of the higher degree of stretching in these materials due to the configuration of the collector. The results are confirmed in table 4.4. The second metastable crystalline phase of polyamide 6 is observed in the pure polyamide networks, while this phase is reduced or is not present in the composite networks, which confirms the influence of CNTs on the crystalline behavior.

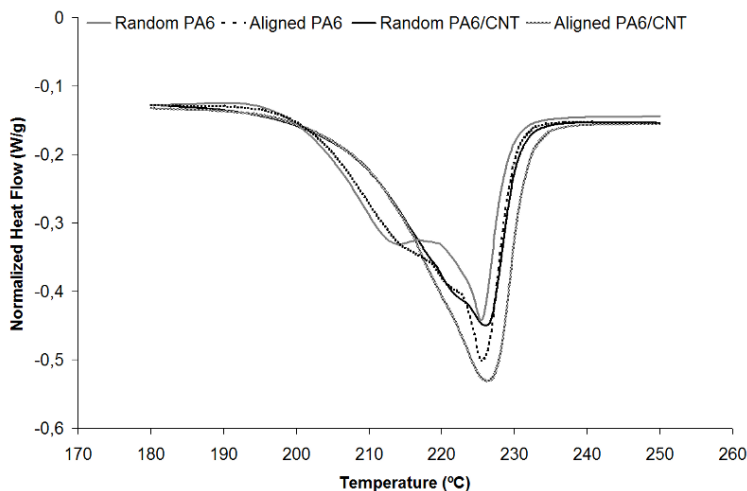


Figure 4.14: First scan partial thermogram depicting the melting region.

Several authors showed how carbon nanotubes influence the crystalline behavior of polymeric nanocomposites [6, 153, 154, 155]. Carbon nanotubes act as nucleant agents in polymeric nanocomposites affecting the crystallization process. Li *et al.* demonstrated that CNTs act as nucleant agents and induce the formation of the nanohybrid shish-kebab (NHSK) structures as presented in figure 4.17. In fact, the nucleating effect of the CNTs on the electrospun composite nets are clearly observed during the cooling run (figure 4.15), where the crystallization of the com-

posite networks start earlier. The onset temperatures during crystallization are 195.82, 194.86, 200.56 and 206.34 °C for random PA6, aligned PA6, random PA6/CNT and aligned PA6/CNT, respectively. In addition, it was observed that the presence of nanotubes reduce the crystallization. We assume that the nanotubes work as a physical barrier and reduce the mobility of the polymer chains, similar result was observed by Chen *et al.* [155].

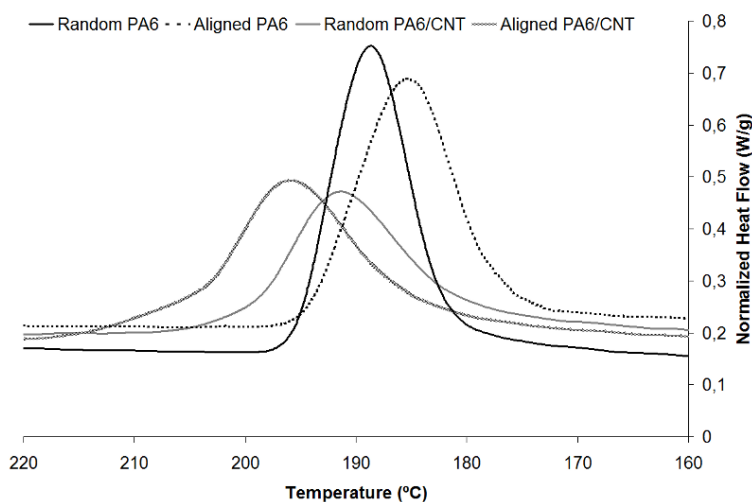


Figure 4.15: Partial thermogram depicting the crystallization region.

The glass transition temperature,  $T_g$ , was not observed in the DSC analysis. We assume that this fact is correlated to the heating rate applied in this work.

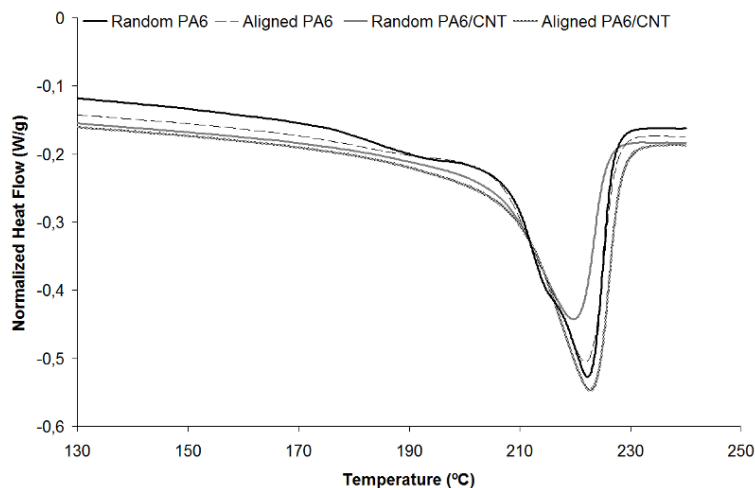


Figure 4.16: Second scan partial thermogram depicting the melting region.

## 4.4 Mechanical Analysis

In order to determine the extent of the anisotropic mechanical properties exhibited by the neat and composite nanofibers, tensile tests were performed both orthogonal and parallel to the spinning direction of the nets. The results of the mechanical analysis are presented in table 4.5 and the typical stress-strain curve at both angles is shown in figure 4.18. The networks showed a nonlinear elastic behavior in lower stress region, 0-4 MPa (parallel) and 0-0.03 MPa (orthogonal), and plastic deformation at higher stress. Due to the nonlinear elastic behavior of the materials the elastic modulus was determined by taking the slope of the stress-strain curve at some specified level of strain (0-5%) and this elastic modulus was defined stiffness. The stiffness and ultimate tensile stress have decreased for the CNT-based networks. It was an unexpected result since several authors have published the enhancement of the mechanical prop-

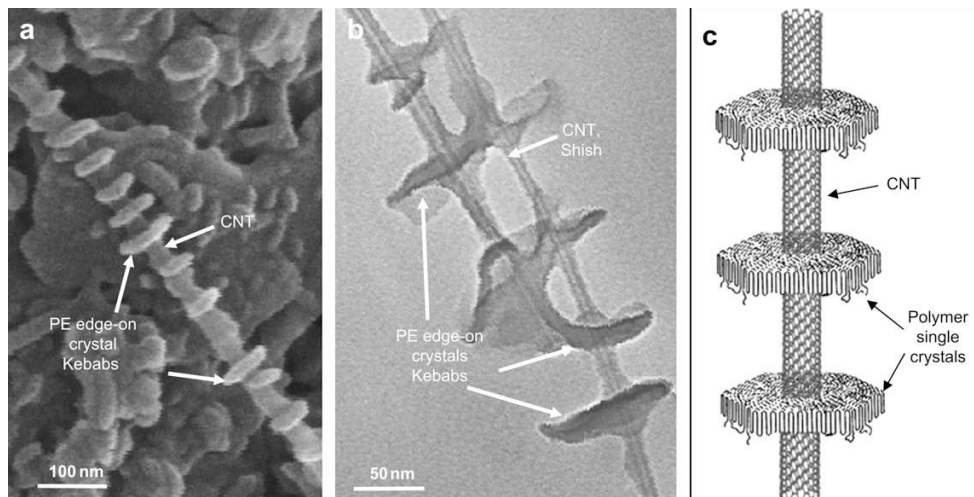


Figure 4.17: PE/MWCNT NHSK structure produced by solution crystallization of PE on MWCNTs at 103 °C in p-xylene for 30 min. (a) SEM image of MWCNTs decorated by disc-shaped PE single crystals. (b) TEM image of the PE/MWCNT NHSK structure. (c) Schematic representation of the PE/CNT NHSK structure. PE forms lamellar single crystals on CNT surface with polymer chains parallel to the CNT axis. [6]

erties by the addition of CNTs [156, 157, 158, 159]. Nevertheless, few authors have studied the mechanical behavior of CNT reinforced electrospun networks [156, 157], however it is agreed that in most of the cases the presence of CNTs enhance the mechanical behavior.

We expected that the mechanical properties would increase as a response to the polar functionalities in the MWCNT, which should be an opportunity to the formation of hydrogen bonds between the polymer and matrix or to amidation reactions between free amine in the MWCNTs. We assume that the lack of tensile properties in the composite nets could be a result of the presence of fiber defects as seen in figure 4.10, and also due to the poor interfacial adhesion between the nanotubes and the matrix. Weak surface adhesion reduces the effectiveness of the load

transfer between the matrix and the nanotubes, and this effect could be inhibitory rather than supportive mechanical strength [140]. Nevertheless, the anisotropic mechanical behavior of the networks was observed which is consequence of the alignment of the fibers in the spinning direction and can be in part attributed to the collector geometry and the voltage adjustments.

Further studies should be held to understand the interactions between CNT filler and the electrospun nets. The possible application of compatibilizer agents should also be thought.

	PA6		PA6/CNT	
	0°	90°	0°	90°
Stiffness (MPa)	89.33 ± 19.42	1.31 ± 0.37	76.32 ± 15.71	1.15 ± 0.20
Ultimate Tensile Stress (MPa)	13.36 ± 1.69	2.91 ± 0.31	10.06 ± 1.37	2.07 ± 0.15
Strain	0.67 ± 0.05	1.98 ± 0.16	0.57 ± 0.13	1.95 ± 0.27

Table 4.5: Mechanical properties of PA6 and PA6/CNT.

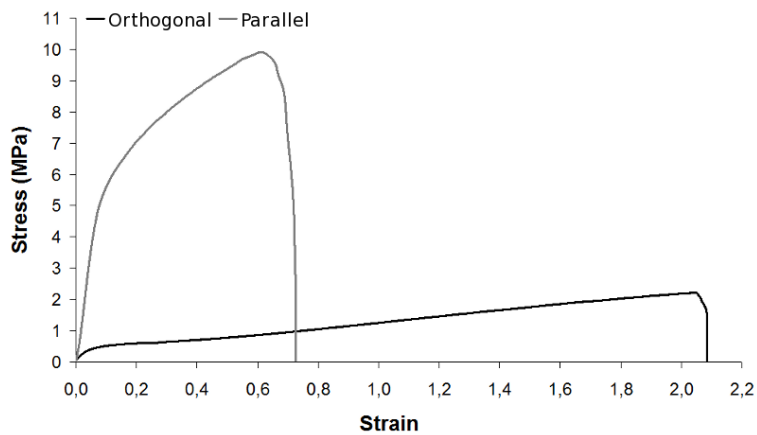


Figure 4.18: Typical stress-strain curves of orthogonal and parallel regarding the spinning direction.

## 4.5 Biological Analysis

### 4.5.1 Protein analyses

Protein adsorption is the first event occurring on the surface of any system in the biological environment. Proteins adsorbed on foreign materials can either keep their native structure or undergo changes in concentration, orientation or conformation. These properties determine the subsequent cellular interactions, which can significantly impact the performance of biomaterials in a biological environment. The extent of the protein selection and rearrangement is affected by the nature and the properties of the material surface.

Aiming to understand the nature of protein adsorption of the produced materials, electrophoretic analyses were carried out. Two different protocols were used to analyze total protein desorption, and to qualitatively evaluate protein binding strength. Firstly, the proteins adsorbed on the materials surface have been eluted with 0.1% SDS and the results are presented in figure 4.19. Secondly, the strength of proteins binding to the surfaces was evaluated applying a sequence of eluting solutions with increasing chemical strength. The results of binding strength analysis are presented in figure 4.21. Even if the electrophoretic analysis is not a quantitative evaluation, it represents an initial assessment of the adsorption behavior.

The higher surface area of the sample compared to the TCP control has shown to be crucial to the analysis of the eluted proteins. The protein amount desorbed from the electrospun networks was significantly higher than the control. To better evaluate the controls a further electrophoretic analysis was carried out with a more sensible stain system, as shown in figure 4.20. It was not possible to stain the samples analysis with the same system since there would be a saturation of the gel labels. Furthermore, the comparison between pure and composite systems

as well as between random and aligned nets showed the higher protein adsorption on the pure polyamide 6, as well as on the random surfaces. The information acquired from the electrophoretic analyses reveals the presence of typical bands corresponding to Bovine Serum Albumin (66 kDa ca), recognized by its shape and position, and immunoglobulin's at 160 kDa. Some other intense bands are shown in the mid-MW range, where, for example, could be present fibronectin around 220 kDa.

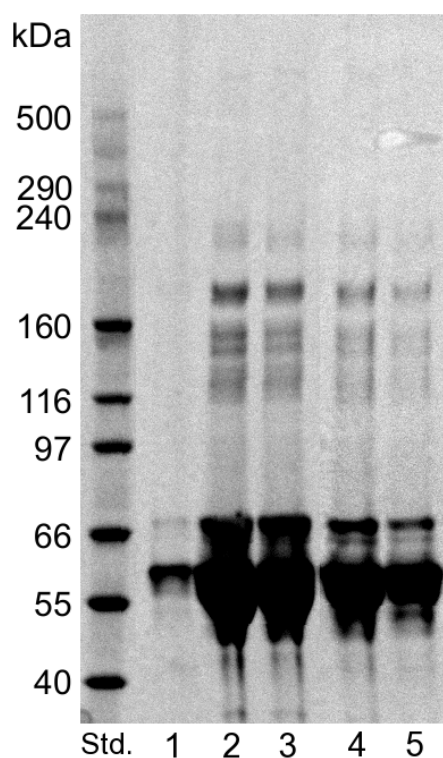


Figure 4.19: Protein adsorption after treatment with 0.1% SDS, where (Std.) HImark Standard, (1) TCP control, (2) Random PA6, (3) Aligned PA6, (4) Random PA6/CNT and (5) Aligned PA6/CNT. Imperial<sup>TM</sup> stain.

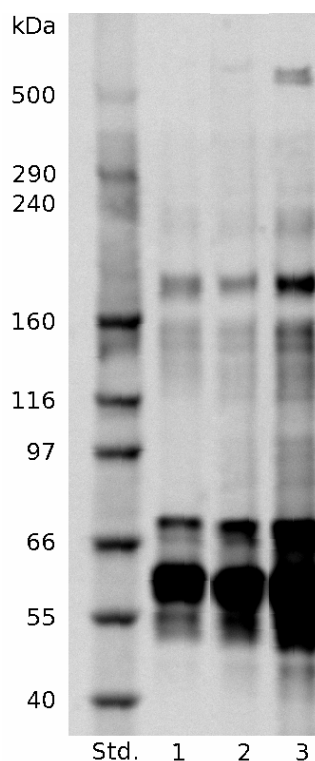


Figure 4.20: Protein adsorption after treatment with 0.1% SDS, where (Std.) HImark Standard, (1) TCP control, (2) MG63 medium and (3) inactive FBS. ProteoSilver<sup>TM</sup> stain.

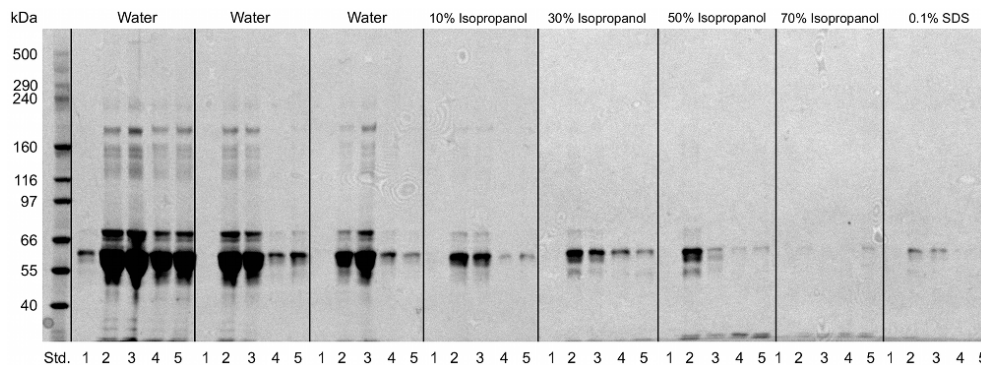


Figure 4.21: Binding strength analysis of (Std.) HI-mark Standard, (1) TCP control, (2) Random PA6, (3) Aligned PA6, (4) Aligned PA6/CNT and (5) Random PA6/CNT.

The proteins known to regulate the cellular attachment such as fibronectin and vitronectin, [93, 160, 161] could not be univocally detected in the electrophoretic analysis, which confirms our need for more specific analyses. Further qualitative analyses such Enzyme-Linked ImmunoSorbent Assay (ELISA) and Western Blot have to be carried out to evaluate a significant difference between our materials and to investigate the role of specific adhesion proteins in cellular attachment on the surfaces.

The binding strength measurements have confirmed the higher adsorption by the pure polyamide as well as the random networks previously discussed. Moreover, the proteins adsorbed on the neat PA6 showed a stronger binding strength than the composite networks, as presented in figure 4.21. The proteins on the composites surface are significantly released after the water washes while the pure polymer present a consistent amount of protein till the wash with a 50% isopropanol solution. The analysis of proteins eluted by media with different chemical strength can help to give an idea of protein affinity for the materials.

A number of features can affect the protein adsorption, such as surface chemistry, wettability. Measurements of wettability have been carried out on electrospun networks, however the natural morphology of the

nanofibers did not allowed the measurements. On the other side, contact angle measurements on flat films of PA with and without CNT could not be significant, since the effect of the nanofibers structure will be lost. Due to technical complexity of the measurements, surface chemistry at the molecular level was not accessed at this point of the research.

### 4.5.2 Proliferation analysis

Cell proliferation analysis was obtained through Alamar Blue assay and the results are shown in figures 4.22 and 4.23 for MG63 and MRC5 cell lines, respectively. As described in section 3.5.3, the active reagent of alamar blue reduces in contact with living cells which permits us to evaluate the proliferation trend at each culture time. After 3 days of culture, it is possible to observe that there is no significant difference between the tested materials for both cell lines. However, it was observed that the attachment kinetics is different for the diverse cell phenotypes. The fibroblast seeding concentration was higher than for the osteoblasts; nevertheless, at day 3 there were less fibroblasts in the networks when compared to the osteoblast seeded samples. It is possible that different adhesion mechanisms are acting in this case.

Of particular interest is the proliferation of the composite networks cultured with MG63 after 7 days which is significantly higher than the pure polymer. However, when cultured with MRC5 there are still no significant difference. Fibroblasts are know to have a slower proliferation kinetics than osteoblasts, however we assume that at the early stages fibroblasts are less sensitive to the patterned surface. It has been previously discussed how cells can interact with surfaces and topography and the corresponding response. Several authors have elucidated this by culturing various cells on nano-patterned surfaces [36, 72, 73, 74, 162]. Nano-patterned structures have promising implications in the biomedical field since they interact with subcellular structures and proteins with

the substrate. The protein analysis previously presented did not clarify the enhancement of the proliferation behavior observed. Moreover, the analysis shows a higher protein adsorption from the pure PA6 networks. As discussed, the electrophoretic analysis could not detect univocally the presence of the proteins known to regulate the cellular attachment such as fibronectin and vitronectin [93, 160, 161]. Moreover, we assumed that the sensitivity of the technique was not high enough to detect low concentration of these proteins.

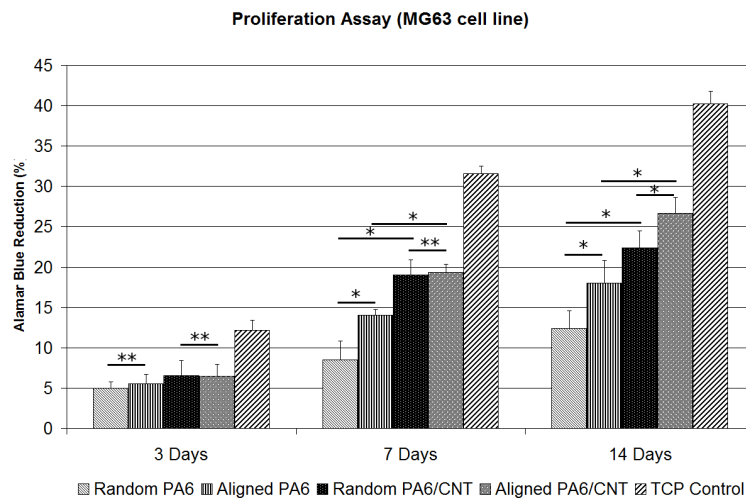


Figure 4.22: Alamar Blue proliferation assay of the tested networks cultured with MG63 cell line. \*  $p < 0.0001$  and \*\*  $p < 0.5$ .

The significant enhancement of the proliferation on the composite networks is observed at day 14 for the MRC5 cell line, as can be seen in figure 4.23. Which confirm our previous assumption that fibroblasts are less sensitive to the surface roughness. The trend presented by the scaffolds cultured with MG63 was kept also in day 14.

Statistical analysis was carried out between the random and aligned PA6 and PA6/CNT groups and inside of each material. What was detected is that from day 7, for osteoblasts, there is a significant enhance-

ment of the proliferation of the random and aligned PA6/CNT nets when compared to the PA6 nets.

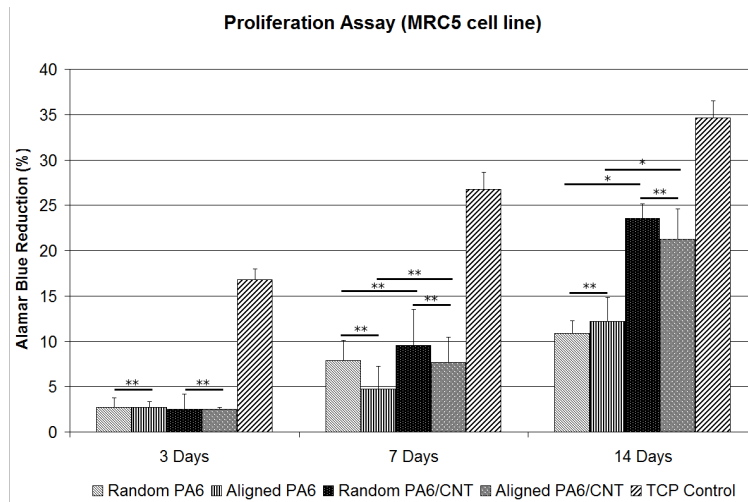


Figure 4.23: Alamar Blue proliferation assay of the tested networks cultured with MRC5 cell line. \*  $p < 0.0001$  and \*\*  $p < 0.5$ .

Interestingly, it was observed that MG63 and MRC5 behave differently after 14 days of culture. The aligned PA6/CNT network induces more proliferation than the random PA6/CNT when cultured with osteoblasts, while it is observed a higher proliferation on the random PA6/CNT samples when cultured with fibroblasts. We assume that the presented result is related to the natural organization of the soft and hard tissues. Bone is known to have an anisotropic structure, while fibroblasts are most present in the ECM among random collagen fibers as can be seen in figure 4.24.

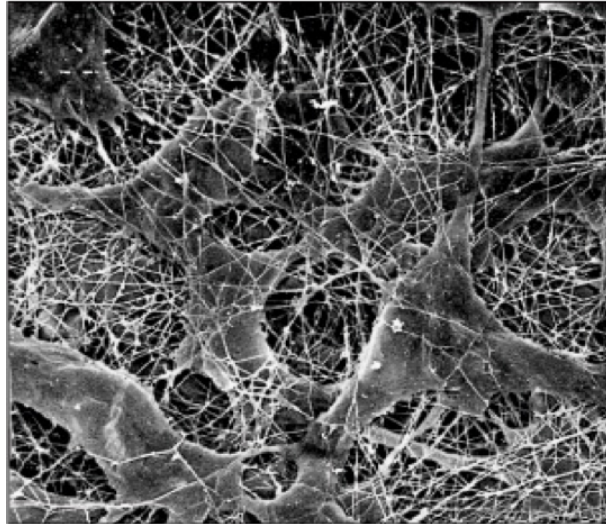


Figure 4.24: Fibroblasts surrounded by (collagen fibrils) a scaffold.

### 4.5.3 Cell viability

The cell viability was evaluated using confocal laser microscopy (CLM) after fluorescein diacetate-propidium iodide (FDA-PI). The results have shown the predominant presence of viable cells in all materials when cultured with both (MG63 and MRC5) cell lines. This results are in agreement with the alamar blue assay, which has shown an increase in cell number in each period of time. After 14 days cells were still viable and well distributed on the scaffolds surface. However, a few quantity of non viable cells are present in the networks cultured with MG63, most likely caused by the large number of cells on the surface.

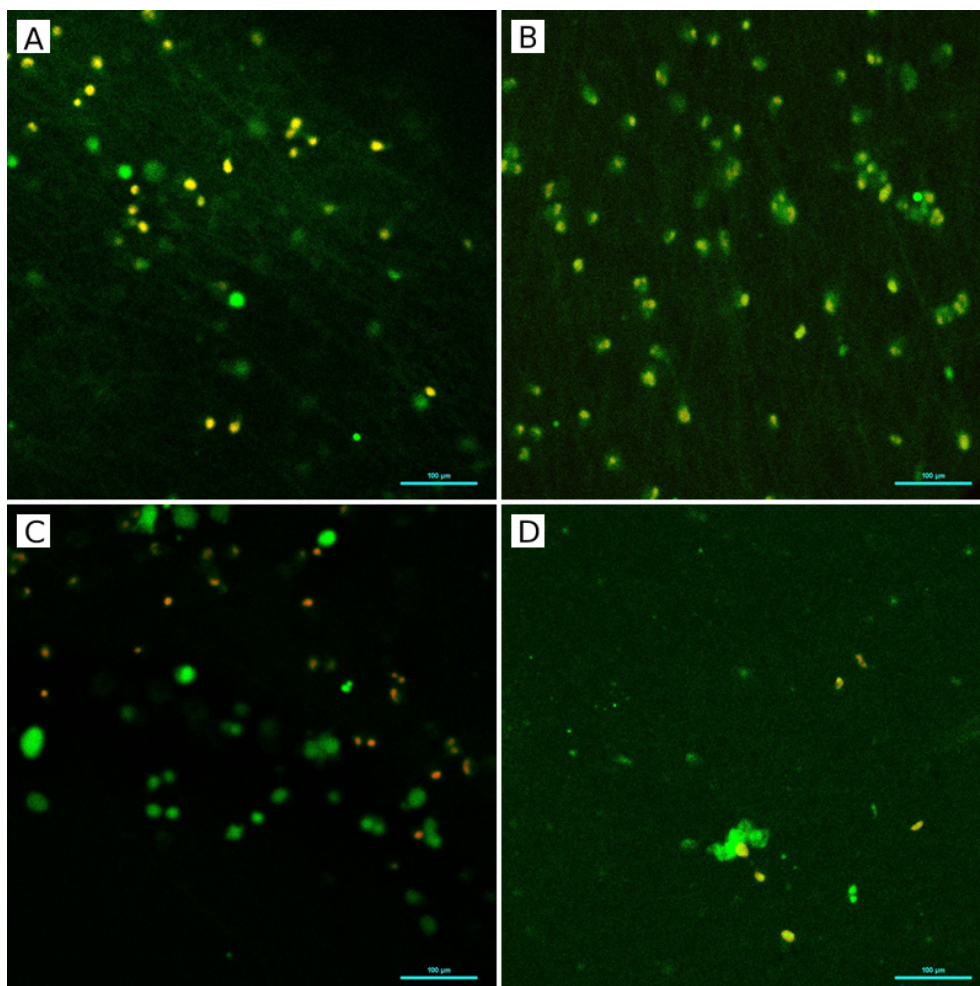


Figure 4.25: Cell viability analysis of MG63 cell culture on different surfaces for 3 days. (A) Random PA6, (B) Aligned PA6, (C) Random PA6/CNT and (D) Aligned PA6/CNT networks.

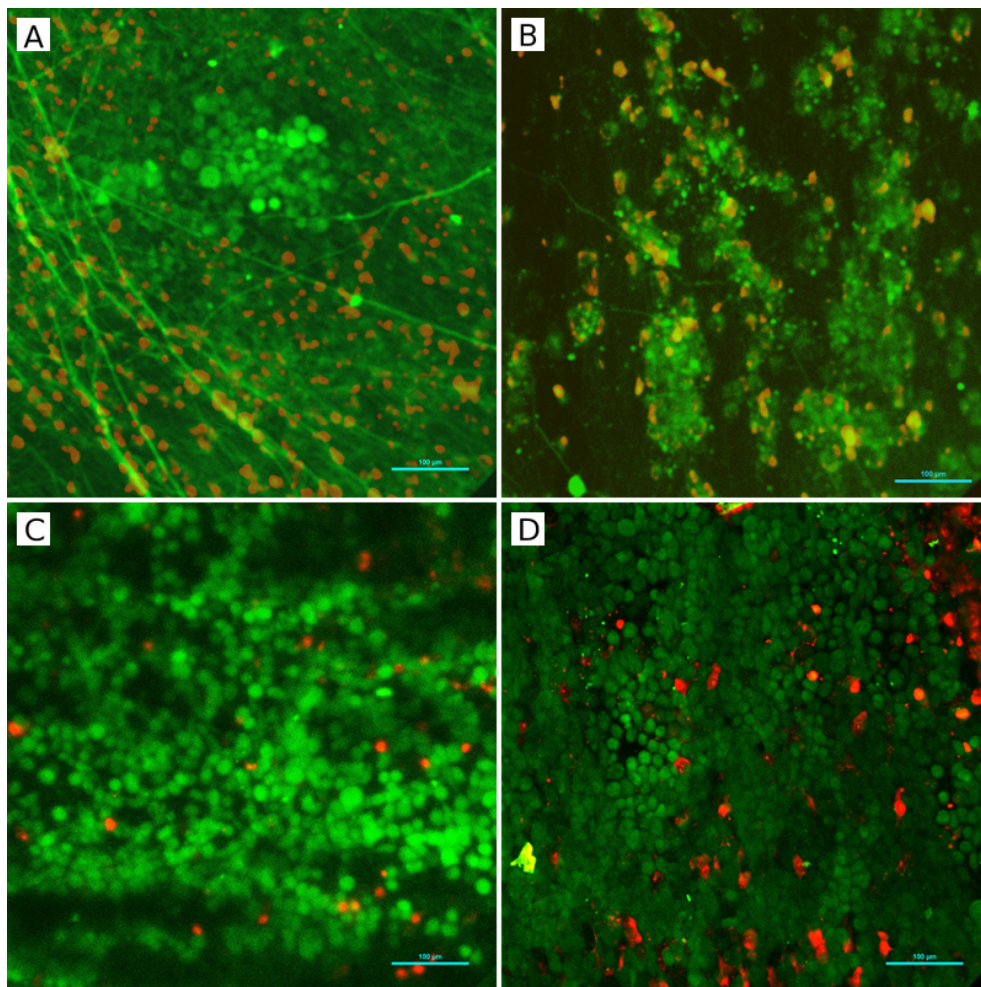


Figure 4.26: Cell viability analysis of MG63 cell culture on different surfaces for 7 days. (A) Random PA6, (B) Aligned PA6, (C) Random PA6/CNT and (D) Aligned PA6/CNT networks.

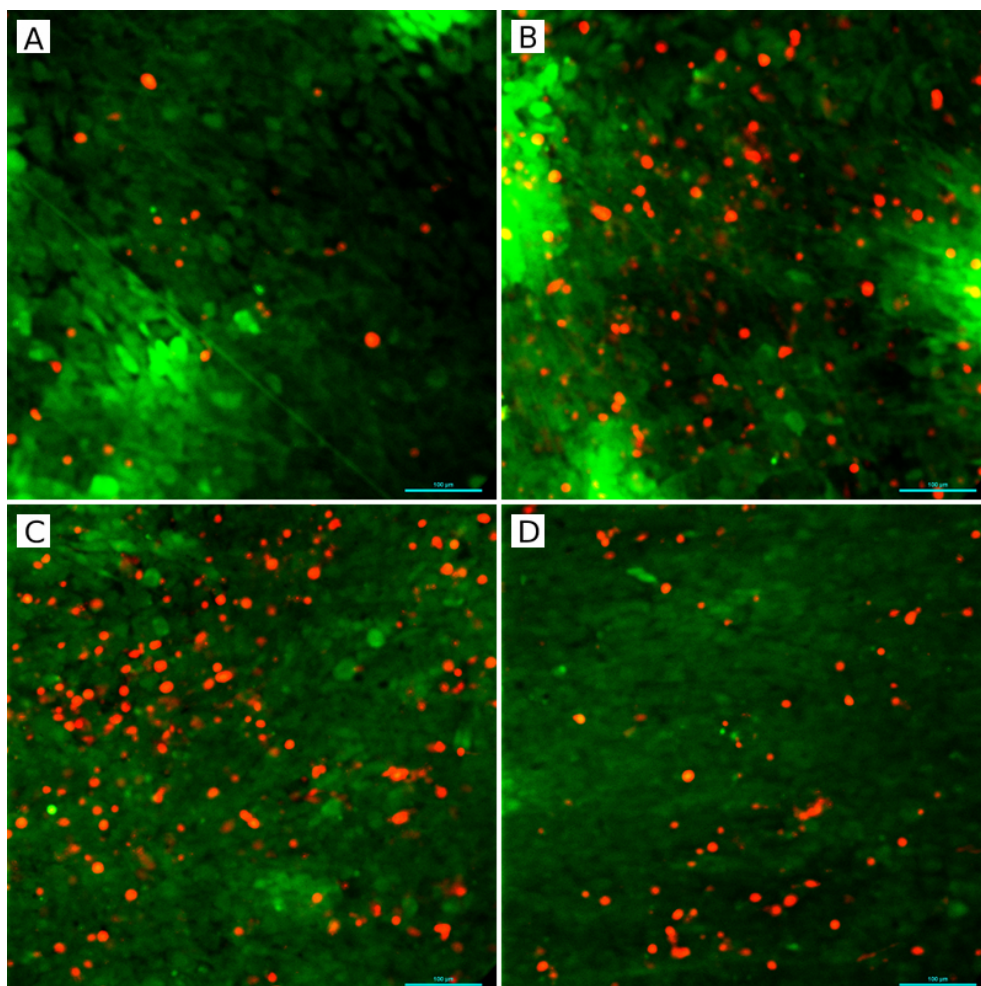


Figure 4.27: Cell viability analysis of MG63 cell culture on different surfaces for 14 days. (A) Random PA6, (B) Aligned PA6, (C) Random PA6/CNT and (D) Aligned PA6/CNT networks.

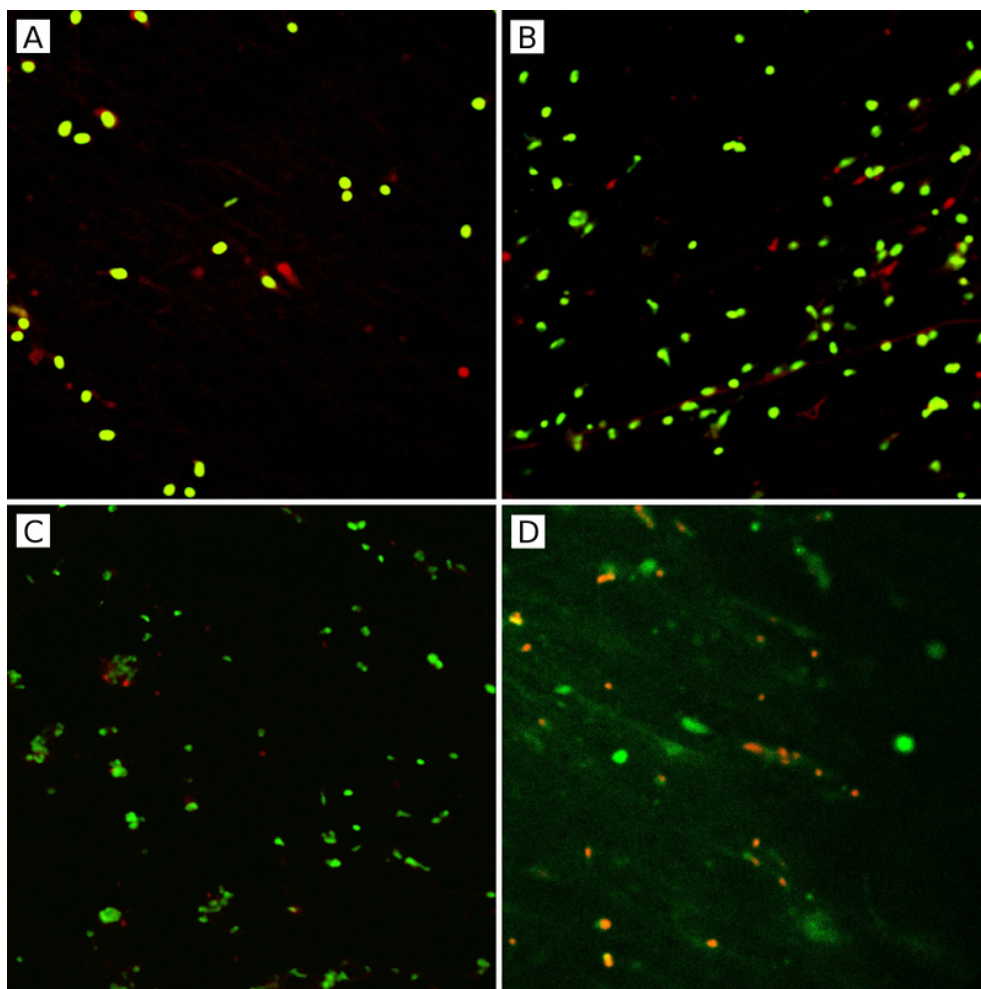


Figure 4.28: Cell viability analysis of MRC5 cell culture on different surfaces for 3 days. (A) Random PA6, (B) Aligned PA6, (C) Random PA6/CNT and (D) Aligned PA6/CNT networks.

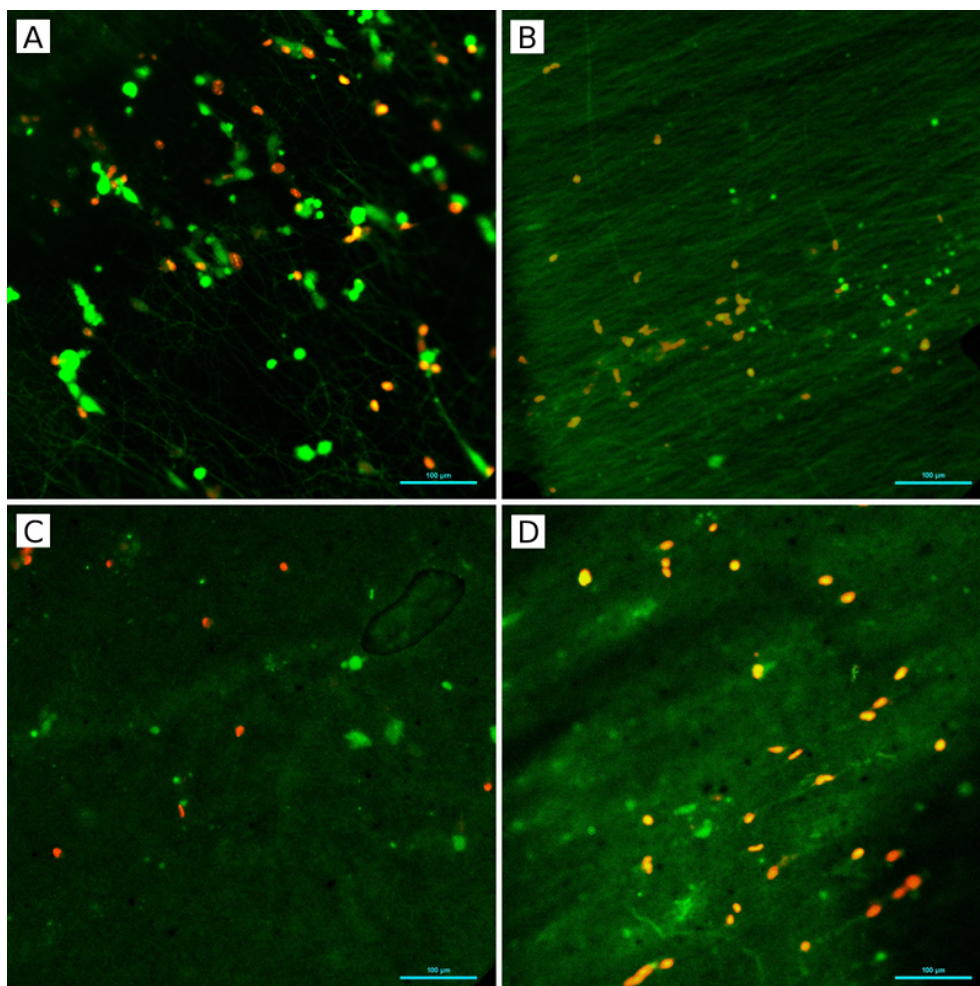


Figure 4.29: Cell viability analysis of MRC5 cell culture on different surfaces for 7 days. (A) Random PA6, (B) Aligned PA6, (C) Random PA6/CNT and (D) Aligned PA6/CNT networks.

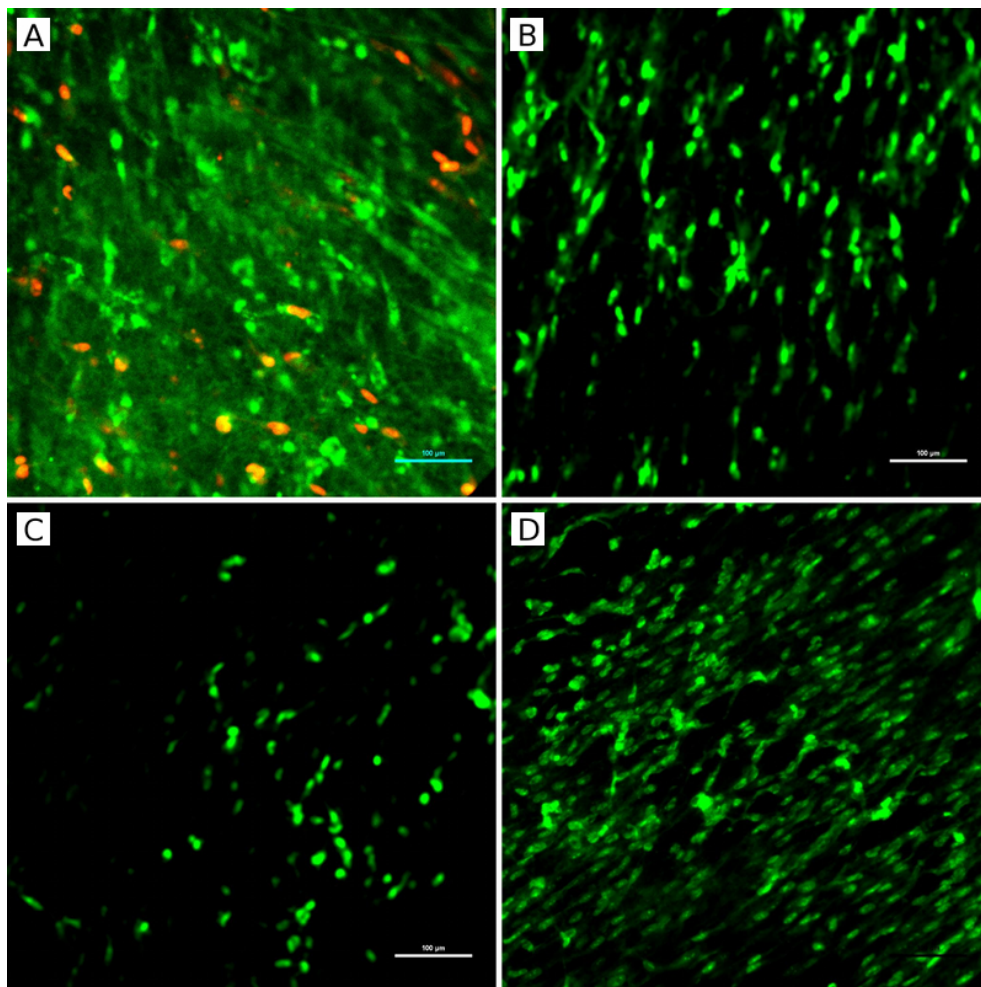


Figure 4.30: Cell viability analysis of MRC5 cell culture on different surfaces for 14 days. (A) Random PA6, (B) Aligned PA6, (C) Random PA6/CNT and (D) Aligned PA6/CNT networks.

#### 4.5.4 Cell morphology

The morphology of the cells cultured on the produced scaffolds was observed under SEM microscope. The interaction of biomaterials surfaces at the molecular level with proteins, ions and enzymes affect the behavior of the cells. The morphology is an important evaluation in order to un-

derstand how cells attach, organize and spread on the prepared materials.

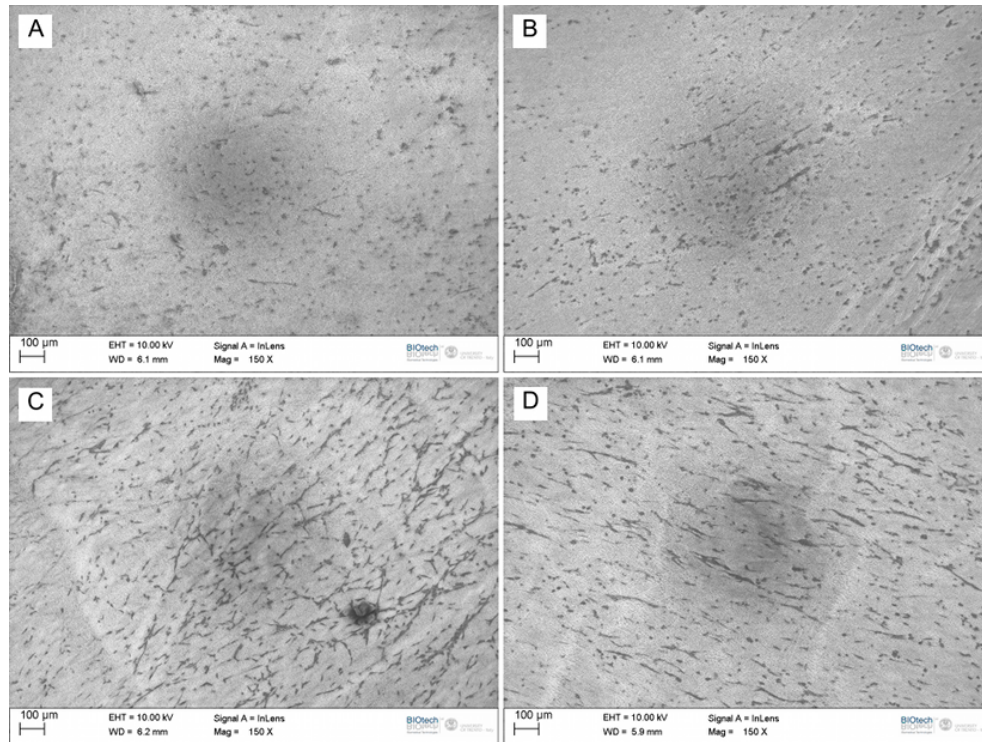


Figure 4.31: SEM images of MG63 cell culture on different surfaces for 3 days. (A) Random PA6, (B) Aligned PA6, (C) Random PA6/CNT and (D) Aligned PA6/CNT networks.

The morphology of MG63 cell line when cultured on the produced materials is presented in figures 4.31, 4.32 and 4.33 for 3, 7 and 14 days, respectively. Important information regarding the organization of the cells has been extracted from the low magnification SEM images. It is possible to observe in figures 4.31 and 4.32 the osteoblasts aligning themselves according to the fiber direction on the aligned networks, while no orientation is presented when cultured on the random networks. The alignment of the cell cytoskeletons when cultured on patterned surfaces has been intensively studied [76, 72, 120, 73, 55] and it is further con-

firmed with these experiments. After 14 days of culture, shown in figure 4.33, the composite nets present an enhanced homogeneous cell layer when compared with the neat polyamide.

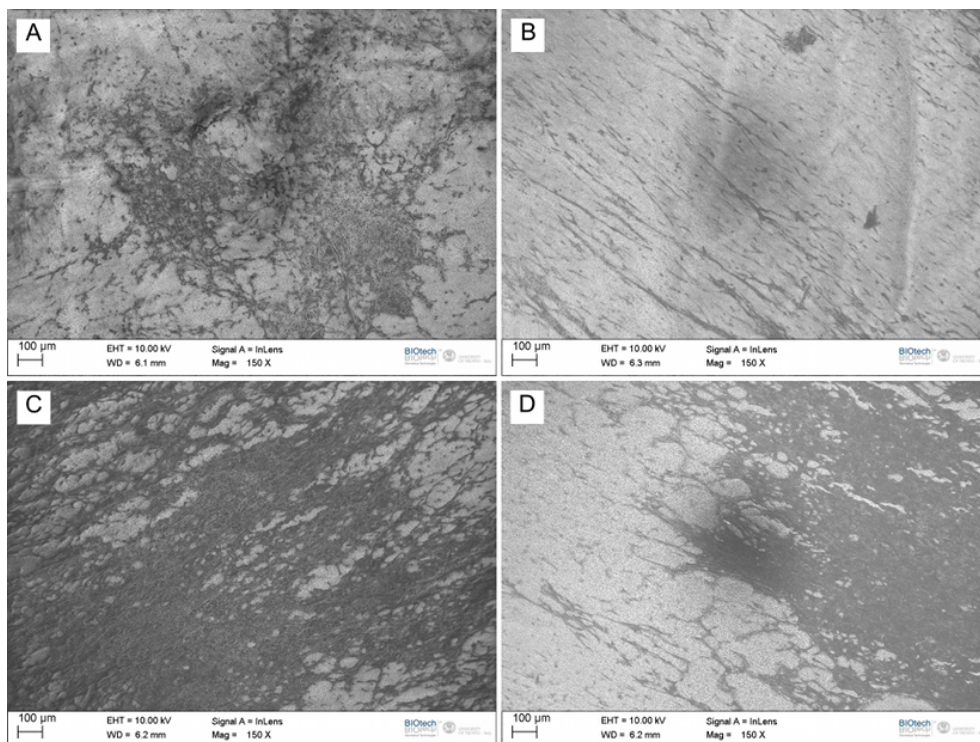


Figure 4.32: SEM images of MG63 cell culture on different surfaces for 7 days. (A) Random PA6, (B) Aligned PA6, (C) Random PA6/CNT and (D) Aligned PA6/CNT networks.

Interestingly, the alignment of the upper layer of osteoblasts when cultured on the aligned composite networks has been observed, while this organization was not evident on the aligned neat polyamide, as seen in figure 4.37. Since cell alignment is present in both networks at the early proliferation stages, as seen in figures 4.31 and 4.32, two explanations are proposed for these results. First, considering integrin-based receptors are the responsible for cell attachment [163, 164], the surface roughness displayed on the composite networks could have activated the

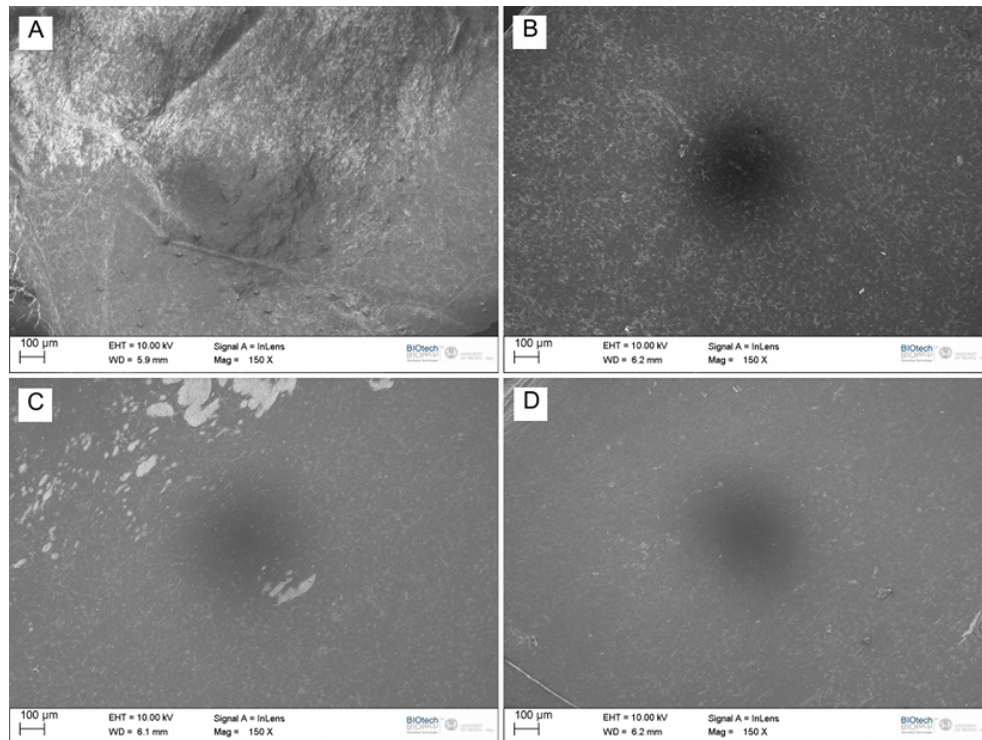


Figure 4.33: SEM images of MG63 cell culture on different surfaces for 14 days. (A) Random PA6, (B) Aligned PA6, (C) Random PA6/CNT and (D) Aligned PA6/CNT networks.

cells differently. They also play a role in cell signaling and thereby define cellular shape, mobility, and regulate the cell cycle. The second hypothesis is that the density of the first cell layer regulates how the subsequent layers will organize. Evidence of this is the higher density of cells on the composite networks.

The morphology of MRC5 cell line was also studied at 3, 7 and 14 days and shown in figures 4.34, 4.35 and 4.36, respectively. The fibroblasts, similarly to MG63, displays an aligned morphology when cultured on the aligned networks, while no cell alignment is present in the random nets. Interestingly, according to the alamar blue results, no significant variation on cell density appears on the tested networks at day 7, while at

day 14 the cell density in the composite nets are clearly higher. It seems that fibroblasts take longer to attach, activate and grow. Nevertheless, at day 14, the fibroblasts are almost in confluence, which confirms the alamar blue results.

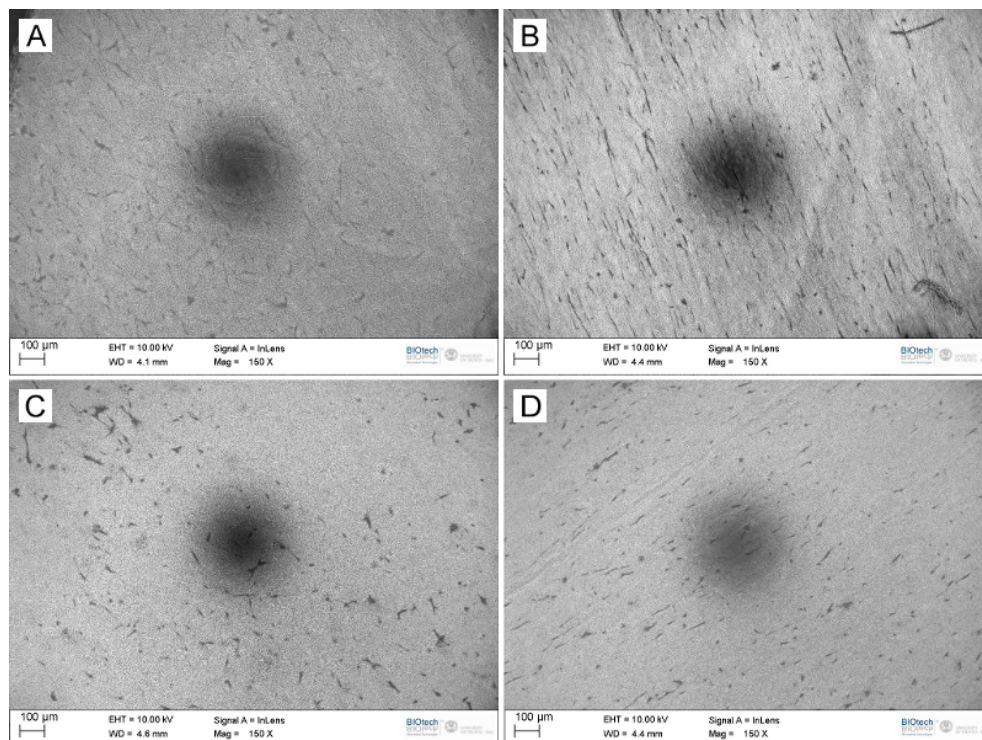


Figure 4.34: SEM images of MRC5 cell culture on different surfaces for 3 days. (A) Random PA6, (B) Aligned PA6, (C) Random PA6/CNT and (D) Aligned PA6/CNT networks.

Tissue integration is one of the most important properties that an implanted material must have. Among the parameters that regulate tissue integration are material porosity, pore size, affinity between scaffold and tissue and scaffold composition. Tissue integration has shown to be an important concern in electrospun nets especially because of the small porous size present in the produced networks. Cell ingrowth has shown to be diminished in electrospun nets [126, 10, 165]. However, significant

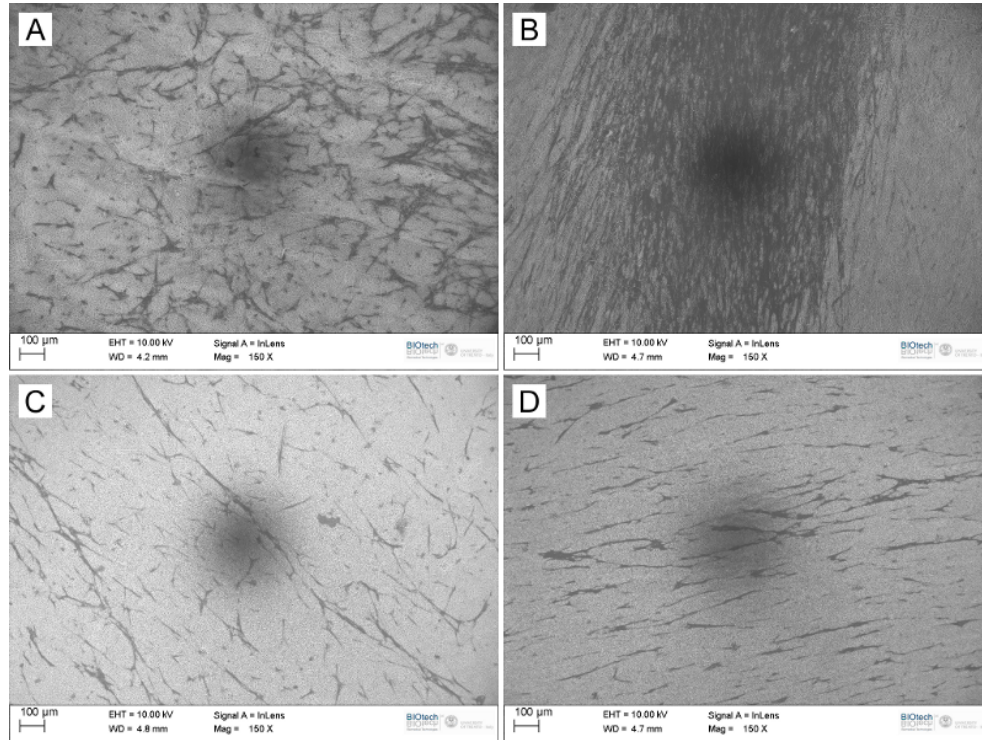


Figure 4.35: SEM images of MRC5 cell culture on different surfaces for 7 days. (A) Random PA6, (B) Aligned PA6, (C) Random PA6/CNT and (D) Aligned PA6/CNT network.

cell ingrowth was observed in our nets when cultured with either MG63 and MRC5 cell lines, as can be seen in figures 4.38 and 4.39. Our results show it is possible to observe that the cells can penetrate the outer fiber layers, which allow us to speculate that this material would have a better integration with natural tissues. Furthermore, it is important to highlight how cells surround the single fibers, which confirm the hypothesis of enhancement of the tissue integration. Although this result is not common in electrospun nets, we assume that it is related to the production parameters selected for this work. It is believed that the complete evaporation of the solvent occur before the fibers hit the grounded target,

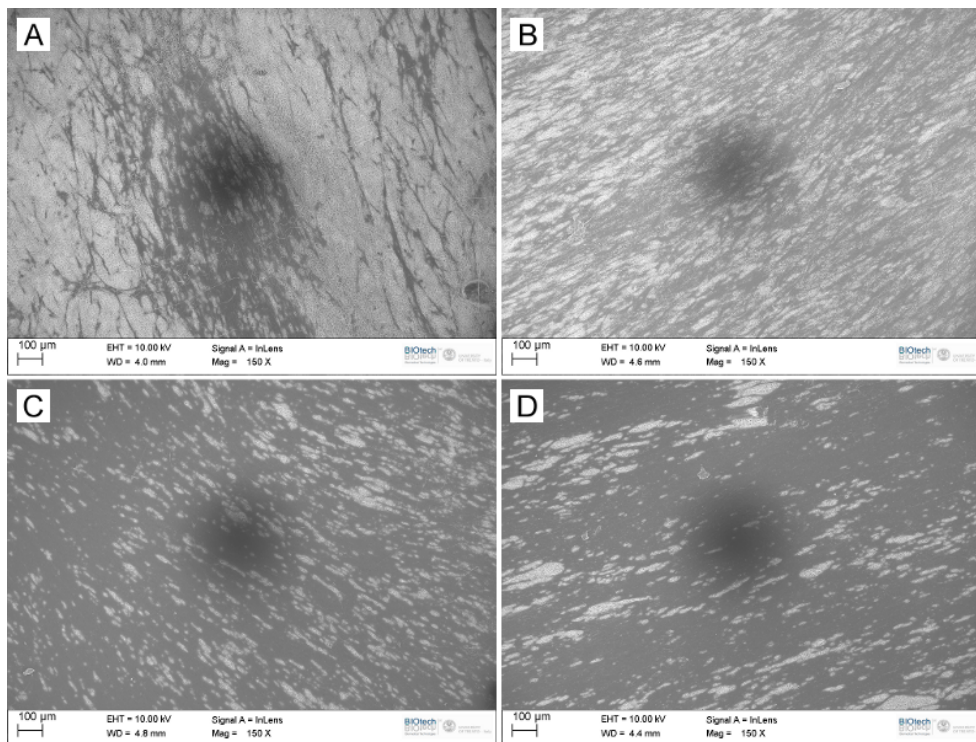


Figure 4.36: SEM images of MRC5 cell culture on different surfaces for 14 days. (A) Random PA6, (B) Aligned PA6, (C) Random PA6/CNT and (D) Aligned PA6/CNT networks.

which reduces the fiber connectivity, ultimately permitting the cells to penetrate when the sample is swollen as can be seen in figure 4.40.

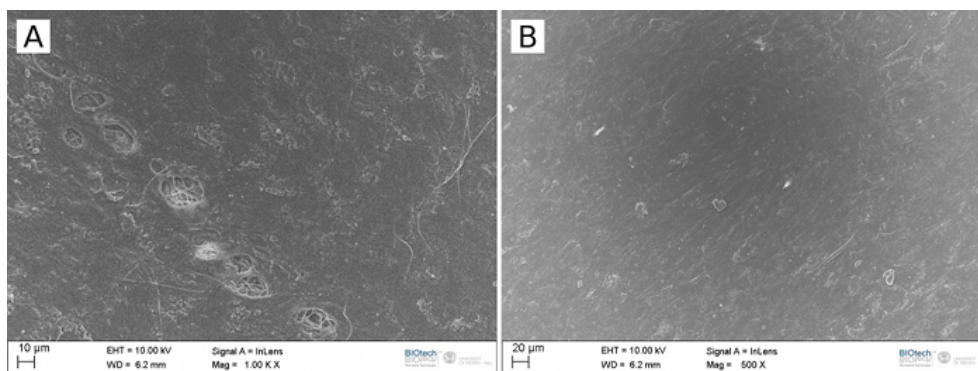


Figure 4.37: Micrography depicting the upper cell layer alignment after 14 days of culture with MG63. Aligned (A) PA6 and (B) PA6/CNT network.

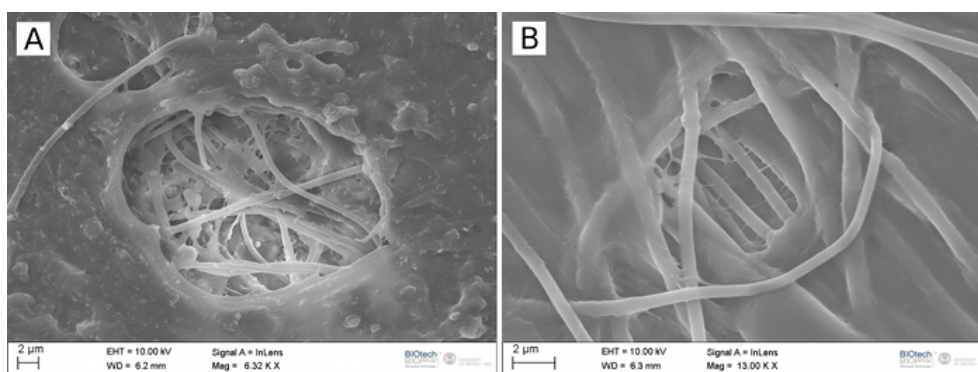


Figure 4.38: High magnification SEM micrography depicting the cellular ingrowth on the scaffolds surface after 14 days of culture with MG63. Aligned (A) PA6 and (B) PA6/CNT network.

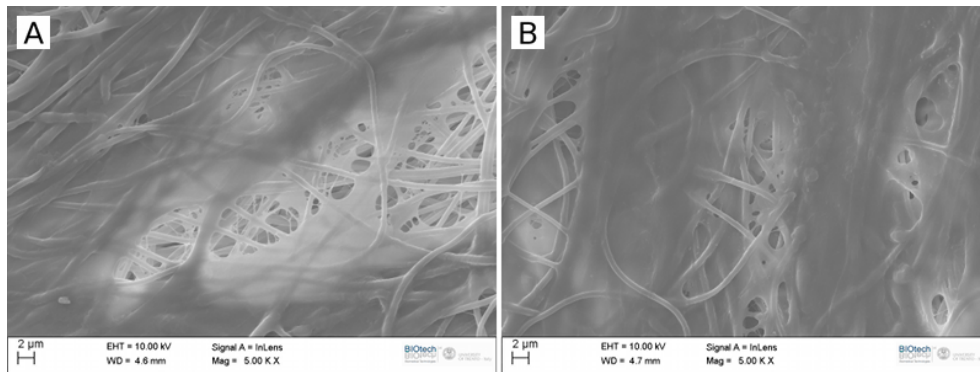


Figure 4.39: High magnification SEM micrograph illustrating the cellular ingrowth on the scaffolds surface after 14 days of culture with MRC5. (A) Aligned PA6 and (B) Random PA6/CNT network.

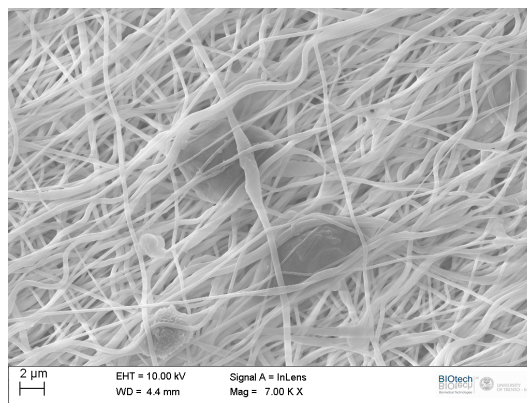


Figure 4.40: High magnification SEM micrograph depicting the cellular penetration in the outer nanofibers of the aligned PA6/CNT at 3 days of culture with MRC5.

# Chapter 5

## CONCLUSIONS

Tissue engineering, involving the use of living cells and extracellular components from either natural and synthetic polymers, aims to regenerate tissue and restore or replace biological structures.

Electrospinning has shown to be an important technique to be applied in the biomedical field. The opportunity to tune the fiber properties increases its potential. This work has applied electrospinning to produce the novel composite system previous described. The technique allowed the production of tunable network morphologies, highly aligned or random, as well as the dispersion and alignment of the multi-walled carbon nanotubes within the polymer matrix. Furthermore, consequences of the electrospinning process, such as polymer concentration, solvent evaporation and fiber stretching, combined with the presence of the MWCNT filler resulted in the formation of surface roughness. This formation has been verified also by AFM and TEM analyses.

The tuned morphology produced was further confirmed by the mechanical experiments. It was demonstrated that the electrospun fibers were able to align in the spinning axis which resulted in the diverse mechanical properties in the network. Additionally, the tensile properties showed no significant enhancement when the filler was added, which we

assume is the consequence of the poor interfacial adhesion and the residual solution aggregates. The solution aggregates caused defects on the fiber surface which was evidenced by the TEM images. Nevertheless, the materials presented favorable mechanical properties. It suggests the possibility of using these networks for applications where low mechanical support is required, such as vertebra and spongy bone scaffolds, nerve or skin regeneration.

Tissue integration is a prerequisite for implant success. Several features can affect tissue integration such as porosity, pore size, affinity between scaffold and tissue, surface chemistry, topography, and scaffold composition. The biological evaluation presented in this work aimed to assess the behavior of two different tissue models (hard and soft) when in contact with the produced materials. Results indicated the enhancement of the proliferation of both cell lines when cultured on the composite system when compared to the raw material. As previously published, we assume these results are related to the surface roughness prior discussed in this manuscript. The qualitative analysis of protein adsorption did not show significant difference between the produced materials. There was no clear evidence of the presence of the specific proteins related to the cell attachment, proliferation and migration. We suppose the analysis was not sensitive enough to provide evidence of the low protein amount.

Furthermore, the cell morphology was extremely dependent of the cultured surface. We have been able to modify the cell shape when cultured on an aligned or random network. It was observed the elongation of the cell cytoskeleton along with the fibers in the aligned network, while completely random cell morphology was observed when cultured on random networks.

These are encouraging results for the application of these networks in the biomedical field. Fiber diameter, network morphology, mechanical properties and surface roughness are some of the composite features that

can be adjusted to mimic the target tissue to be replaced or regenerated. Scientists can apply this system aiming to enhance biological responses, patient quality life, easy of application and process simplicity.



## Chapter 6

### FUTURE INVESTIGATIONS

The future investigations has to fulfil the lacks on the mechanical properties, stability of the matrix and biological interaction between scaffold and cells. Analyses under electrical and mechanical stimuli should also be carried out.

As is well known, the interfacial adhesion in composites plays an important role on the final mechanical properties. The poor adhesion between filler and matrix would reduce the properties, since it would work as defects instead load transfers. For this project we have been using surface modified carbon nanotubes, as received. Previous analysis by XPS have shown the low amount of carboxyl and hydroxyl groups present at the CNT surface. We expect to improve the chemical interactions between CNT/polymer by the further functionalization of the filler. The presence of higher amount of reactive groups at the CNT surface should enhance the chemical interaction with the polymer and then increase the mechanical behaviour. There is also the possibility of using metal complexes to cross-link the composite and most probably enhance the chemical interaction of the interface.

It is also extremely relevant the stability of matrix. There are several published studies that report the cytotoxicity of carbon nanotubes

when in contact with the human tissue, in this context it is interesting to evaluate how and if the nanotubes will be released in the biological environmental. We have selected slow bioresorbable polymers for this project, however is important to analyse the behaviour of the matrix when in contact with simulated body fluids. This would allow us to start with in vivo experiments.

In this thesis, it was presented the different cell behavior when cultured in our surfaces. We believe that is an important point understand how and why cells respond differently to this patterned surfaces. Many authors are studying this behavior lately, however this behavior is still not fully understood. Human cells have different responses also when incubated under electrical and mechanical stimuli. Morphology, proliferation and activation of the cells can be affected by these stimuli. We expect to evaluate the behaviour of the cells when incubated under defined conditions.

## Chapter 7

# ACKNOWLEDGEMENTS

I would like to acknowledge to all of them that have contributed to the realization of the PhD school in the University of Trento, especially to:

My parents, José Assis Volpato and Josiane Zomer Volpato, which have always supported me during all these years. My brother, Fernando Zomer Volpato, for the advices and comprehension in all difficult times.

My advisor, Professor Claudio Migliaresi for his patience, incentive, financial and intellectual support during this PhD course.

Dr. Antonella Motta for her assistance on the biological sections of this work.

My colleagues from the laboratory Beppe, Cristina, Christian, Dario, David, Eleonora, Enrico, Eva, Gian, LDB, Luca, Lucia, Matteo, Mari, Massimo, Mike, Traina and Walter for the long work discussions, beer and football during all these years.

My friends André, Tatiani, Nério, Camila, Palloma, Ketner, Mike and Lea for their friendship and relaxing times spent together.



# Bibliography

- [1] J. F. Cooley. Apparatus for electrically dispersing fluids, 1902.
- [2] Jon Stanger, Nick Tucker, and Mark Staiger. *Electrospinning*, volume 16. Rapra, 2005.
- [3] Ji-huan He, Yong Liu, Lu-Feng Mo, Yu-Qin Wan, and Lan Xu. *Electrospun Nanofibres and Their Applications*. iSmithers, 2008.
- [4] Anthony L. Andrady. *Science and Technology of Polymer Nanofibers*. John Wiley & Sons, 2008.
- [5] D. H. Reneker, W Kataphinan, A. Theron, E. Zussman, and A. L. Yarin. Nanofiber garlands of polycaprolactone by electrospinning. *Polymer*, 43(25):6785–6794, 2002.
- [6] Lingyu Li, Bing Li, Matthew A. Hood, and Christopher Y. Li. Carbon nanotube induced polymer crystallization: The formation of nanohybrid shish–kebabs. *Polymer*, 50(4):953–965, 2009.
- [7] Paul K. Chu and Xuanyong Liu, editors. *Biomaterials Fabrication and Processing Handbook*. CRC Press, 2008.
- [8] R Langer and J. Vacanti. Tissue engineering. *Science*, 260(5110):920–926, 1993.

- [9] T. Livingston Arinzeh, T. Tran, J. Mcalary, and G. Daculsi. A comparative study of biphasic calcium phosphate ceramics for human mesenchymal stem-cell-induced bone formation. *Biomaterials*, 26:3631–3638, 2005.
- [10] Paulo Bártolo and Bopaya Bidanda, editors. *Bio-Materials and Prototyping Applications in Medicine*. Springer, 2008.
- [11] Mariangela Fedel, Antonella Motta, Devid Maniglio, and Claudio Migliaresi. Surface properties and blood compatibility of commercially available diamond-like carbon coatings for cardiovascular devices. *Journal of biomedical materials research. Part B: Applied biomaterials*, 90(1):338–49, 2009.
- [12] Teoh Swee Hin, editor. *Engineering Materials for Biomedical Applications*. World Scientific, 2004.
- [13] J Meng, H Kong, H Y Xu, L Song, C Y Wang, and S S Xie. Improving the blood compatibility of polyurethane using carbon nanotubes as fillers and its implications to cardiovascular surgery. *Journal of biomedical materials research. Part A*, 74(2):208–14, 2005.
- [14] W. Eugene Roberts and James K. Jr. Hartsfield. Bone Development and Function: Genetic and Environmental Mechanisms. *Seminar in Orthodontics*, 10(2):100–122, 2004.
- [15] G. I. Taylor. Deposition of a viscous fluid on the wall of a tube. *Journal of Fluid Mechanics*, 10(02):161–165, 1961.
- [16] Eugene D. Boland, Jamil A. Matthews, Kristin J. Pawlowski, David G. Simpson, Gary E. Wnek, and Gary L. Bowlin. Electrospinning collagen and elastin: preliminary vascular tissue . . . . *Frontiers in Bioscience*, 9:1422–1432, 2004.

- [17] D.S. Katti, K.W. Robinson, F.K. Ko, and C.T. Laurencin. Biore-sorbable nanofiber-based systems for wound healing and drug deliv-ery: optimization of fabrication parameters. *Journal of Biomedical Materials Research*, 70(2):286–296, 2004.
- [18] G. Verreck, I. Chun, J. Peeters, J. Rosenblatt, and M.E. Brew-ster. Preparation and characterization of nanofibers containing amorphous drug dispersions generated by electrostatic spinning. *Pharmaceutical research*, 20(5):810–817, 2003.
- [19] Yael Dror, Wael Salalha, Rafail L. Khalfin, Yachin Cohen, Alexan-der L. Yarin, and Eyal Zussman. Carbon Nanotubes Embedded in Oriented Polymer Nanofibers by Electrospinning. *Langmuir*, 19(17):7012–7020, 2003.
- [20] Frank Ko, Yury Gogotsi, Ashraf Ali, Nevin Naguib, Haihui Ye, Guoliang Yang, Christopher Li, and Peter Willis. Electrospinning of Continuous Carbon Nanotube-Filled Nanofiber Yarns. *Advanced Materials*, 15(14):1161–1165, 2003.
- [21] Matthew G. Mckee, Taigyoo Park, Serkan Unal, Iskender Yil-gor, and Timothy E. Long. Electrospinning of linear and highly branched segmented poly(urethane urea)s. *Polymer*, 46:2011–2015, 2005.
- [22] Kousaku Ohkawa, Dongil Cha, Hakyong Kim, Ayako Nishida, and Hiroyuki Yamamoto. Electrospinning of Chitosan. *Macromolecules*, 25:1600–1605, 2004.
- [23] Xinfeng Shi, Balaji Sitharaman, Quynh P. Pham, Feng Liang, Katherine Wu, W. Edward Billups, Lon J. Wilson, and Antonios G. Mikos. Fabrication of porous ultra-short single-walled carbon nan-otube nanocomposite scaffolds for bone tissue engineering. *Biomaterials*, 28:4078–4090, 2007.

- [24] Benjamin S. Harrison and Anthony Atala. Carbon nanotube applications for tissue engineering. *Biomaterials*, 28:344–353, 2007.
- [25] Masanori Kikuchi, Yoshihisa Koyama, Takeki Yamada, Yukari Imamura, Takao Okada, Noriaki Shirahama, Kazumi Akita, Kazuo Takakuda, and Junzo Tanaka. Development of guided bone regeneration membrane composed of  $\beta$ -tricalcium phosphate and poly (-lactide-co-glycolide-co-[var epsilon]-caprolactone) composites. *Biomaterials*, 25(28):5979 – 5986, 2004.
- [26] M. Kobayashi, T. Kikutani, T. Kokubo, and T. Nakamura. Direct bone formation on alumina bead composite. *Journal of biomedical materials research*, 37(4):554–565, 1997.
- [27] V. Sanginario, M.P. Ginebra, K.E. Tanner, J.A. Planell, and L. Ambrosio. Biodegradable and semi-biodegradable composite hydrogels as bone substitutes: morphology and mechanical characterization. *Journal of Materials Science: Materials in Medicine*, 17(5):447–454, 2006.
- [28] C. Stephan, T. P. Nguyen, M. Lamy De La Chapelle, S. Lefrant, C. Journet, and P. Bernier. Characterization of singlewalled carbon nanotubes-PMMA composites. *Synthetic Metals*, 108:139–149, 2000.
- [29] K. Tanaka and H. Kozuka. Preparation of acetylcellulose/silica composites by sol-gel method and their mechanical properties. *Journal of Materials Science*, 40(19):5199–5206, 2005.
- [30] A. Krishnan, E. Dujardin, T. W. Ebbesen, P. N. Yianilos, and M. M. J. Treacy. Young’s modulus of single-walled nanotubes. *Physical Review B*, 58(20):14013–14019, 1998.

- [31] Min-Feng Yu, Oleg Lourie, Mark J. Dyer, Katerina Moloni, Thomas F. Kelly, and Rodney S. Ruoff. Strength and breaking mechanism of multiwalled carbon nanotubes under tensile load. *Science*, 287(28):637–640, 2000.
- [32] D. B. Warheit, B. R. Laurence, K. L. Reed, D. H. Roach, G. A. M. Reynolds, and T. R. Webb. Comparative pulmonary toxicity assessment of single-wall carbon nanotubes in rats. *Toxicological Sciences*, 77:117–125, 2004.
- [33] P. Cherukuri, S. M. Bachilo, S. H. Litovsky, and R. B. Weisman. Near-infrared fluorescence microscopy of single-walled carbon nanotubes in phagocytic cells. *Journal of the American Chemical Society*, 126:15638–15639, 2004.
- [34] H.X. Ren, X. Chen, J.H. Liu, N. Gu, and X.J. Huang. Toxicity of single-walled carbon nanotube: How we were wrong? *Materials Today*, 13(1-2):6–8, 2010.
- [35] Ben D. MacArthur and Richard O. C. Oreffo. Bridging the gap. *Nature*, 433(7021):19, 2005.
- [36] T-W. Chung, D-Z. Liu, S-Y. Wang, and S-S. Wang. Enhancement of the growth of human endothelial cells by surface roughness at nanometer scale. *Biomaterials*, 24:4655–4661, 2003.
- [37] Michael Strosio and Mitra Dutt, editors. *Biological Nanostructures and Applications of Nanostructures in Biology: Electrical, mechanical and Optical Properties*. Kluwer Academic Publishers, 2004.
- [38] Thomas J. Webster, Michael C. Waid, Janice L. McKenzie, Rachel L. Price, and Jeremiah U. Ejiofor. Nano-biotechnology:

- carbon nanofibres as improved neural and orthopaedic implants. *Nanotechnology*, 15(1):48–54, 2004.
- [39] Chih-sheng Ko, Jui-pin Huang, Chia-wen Huang, and I-ming Chu. Type II collagen-chondroitin sulfate-hyaluronan scaffold cross-linked by genipin for cartilage tissue engineering. *Journal of Bioscience and Bioengineering*, 107(2):177–182, 2009.
- [40] Nathan A. Mauntler, Tony L. Schmitz, and John C. Ziegert. The Influence of Process Variation on a Cortical Bone Interference Fit Pin Connection. *Journal of Manufacturing Science and Engineering*, 130:1–7, 2008.
- [41] C. E. Schmidt, V. R. Shastri, J. P. Vacanti, and R. Langer. Stimulation of neurite outgrowth using an electrically conducting polymer. *Proceedings of the National Academy of Sciences of the United States of America*, 94(August):8948–8953, 1997.
- [42] Yongzhong Wang, Darya D. Rudym, Ashley Walsh, Lauren Abrahamsen, Hyeon-joo Kim, Hyun S. Kim, Carl Kirker-Head, and David L. Kaplan. Biomaterials In vivo degradation of three-dimensional silk fibroin scaffolds. *Biomaterials*, 29:3415–3428, 2008.
- [43] Wei-Bor Tsai, Chun-Hong Chen, Jing-Fu Chen, and Ken-Yuan Chang. The effects of types of degradable polymers on porcine chondrocyte adhesion , proliferation and gene expression. *Journal of materials Science: Materials in Medicine*, 17:337–343, 2006.
- [44] Archel M. A. Ambrosio, Janmeet S. Sahota, Yusuf Khan, and Cato T. Laurencin. A novel amorphous calcium phosphate polymer ceramic for bone repair: I. Synthesis and characterization. *Journal of Biomedical Materials Research*, 58:295–301, maio 2001.

- [45] Han Gi Chae, Marilyn L Minus, and Satish Kumar. Oriented and exfoliated single wall carbon nanotubes in polyacrylonitrile. *Polymer*, 47:3494–3504, 2006.
- [46] Chin-san Wu and Hsin-tzu Liao. Study on the preparation and characterization of biodegradable polylactide/multi-walled carbon nanotubes nanocomposites. *Polymer*, 48:4449–4458, 2007.
- [47] Hockin H. K. Xu, Douglas T. Smith, and Carl G. Simon. Strong and bioactive composites containing nano-silica-fused whiskers for bone repair. *Biomaterials*, 25:4615–4626, 2004.
- [48] Byung-Soo Kim and David J. Mooney. Development of biocompatible synthetic extracellular matrices for tissue engineering. *Trends in Biotechnology*, 16(5):224–230, 1998.
- [49] Lorenz Meinel, Sandra Hofmann, Vassilis Karageorgiou, Carl Kirker-Head, John McCool, Gloria Gronowicz, Ludwig Zichner, Robert Langer, Gordana Vunjak-Novakovic, and David L Kaplan. The inflammatory responses to silk films in vitro and in vivo. *Biomaterials*, 26:147–55, 2005.
- [50] F. Witte, H. Ulrich, M. Rudert, and E. Willbold. Biodegradable magnesium scaffolds: Part 1: appropriate inflammatory response. *Journal of biomedical materials research. Part A*, 81(3):748–56, 2007.
- [51] J. E. Bergsma, F. R. Rozema, R. R. M. Bos, G. Boering, W. C. De Bruijn, and A. J. Pennings. In vivo degradation and biocompatibility study of in vitro pre-degraded as-polymerized polylactide particles. *Biomaterials*, 16(4):267–274, 1995.
- [52] I. V. Yannas. *Classes of materials used in medicine: natural materials*. Elsevier Academic Press, 2004.

- [53] R. A. Brown, M. Wiseman, C.-B. Chuo, U. Cheema, and S. N. Nazhat. Ultrarapid Engineering of Biomimetic Materials and Tissues: Fabrication of Nano- and Microstructures by Plastic Compression. *Advanced Functional Materials*, 15(11):1762–1770, 2005.
- [54] L. Buttafoco, N. G. Kolkman, P. Engbers-Buijtenhuijs, A. A. Poot, P. J. Dijkstra, I. Vermes, and J. Feijen. Electrospinning of collagen and elastin for tissue engineering applications. *Biomaterials*, 27(5):724–34, 2006.
- [55] Dehai Liang, Benjamin S. Hsiao, and Benjamin Chu. Functional electrospun nanofibrous scaffolds for biomedical applications. *Advanced Drug Delivery Reviews*, 59:1392 – 1412, 2007.
- [56] Takahiro Morita, Yuji Horikiri, Takehiko Suzuki, and Hiroyuki Yoshino. Preparation of gelatin microparticles by co-lyophilization with poly(ethylene glycol): characterization and application to entrapment into biodegradable microspheres. *International Journal of Pharmaceutics*, 219:127–37, maio 2001.
- [57] A. Motta, C. Migliaresi, A. W. Lloyd, St. P. Denyer, and M. Santin. Serum Protein Absorption on Silk Fibroin Fibers and Films: Surface Opsonization and Binding Strength. *Journal of Bioactive and Compatible Polymers*, 17(1):23–35, janeiro 2002.
- [58] P. Gunatillake, R. Mayadunne, and R. Adhikari. Recent developments in biodegradable synthetic polymers. *Biotechnology Annual Review*, 12:301–347, 2006.
- [59] S. M. Zhang, J. Liu, W. Zhou, L. Cheng, and X. D. Guo. Interfacial fabrication and property of hydroxyapatite/poly(lactide) resorbable bone fixation composites. *Current Applied Physics*, 5:516–518, 2005.

- [60] X. Deng, S. Zhou, X. Li, J. Zhao, and M. Yuan. In vitro degradation and release profiles for poly-dl-lactide-poly(ethylene glycol) microspheres containing human serum albumin. *Journal of the Controlled Release*, 71:165–173, abril 2001.
- [61] Todd C. McDevitt, Kimberly A. Woodhouse, Stephen D. Hauschka, Charles E. Murry, and Patrick S. Stayton. Spatially organized layers of cardiomyocytes on biodegradable polyurethane films for myocardial repair. *Biomedical Materials Research A*, 66:586–595, 2003.
- [62] John J. Stankus, Jianjun Guan, and William R. Wagner. Fabrication of biodegradable elastomeric scaffolds with sub-micron morphologies. *Journal of Biomedical Materials Research. Part A*, 70(4):603–14, 2004.
- [63] Ingo N. G. Springer, Bernd Fleiner, Soren Jepsen, and Yahya Acil. Culture of cells gained from temporomandibular joint cartilage on non-absorbable scaffolds. *Biomaterials*, 22:2569–2577, 2001.
- [64] Huanan Wang, Yubao Li, Yi Zuo, Jihua Li, Sansi Ma, and Lin Cheng. Biocompatibility and osteogenesis of biomimetic nano-hydroxyapatite/ polyamide composite scaffolds for bone tissue engineering. *Biomaterials*, 28:3338–3348, 2007.
- [65] F. L. Matthews and R. D. Rawlings. *Composite materials: engineering and science*. Woodhead Publishing, 1999.
- [66] W. D. Callister. *Materials science and engineering: an introduction*. Wiley, New York, 2nd edition, 2003.
- [67] K. Chrissafis, G. Antoniadis, K. M. Paraskevopoulos, A. Vassiliou, and D. N. Bikiaris. Comparative study of the effect of different

- nanoparticles on the mechanical properties and thermal degradation mechanism of in situ prepared poly( $\epsilon$ -caprolactone) nanocomposites. *Composites Science and Technology*, 67:2165–2174, 2007.
- [68] P. R. Supronowicz, P. M. Ajayan, K. R. Ullmann, B. P. Arulananadam, D. W. Metzger, and R. Bizios. Novel current-conducting composite substrates for exposing osteoblasts to alternating current stimulation. *Journal of biomedical materials research*, 59(3):499–506, 2002.
- [69] V. Bounor-Legare, C. Angeloz, P. Blanc, P. Cassagnau, and A. Michel. A new route for organic-inorganic hybrid material synthesis through reactive processing without solvent. *Polymer*, 45(5):1485–1493, 2004.
- [70] S. L. Ruan, P. Gao, X. G. Yang, and T. X. Yu. Toughening high performance ultrahigh molecular weight polyethylene using multi-walled carbon nanotubes. *Polymer*, 44:5643–5654, 2003.
- [71] Blanca Vázquez, María Pau Ginebra, Xavier Gil, Josep Antón Planell, and Julio San Román. Acrylic bone cements modified with beta-TCP particles encapsulated with poly(ethylene glycol). *Biomaterials*, 26(20):4309–16, 2005.
- [72] Ngan F. Huang, Shyam Patel, Rahul G. Thakar, Jun Wu, Benjamin S. Hsiao, Benjamin Chu, Randall J. Lee, and Song Li. Myotube assembly on nanofibrous and micropatterned polymers. *Nano letters*, 6(3):537–542, 2006.
- [73] Dongwoo Khang, Jing Lu, Chang Yao, Karen M. Haberstroh, and Thomas J. Webster. The role of nanometer and sub-micron surface features on vascular and bone cell adhesion on titanium. *Biomaterials*, 29:970–983, 2008.

- [74] Shyam Patel, Kyle Kurpinski, Ryan Quigley, Hongfeng Gao, Benjamin S Hsiao, Mu-Ming Poo, and Song Li. Bioactive nanofibers: synergistic effects of nanotopography and chemical signaling on cell guidance. *Nano letters*, 7(7):2122–2128, 2007.
- [75] Chang-Hwan Choi, Sepideh H Hagvall, Benjamin M Wu, James C Y Dunn, Ramin E Beygui, and Chang-Jin CJ Kim. Cell interaction with three-dimensional sharp-tip nanotopography. *Biomaterials*, 28(9):1672–9, 2007.
- [76] M. J. Dalby, M. O. Riehle, H. Johnstone, S. Affrossman, and A. S. G. Curtis. In vitro reaction of endothelial cells to polymer demixed nanotopography. *Biomaterials*, 23(14):2945–54, julho 2002.
- [77] Ketul C. Popat, Lara Leoni, Craig A. Grimes, and Tejal A. Desai. Influence of engineered titania nanotubular surfaces on bone cells. *Biomaterials*, 28:3188–3197, 2007.
- [78] Sumio Iijima. Helical microtubes of graphitic carbon. *Nature*, 354(7):56–58, 1991.
- [79] M. S. Dresselhaus, G. Dresselhaus, and Ph. Avouris, editors. *Carbon Nanotubes*, volume 80. Topics in Applied Physics, 2001.
- [80] M. Meyyappan, editor. *Carbon Nanotubes Science and Applications*. CRC Press, 2005.
- [81] Rodney S. Ruoff, Dong Qian, and Wing Kam Liu. Mechanical properties of carbon nanotubes: theoretical predictions and experimental measurements. *Comptes Rendus Physique*, 4(9):993–1008, 2003.

- [82] Noriaki Hamada, Shin-ichi Sawada, and Atsushi Oshiyama. New one-dimensional conductors: Graphitic microtubules. *Physical Review Letters*, 68(10):1579–1581, 1992.
- [83] J. Mintmire, B. Dunlap, and C. White. Are fullerene tubules metallic? *Physical Review Letters*, 68(5):631–634, 1992.
- [84] Stefan Frank, Philippe Poncharal, Z. L. Wang, and Walt A. de Heer. Carbon nanotube quantum resistors. *Science*, 280:1744–1746, 1998.
- [85] Stefano Sanvito, Young-Kyun Kwon, David Tománek, and Colin J. Lambert. Fractional quantum conductance in carbon nanotubes. *Physical Review Letters*, 84(9):1974–1977, 2000.
- [86] Achim Hartschuh, Hermenegildo N. Pedrosa, Lukas Novotny, and Todd D. Krauss. Simultaneous fluorescence and Raman scattering from single carbon nanotubes. *Science*, 301:1354–1356, 2003.
- [87] Axel Hagen and Tobias Herbel. Quantitative analysis of optical spectra from individual single-wall carbon nanotubes. *Nano letters*, 3(3):383–388, 2003.
- [88] J. A. Misewich, R. Martel, Ph Avouris, J. C. Tsang, S. Heinze, and J. Tersoff. Electrically induced optical emission from a carbon nanotube FET. *Science (New York, N.Y.)*, 300(5620):783–6, 2003.
- [89] M. Freitag, Y. Martin, J. A. Misewich, R. Martel, and P. Avouris. Photoconductivity of Single Carbon Nanotubes. *Nano letters*, 3(8):1067–1071, 2003.
- [90] Giada Cellot, Emanuele Cilia, Sara Cipollone, Vladimir Rancic, Antonella Sucapane, Silvia Giordani, Luca Gambazzi, Henry Markram, Micaela Grandolfo, Denis Scaini, Fabrizio Gelain,

- Loredana Casalis, Maurizio Prato, Michele Giugliano, and Laura Ballerini. Carbon nanotubes might improve neuronal performance by favouring electrical shortcuts. *Nature nanotechnology*, 4(2):126–33, 2009.
- [91] Pedro Galvan-Garcia, Edward W Keefer, Fan Yang, Mei Zhang, Shaoli Fang, Anvar A Zakhidov, Ray H Baughman, and Mario I Romero. Robust cell migration and neuronal growth on pristine carbon nanotube sheets and yarns. *Journal of biomaterials science. Polymer edition*, 18(10):1245–61, janeiro 2007.
- [92] Joseph J Pancrazio. Neural interfaces at the nanoscale. *Nanomedicine (London, England)*, 3(6):823–30, dezembro 2008.
- [93] Dongwoo Khang, Grace E. Park, and Thomas J. Webster. Enhanced chondrocyte densities on carbon nanotube composites: the combined role of nanosurface roughness and electrical stimulation. *Journal of biomedical materials research. Part A*, 86(1):253–60, 2008.
- [94] A. R. Boccaccini, F. Chicatun, J. Cho, O. Bretcanu, J. A. Roether, S. Novak, and Q. Z. Chen. Carbon Nanotube Coatings on Bioglass-Based Tissue Engineering Scaffolds. *Advanced Functional Materials*, 17(15):2815–2822, 2007.
- [95] Dongwoo Khang. *Bio-inspired Carbon Nano-structures: Orthopedic Applications*, chapter 4. World Scientific Publishing, 2007.
- [96] Naoto Saito, Yuki Usui, Kaoru Aoki, Nobuyo Narita, Masayuki Shimizu, Nobuhide Ogiwara, Koichi Nakamura, Norio Ishigaki, Hiroyuki Kato, Seiichi Taruta, and Morinobu Endo. Carbon Nanotubes for Biomaterials in Contact with Bone. *Current Medicinal Chemistry*, 15(5):523–527, 2008.

- [97] Rose L. Spear and Ruth E. Cameron. Carbon nanotubes for orthopaedic implants. *Journal of Materials Form*, 1:127–133, 2008.
- [98] Xiaoming Li, Hong Gao, Motohiro Uo, Yoshinori Sato, Tsukasa Akasaka, Qingling Feng, Fuzhai Cui, Xinhui Liu, and Fumio Watari. Effect of carbon nanotubes on cellular functions in vitro. *Journal of Biomedical Materials Research. Part A*, 91(1):132–9, 2009.
- [99] Jie Meng, Hua Kong, Zhaozhao Han, Chaoying Wang, Guangjin Zhu, Sishen Xie, and Haiyan Xu. Enhancement of nanofibrous scaffold of multiwalled carbon nanotubes/polyurethane composite to the fibroblasts growth and biosynthesis. *Journal of Biomedical Materials Research Part A*, 88A(1):105–116, 2008.
- [100] E Mooney, P Dockery, U Greiser, M Murphy, and V Barron. Carbon nanotubes and mesenchymal stem cells: Biocompatibility, proliferation and . . . . *Nano Letters*, 2008.
- [101] L. P. Zanello, B. Zhao, H. Hu, and R. C. Haddon. Bone cell proliferation on carbon nanotubes. *Nano letters*, 6(3):562–567, 2006.
- [102] Xiaoke Zhang, Lingjie Meng, and Qinghua Lu. Cell behaviors on polysaccharide-wrapped single-wall carbon nanotubes: a quantitative study of the surface properties of biomimetic nanofibrous scaffolds. *ACS nano*, 3(10):3200–6, 2009.
- [103] Shao-Feng Wang, Lu Shen, Wei-De Zhang, and Yue-Jin Tong. Preparation and mechanical properties of chitosan/carbon nanotubes composites. *Biomacromolecules*, 6(6):3067–72, 2005.
- [104] Chiu-Wing Lam, John T. James, Richard McCluskey, and Robert L. Hunter. Pulmonary toxicity of single-wall carbon nan-

- otubes in mice 7 and 90 days after intratracheal instillation. *Toxicological sciences*, 77:126–34, 2004.
- [105] Guang Jia, Haifang Wang, Lei Yan, Xiang Wang, Rongjuan Pei, Tao Yan, Yuliang Zhao, and Xinbiao Guo. Cytotoxicity of Carbon Nanomaterials: Single-Wall Nanotube, Multi-Wall Nanotube, and Fullerene. *Environmental Science & Technology*, 39(5):1378–1383, 2005.
- [106] Tonya K. Leeuw, R. Michelle Reith, Rebecca A. Simonette, Malory E. Harden, Paul Cherukuri, Dmitri A. Tsyboulski, Kathleen M. Beckingham, and R. Bruce Weisman. Single-walled carbon nanotubes in the intact organism: near-IR imaging and biocompatibility studies in *Drosophila*. *Nano letters*, 7(9):2650–4, 2007.
- [107] Sunil K. Manna, Shubhashish Sarkar, Johnny Barr, Kimberly Wise, Enrique V. Barrera, Olufisayo Jejelowo, Allison C. Rice-Ficht, and Govindarajan T. Ramesh. Single-walled carbon nanotube induces oxidative stress and activates nuclear transcription factor-kappaB in human keratinocytes. *Nano letters*, 5(9):1676–84, 2005.
- [108] D. B. Warheit. What is currently known about the health risks related to carbon nanotube exposures? *Carbon*, 44(6):1064–1069, 2006.
- [109] J. Doshi and D. H. Reneker. Electrospinning process and applications of electrospun fibers. *Journal of Electrostatics*, 35, 1995.
- [110] Zheng-Ming Huang, Y. Z. Zhang, M. Kotaki, and S. Ramakrishna. A review on polymer nanofibers by electrospinning and their applications in nanocomposites. *Composites Science and Technology*, 63:2223–2253, 2003.

- [111] S. N. Reznik, A. L. Yarin, and A. Theron. Transient and steady shapes of droplets attached to a surface in a strong electric field. *Journal of Fluid Mechanics*, 516(1):349, 2004.
- [112] Y. M. Shin, M. M. Hohman, M. P. Brenner, and G. C. Rutledge. Experimental Characterization of Electrospinning: the electrically forced jet and instabilities. *Polymer*, 42:9955–9967, 2001.
- [113] C. R. Jaeger, M. M. Bergshoef, C. M. Batlle, H. Schonherr, and G. J. Vancso. Electrospinning of ultra-thin polymer fibers. *Macromolecular Symposia*, 127:141–150, 1998.
- [114] S. B. Warner, A. Buer, M. Grimler, S. C. Ugbohue, G. C. Rutledge, and M. Y. Shin. A Fundamental Investigation of the Formation and Properties of Electrospun Fibers, 1999.
- [115] A Buer, S. C. Ugbohue, and S. B. Warner. Electrospinning and properties of some nanofibers. *Textile Research Journal*, 71(4):323–328, 2001.
- [116] Darrell H. Reneker, Alexander L. Yarin, Hao Fong, and Sureeporn Koombhongse. Bending instability of electrically charged liquid jets of polymer solutions in electrospinning. *Journal of Applied Physics*, 87(9):4531, 2000.
- [117] Yuris Dzenis. Material science. Spinning continuous fibers for nanotechnology. *Science*, 304(5679):1917–9, 2004.
- [118] G Larsen, S Noriega, and R Spretz. Electrohydrodynamics and hierarchical structure control: submicron-thick . . . . . of *Materials Chemistry*, 2004.
- [119] Sureeporn Koombhongse, Wenxia Liu, and Darrell H. Reneker. Flat polymer ribbons and other shapes by electrospinning. *Journal of Polymer Science Part B: Polymer Physics*, 39:2598–2606, 2001.

- [120] Geunhyung Kim and Wandoo Kim. Designed PCL Nanofibers Fabricated Using a Modified Electrohydrodynamic Process for Tissue Engineering. *Journal of Manufacturing Science and Engineering*, 130, 2008.
- [121] Sachiko Sukigara, Milind Gandhi, Jonathan Ayutsede, Michael Micklus, and Frank Ko. Regeneration of Bombyx mori silk by electrospinning. Part 2. Process optimization and empirical modeling using response surface methodology. *Polymer*, 45:3701–3708, 2004.
- [122] Homa Homayoni, Seyed Abdolkarim Hosseini Ravandi, and Masoumeh Valizadeh. Electrospinning of chitosan nanofibers: Processing optimization. *Carbohydrate Polymers*, 77:656–661, 2009.
- [123] Zeng Jun, Haoqing Hou, Andreas Schaper, Joachim H. Wendorff, and Andreas Greiner. Poly-L-lactide nanofibers by electrospinning – Influence of solution viscosity and electrical conductivity on fiber diameter and fiber morphology. *e-Polymers*, (009):1–9, 2003.
- [124] Satoru Kidoaki, Il Keun Kwon, and Takehisa Matsuda. Structural features and mechanical properties of in situ-bonded meshes of segmented polyurethane electrospun from mixed solvents. *Journal of biomedical materials research. Part B: Applied biomaterials*, 76(1):219–29, 2006.
- [125] J.P. Jeun, Y.M. Lim, and Y.C. Nho. Study on morphology of electrospun poly (caprolactone) nanofiber. *Journal of Industrial and Engineering Chemistry*, 11(4):573, 2005.
- [126] Peter X. Ma and Jennifer Elisseeff, editors. *Scaffolding in Tissue Engineering*. CRC Press, 2006.
- [127] R. Samatham, I-S. Park, K. J. Kim, J-D Nam, N. Whisman, and

- J. Adams. Electrospun nanoscale polyacrylonitrile artificial muscle. *Smart Materials and Structures*, 15:152–156, 2006.
- [128] Y. Wang and Y.-L. Hsieh. Enzyme immobilization via electrospinning of polymer/enzyme blends. *Polymer Preprints*, 44:1212–1213, 2003.
- [129] L. Wu, X. Yuan, and J. Sheng. Immobilization of cellulase in nanofibrous PVA membranes by electrospinning. *Journal of Membrane Science*, 250(1-2):167–173, 2005.
- [130] Zuwei Ma, Masaya Kotaki, Thomas Yong, Wei He, and Seeram Ramakrishna. Surface engineering of electrospun polyethylene terephthalate (PET) nanofibers towards development of a new material for blood vessel engineering. *Biomaterials*, 26(15):2527–36, 2005.
- [131] T. J. Webster, editor. *Nanotechnology for the Regeneration of Hard and Soft Tissues*. World Scientific Publishing, 2007.
- [132] C. T. Laurencin, A. M. Ambrosio, M. D. Borden, and J. A. Cooper. Tissue engineering: orthopedic applications. *Annual review of biomedical engineering*, 1:19–46, 1999.
- [133] S. Srouji, T. Kizhner, E. Suss-Tobi, E. Livne, and E. Zussman. 3-D Nanofibrous electrospun multilayered construct is an alternative ECM mimicking scaffold. *Journal of materials science: Materials in medicine*, 19(3):1249–55, 2008.
- [134] S. Y. Chew, Y. Wen, Y. Dzenis, and K. W. Leong. The role of electrospinning in the emerging field of nanomedicine. *Current Pharmaceutical Design*, 12(36):4751–4770, 2006.
- [135] F. Ignatious and J. M. Baldoni. Electrospun pharmaceutical compositions, 2002.

- [136] Joseph D. Bronzino, editor. *The Biomedical Engineering Handbook*. CRC Press, second edition, 2000.
- [137] James E. Mark, editor. *Physical Properties of Polymers Handbook*. Springer, second edi edition, 2007.
- [138] Aldo R. Boccaccini and Julie E. Gough, editors. *Tissue engineering using ceramics and polymers*. CRC Press, 2007.
- [139] M. Kawashita, M. Nakao, M. Minoda, H.-M. Kim, T. Beppu, T. Miyamoto, T. Kokubo, and T. Nakamura. Apatite-forming ability of carboxyl group-containing polymer gels in a simulated body fluid. *Biomaterials*, 24:2477–2484, 2003.
- [140] G. A. Shen, S. Namilae, and N. Chandra. Load transfer issues in the tensile and compressive behavior of multiwall carbon nanotubes. *Materials Science and Engineering A*, 429:66–73, 2006.
- [141] Jinglei Yang, Zhong Zhang, Klaus Friedrich, and Alois K. Schlarb. Creep Resistant Polymer Nanocomposites Reinforced with Multiwalled Carbon Nanotubes. *Macromolecular Rapid Communications*, 28:955–961, 2007.
- [142] A.L. Andradý. *Science and Technology of Polymer Nanofibers*. John Wiley & Sons, New Jersey, 2008.
- [143] E.D. Boland, J.A. Matthews, K.J. Pawlowski, D.G. Simpson, G.E. Wnek, and G.L. Bowlin. Electrospinning collagen and elastin: preliminary vascular tissue engineering. *Front Biosci*, 9:1422–1432, 2004.
- [144] Krystyna Kelar and Boleslaw Jurkowski. Properties of Anionic Polymerized e-Caprolactam in the Presence of Carbon Nanotubes. *Polymer*, 104:3010–3017, 2007.

- [145] Derek M. Lincoln, Richard A. Vaia, Zhi-Gang Wang, Benjamin S. Hsiao, and Ramanan Krishnamoorti. Temperature dependence of polymer crystalline morphology in nylon 6/montmorillonite nanocomposites. *Polymer*, 42(25):9975–9985, 2001.
- [146] Anthony L. Andrady. *Science and Technology of Polymer Nanofibers*. John Wiley & Sons, 2008.
- [147] Gianluca D’Ippolito, Paul C. Schiller, Camillo Ricordi, Bernard A. Roos, and Guy A. Howard. Age-related osteogenic potential of mesenchymal stromal stem cells from human vertebral bone marrow. *Journal of bone and mineral research*, 14(7):1115–22, julho 1999.
- [148] M. Martina, G. Subramanyam, J. C. Weaver, D. W. Hutmacher, D. E. Morse, and S. Valiyaveetil. Developing macroporous bicontinuous materials as scaffolds for tissue engineering. *Biomaterials*, 26:5609–5616, 2005.
- [149] F. Ko, Y. Gogotsi, A. Ali, N. Naguib, H. Ye, G.L. Yang, C. Li, and P. Willis. Electrospinning of continuous carbon nanotubes-filled nanofiber yarns. *Advanced Materials*, 15(14):1161–1165, 2003.
- [150] X. Xiao-Lin, M. Yiu-Wing, and Xing-Ping Z. Dispersion and alignment of carbon nanotubes in polymer matrix: A review. *Materials Science and Engineering R*, 49:89–112, 2005.
- [151] R. Sengupta, A. Bandyopadhyay, S. Sabharwal, T. Chaki, and A. Bhowmick. Polyamide-6,6/in situ silica hybrid nanocomposites by sol-gel technique: synthesis, characterization and properties. *Polymer*, 46(10):3343–3354, 2005.
- [152] D. Vlasveld, J. Groenewold, H. Bersee, and S. Picken. Moisture

- absorption in polyamide-6 silicate nanocomposites and its influence on the mechanical properties. *Polymer*, 46(26):12567–12576, 2005.
- [153] Lingyu Li, Christopher Y. Li, Chaoying Ni, Lixia Rong, and Benjamin Hsiao. Structure and crystallization behavior of Nylon 66/multi-walled carbon nanotube nanocomposites at low carbon nanotube contents. *Polymer*, 48(12):3452–3460, 2007.
- [154] Khalid Saeed and Soo-young Park. Preparation of multiwalled carbon nanotube/nylon-6 nanocomposites by in situ polymerization. *Journal of Applied Polymer Science*, 106(6):3729–3735, 2007.
- [155] Erh-Chian Chen and Tzong-Ming Wu. Isothermal and nonisothermal crystallization kinetics of nylon 6/functionalized multi-walled carbon nanotube composites. *Journal of Polymer Science Part B: Polymer Physics*, 46(2):158–169, 2008.
- [156] Satish Kumar, Thuy D. Dang, Fred E. Arnold, Arup R. Bhattacharyya, Byung G. Min, Xiefei Zhang, Richard A. Vaia, Cheol Park, W. Wade Adams, Robert H. Hauge, Richard E. Smalley, Sivaraman Ramesh, and Peter A. Willis. Synthesis, Structure, and Properties of PBO/SWNT Composites. *Macromolecules*, 35(24):9039–9043, 2002.
- [157] Rahul Sen, Bin Zhao, Daniel Perea, Mikhail E. Itkis, Hui Hu, James Love, Elena Bekyarova, and Robert C. Haddon. Preparation of Single-Walled Carbon Nanotube Reinforced Polystyrene and Polyurethane Nanofibers and Membranes by Electrospinning. *Nano Letters*, 4(3):459–464, 2004.
- [158] S. Namilae and N. Chandra. Multiscale Model to Study the Effect of Interfaces in Carbon Nanotube-Based Composites. *Journal of Engineering Materials and Technology*, 127:222–232, 2005.

- [159] Mian Wang, K. P. Pramoda, and Suat Hong Goh. Enhancement of interfacial adhesion and dynamic mechanical properties of poly(methyl methacrylate)/multiwalled carbon nanotube composites with amine-terminated poly(ethylene oxide). *Carbon*, 44:613–617, 2006.
- [160] Kyung Mi Woo, Victor J. Chen, and Peter X. Ma. Nano-fibrous scaffolding architecture selectively enhances protein adsorption contributing to cell attachment. *Journal of biomedical materials research. Part A*, 67(2):531–7, novembro 2003.
- [161] Kenneth M. Yamada. Adhesive Recognition Sequences. *The Journal of Biological Chemistry*, 266(20):12809–12812, 1991.
- [162] Michael Giersig and Gennady B. Khomutov, editors. *Nanomaterials for Application in Medicine and Biology*. Springer, 2006.
- [163] Erik H. J. Danen. Integrin proteomes reveal a new guide for cell motility. *Science signaling*, 2(89):58, 2009.
- [164] Richard O. Hynes. Integrins: Bidirectional, Allosteric Signaling Machines. *Cell*, 110(6):673–687, 2002.
- [165] K. Fujihara, M. Kotaki, and S. Ramakrishna. Guided bone regeneration membrane made of polycaprolactone/calcium carbonate composite nano-fibers. *Biomaterials*, 26:4139–4147, 2005.